UNIVERSITAT POLITÈCNICA DE VALÈNCIA

INSTITUTO INTERUNIVERSITARIO DE INVESTIGACIÓN DE RECONOCIMIENTO MOLECULAR Y DESARROLLO TECNOLÓGICO

Gated mesoporous silica nanoparticles for biomedical applications

PhD. Thesis

Submitted by

Ismael Otri

PhD. Supervisors:

Dr. Félix Sancenón Galarza
Dra. Elena Aznar Gimeno

Valencia, November 2022

FÉLIX SANCENÓN GALARZA, PhD in Chemistry and Full Professor at the *Universitat Politècnica de València*, ELENA AZNAR GIMENO, PhD in Chemistry and Lecturer at the *Universitat Politècnica de València*

Certify:

That the work "***Gated mesoporous silica nanoparticles for biomedical applications***" has been developed by Ismael Otri under their supervision in the Instituto Interuniversitario de Investigación de Reconocimiento Molecular y Desarrollo Tecnológico (IDM) of the *Universitat Politècnica de València*, as a Thesis Project in order to obtain the degree of PhD in Biotechnology at the *Universitat Politècnica de València*.

Valencia, 4th November 2022.

Dr. Félix Sancenón Galarza Dra. Elena Aznar Gimeno

Acknowledgements

Agradecimientos

Thank you to everyone who walked with me on the road, whether he strayed beside me or behind me or left the road and left me... I learned from all of you... I believed that no matter how weak and lonely I was, your kindness and mercy are always close to me, thank you God.

For the one who taught me the pronunciation of the letter and the love of knowledge for my mother and father, all that I am today, and tomorrow is the fruit of your love and knowledge ... All words of thanks are incapable of replying to your kindness and grace.

My beloved family, my brothers, and sisters, I am indebted to everyone who has supported and believed in me all my life.

My life partner and success, my dear wife... Thank you for your presence and support.

My children, I hope that science will always light your way in your life. I love you and strive for the best for you always.

My supervisors, Elena and Felix, thanks for your continuous support and cooperation.

My friends, message moderators and everyone who taught me letters, thank you all. You were candles in my path.

Resumen

Esta tesis doctoral titulada “Nanopartículas de sílice mesoporosas funcionalizadas con puertas moleculares para aplicaciones biomédicas” está centrada en el diseño y la síntesis de nuevos nanosistemas sensores y terapéuticos con aplicaciones en el campo clínico y medioambiental.

En la introducción de esta tesis (capítulo uno) se presenta una visión general de conceptos básicos de nanotecnología, química supramolecular, nanopartículas de sílice mesoporosa y de puertas moleculares.

A continuación, se presentan los objetivos generales y específicos que se van a desarrollar en los capítulos experimentales siguientes.

En el tercer capítulo se presenta el diseño, síntesis y caracterización de un nanodispositivo para la detección de endotoxina en medios acuosos. El nanodispositivo está basado en nanopartículas de sílice mesoporosa con los poros cargados con rodamina B y su superficie externa funcionalizada con grupos carboxilato. Los poros se bloquean, para evitar la liberación de la rodamina B, con polimixina B, un péptido con carga positiva. En presencia de la endotoxina, la polimixina B es desplazada de la superficie de las nanopartículas y se activa la liberación de la rodamina B del interior de los poros a la disolución. Esta liberación genera un aumento significativo de la fluorescencia en la disolución permitiendo la detección de la endotoxina. La respuesta obtenida con el nanodispositivo es muy selectiva ya que otras especies como el arabinogalactan, el β-(1,3)-D-glucano, la pectina, el EDTA, la glucosa, el GTP y el polvo no son capaces de inducir la apertura de los poros y la liberación de la rodamina B. Además, el

nanodispositivo presenta un límite de detección para la endotoxina en el rango picomolar.

En el cuarto capítulo se describe un nanodispositivo, basado en nanopartículas de sílice mesoporosa cargadas con rodamina B y tapadas con curcumina, que se emplea para la detección selectiva de seroalbúmina humana (HSA) mediante medidas de fluorescencia. En este nanodispositivo, de nuevo, la presencia de HSA es capaz de desplazar la curcumina de la superficie de las nanopartículas permitiendo la liberación controlada de la rodamina B. El nanodispositivo preparado presentó una respuesta muy selectiva hacia la HSA con un límite de detección tan bajo como 0.1 mg/mL en PBS (pH 7.4)-acetonitrilo 95:5 *v*/*v*.

El capítulo cinco está centrado en la preparación de un nanodispositivo para la liberación sinérgica del antibiótico linezolida en presencia de bacterias Gram negativas. Este nanomaterial está basado en el empleo de nanopartículas de sílice mesoporosa (como soporte inorgánico) con los poros cargados con linezolida y con la superficie externa funcionalizada con el antibiótico disruptor de membrana polimixina B (mediante interacciones electrostáticas). Cuando estas nanopartículas entran en contacto con bacterias Gram negativas el lipopolisacárido (LPS) de sus membrabas induce el desplazamiento de la polimixina B que actúa eficientemente como permeador y permite la liberación de la linezolida. La liberación simultánea de linezolida y la polimixina B en forma de nanoformulación inducen una reducción significativa de los valores del IC_{50} para bacterias cuando se compara con los valores obtenidos empleando de forma individual ambas especies.

El capítulo sexto está dedicado a la discusión de los resultados experimentales descritos en los capítulos tres, cuatro y cinco.

Finalmente, el capítulo siete de esta tesis doctoral, presenta las conclusiones generales que se derivan del trabajo experimental realizado. También se presentan las perspectivas futuras en el campo de las aplicaciones biomédicas de las nanopartículas de sílice mesoporosa con puertas moleculares. Esperamos que los resultados que se presentan en esta tesis doctoral puedan abrir nuevas oportunidades de investigación en el desarrollo de nuevos nanodispositivos inteligentes que puedan actuar como agentes antimicrobianos, así como en la preparación de sistemas sensores mejorados para detección clínica.

Resum

Aquesta tesi doctoral titulada “Nanopartícules de sílice mesoporoses funcionalitzades amb portes moleculars per a aplicacions biomèdiques” està centrada en el disseny i la síntesi de nous nanosistemes sensors i terapèutics amb aplicacions en el camp clínic i mediambientals.

En la introducció d'aquesta tesi (capítol un) es presenta una visió general de conceptes bàsics de nanotecnologia, química supramolecular, nanopartícules de sílice mesoporosa i de portes moleculars.

A continuació, es presenten els objectius generals i específics que es desenvoluparan en els capítols experimentals següents.

En el tercer capítol es presenta el disseny, síntesi i caracterització d'un nanodispositiu per a la detecció d'endotoxina en mitjans aquosos. El nanodispositiu està basat en nanopartícules de sílice mesoporosa amb els porus carregats amb rodamina B i la seua superfície externa funcionalitzada amb grups carboxilat. Els porus es bloquegen, per a evitar l'alliberament de la rodamina B, amb polimixina B, un pèptid amb càrrega positiva. En presència de l'endotoxina, la polimixina B és desplaçada de la superfície de les nanopartícules i s'activa l'alliberament de la rodamina B de l'interior dels porus a la dissolució. Aquest alliberament genera un augment significatiu de la fluorescència en la dissolució permetent la detecció de l'endotoxina. La resposta obtinguda amb el nanodispositiu és molt selectiva ja que altres espècies com l’arabinogalactan, el β-(1,3)-D-glucà, la pectina, l’EDTA, la glucosa, el GTP i la pols no són capaços d'induir l'obertura dels porus i l'alliberament de la rodamina B. A més, el nanodispositiu presenta un límit de detecció per a l'endotoxina en el rang picomolar.

En el quart capítol es descriu un nanodispositiu, basat en nanopartícules de sílice mesoporosa carregades amb rodamina B i tapades amb curcumina, que s'empra per a la detecció selectiva de seroalbúmina humana (HSA) mitjançant mesures de fluorescència. En aquest nanodispositiu, de nou, la presència de HSA és capaç de desplaçar la curcumina de la superfície de les nanopartícules permetent l'alliberament controlat de la rodamina B. El nanodispositiu preparat va presentar una resposta molt selectiva cap a la HSA amb un límit de detecció tan baix com 0.1 mg/ml en PBS (pH 7.4)-acetonitril 95:5 v/v.

El capítol cinc està centrat en la preparació d'un nanodispositiu per a l'alliberament sinèrgic de l'antibiòtic linezolida en presència de bacteris Gram negatives. Aquest nanomaterial està basat en l'ús de nanopartícules de sílice mesoporosa (com a suport inorgànic) amb els porus carregats amb linezolida i amb la superfície externa funcionalitzada amb l'antibiòtic disruptor de membrana polimixina B (mitjançant interaccions electroestàtiques). Quan aquestes nanopartícules entren en contacte amb bacteris Gram negatives el lipopolisacàrid (*LPS) de les seues membranes indueix el desplaçament de la polimixina B que actua eficientment com permeador i permet l'alliberament de la linezolida. L'alliberament simultani de linezolida i la polimixina B en forma de nanoformulació indueixen una reducció significativa dels valors de l'IC_{50} per a bacteris quan es compara amb els valors obtinguts emprant de manera individual totes dues espècies.

El capítol sisé està dedicat a la discussió dels resultats experimentals descrits en els capítols tres, quatre i cinc.

Finalment, el capítol set d'aquesta tesi doctoral, presenta les conclusions generals que es deriven del treball experimental realitzat. També es presenten les perspectives futures en el camp

de les aplicacions biomèdiques de les nanopartícules de sílice mesoporosa amb portes moleculars. Esperem que els resultats que es presenten en aquesta tesi doctoral puguen obrir noves oportunitats d'investigació en el desenvolupament de nous nanodispositius intel·ligents que puguen actuar com a agents antimicrobians, així com en la preparació de sistemes sensors millorats per a detecció clínica

Abstract

This PhD thesis entitled "Gated mesoporous silica nanoparticles for biomedical applications" is focused on the design and synthesis of novel nanodevices for sensing and therapeutic applications in clinical and environmental fields.

The first introductory chapter presented an overview of the different concepts related to nanotechnology, supramolecular chemistry, mesoporous silica nanoparticles (MSNs), and molecular gates.

Next, the general and specific objectives of this PhD thesis, that are addressed in the different experimental chapters, are presented.

The third chapter presented the design, synthesis, and characterization of a nanodevice for endotoxin detection in aqueous environments. The prepared nanodevice is based on mesoporous silica nanoparticles loaded rhodamine B and with its external surface functionalized with carboxylates. Pores are finally capped upon addition of cationic polymyxin B peptide. In the presence of endotoxin, polymyxin B is detached from the surface of the nanoparticles with subsequent rhodamine B release from the inner of the pores to the solution. This release generated a marked emission enhancement in solution which allow endotoxin detection. The obtained response was highly selective to endotoxin because other interfering agents such as arabinogalactan, β-(1,3)-D-glucan, pectin, EDTA, glucose, GTP and dust were unable to induce pore opening and rhodamine B release. Besides, the system detects endotoxin with a limit of detection in the picomolar range.

The fourth chapter presented a nanodevice, based on mesoporous silica nanoparticles loaded with rhodamine B and capped with anionic curcumin, which is used for the selective and

sensitive fluorogenic detection of human serum albumin (HSA). Again, in the presence of HSA, curcumin was detached from nanoparticles surface allowing rhodamine B release. Prepared nanodevice showed a highly selective response toward HSA with a limit of detection for HSA as low as 0.1 mg/mL in PBS (pH 7.4)-acetonitrile 95:5 *v*/*v*.

Chapter five focus on the design and synthesis of a nanodevice for the synergic release of linezolid antibiotic in the presence of Gram-negative bacteria. This nanodevice is based on the use of mesoporous silica nanoparticles (as inorganic support) with the pores loaded with linezolid and capped with the membrane disruptor polymyxin B through electrostatic interactions. When these particles enter in contact with Gram-negative bacterium, lipopolysaccharide (LPS) present in the cell membrane induces the detachment of polymyxin B, which acts as membrane permeator, from the nanodevice allowing linezolid release. Simultaneous release of linezolid and polymyxin B as a nanoformulation induced a marked reduction in the IC_{50} values for bacteria when compared to the values obtained using free linezolid and polymyxin B alone.

The sixth chapter is devoted to the discussion of the experimental results described in the previous chapters.

Finally, the seventh chapter of this PhD thesis, presented the main conclusions, derived from the experimental work, and future perspectives in the field of gated mesoporous silica nanoparticles for biomedical applications. We hope that the results achieved in this PhD thesis will open new research opportunities to develop advanced smart nanodevices as antimicrobial drugs as well as smart and fast sensing systems for clinical purposes.

Publications

Results of this PhD Thesis and other contributions have resulted in the following scientific publications:

- **Ismael Otri**, Sameh El Sayed, Serena Medaglia, Ramón Martínez-Máñez, Elena Aznar and Félix Sancenón, ‘‘Simple endotoxin detection using polymyxin B-gated nanoparticles’’ Chemistry – A European Journal, **2019**, 25, 3770-3774.
- **Ismael Otri,** Serena Medaglia, Elena Aznar, Félix Sancenón, and Ramón Martínez-Máñez, ‘‘Fluorogenic Detection of Human Serum Albumin Using Curcumin-Capped Mesoporous Silica Nanoparticles’’ Molecules **2022**, 27, 1133-1142.
- Hazem Essam Okda, Sameh El Sayed, **Ismael Otri**, Rosa C.M. Ferreira, Susana P.G. Costa, M. Manuela M. Raposo, Ramón Martínez-Máñez, Félix Sancenón, ‘‘A simple and easy-to-prepare imidazole-based probe for the selective chromo-fluorogenic recognition of biothiols and Cu(II) in aqueous environments’’ Dyes and Pigments, **2019**, 162, 303–308.
- Hazem Essam Okda, Sameh El Sayed, **Ismael Otri**, R. Cristina M. Ferreira, Susana P. G. Costa, M. Manuela M. Raposo, Ramón Martínez-Máñez, Félix Sancenón, ‘‘2,4,5-triaryl imidazole probes for the selective chromo-fluorogenic detection of Cu(II). Prospective use of the Cu(II) complexes for the optical recognition of biothiols’’ Polyhedron, **2019**, 170, 388-394.
- **Ismael Otri**, Serena Medaglia, Elena Aznar, and Félix Sancenón, ‘‘Exploring synergy between nanoformulated linezolid and polymyxin b as a gram-negative effective antibiotic delivery system based on mesoporous silica nanoparticles’’ Nanomaterials, **2022**, submitted.

Abbreviations and Acronyms

AG	Arabinogalactan
AMCA	7-amino-4-methylcoumarin
AMR	Antimicrobial resistance
ATP	Adenosine triphosphate
BET	Brunauer-Emmet-Teller
BIBB	2-bromoisobutyryl bromide
BJH	Barret-Joyner-Halenda
BSA	Bovine serum albumin
CIBER-BBN	Centro de Investigación Biomédica en Red en Bioingeniería, Biomateriales y Nanomedicina
CIPF	Centro Investigación Príncipe Felipe
CTAB	n-cetyltrimethylammonium bromide
DLS	Dynamic Light Scattering
DNA	Deoxyribonucleic acid
dNTP	Deoxynucleoside triphosphate
DOX	Doxorubicin
DTT	DL-Dithiothreitol
EDTA	Ethylenediaminetetraacetic acid
EFSA	European Food Safety Authority
ELISA	Enzyme-linked immunosorbent assay
Em and em	Emission
Ex and ex	Excitation
FDA	Food and Drug Administration
FITC	Fluorescein isothiocyanate

Fl	Fluorescence
FRET	Fluorescence Resonance Energy Transfer
GMP	Guanosine monophosphate
GOx	Glucose oxidase enzyme
GTP	Guanosine-5'-triphosphate
HSA	Human serum albumin
IDM	Instituto de Reconocimiento Molecular y Desarrollo Tecnológico
IISLAFE	Instituto de Investigación Sanitaria La Fe
IR	Infrared
IUPAC	International Union of Pure and Applied Chemistry
LAL	Limulus amebocyte lysate
LbL	layer-by-layer
LCST	lower critical solution temperature
LOD	Limit of Detection
LPS	Lipopolysaccharide
LPS-RS	Lipopolysaccharide from Rhodobacter sphaeroides
MCM-41	Mobil Composition of Matter No. 4
MIC	Minimum Inhibitory Concentration
mRNA	Messenger RNA
MRSA	Methicillin-resistant Staphylococcus aureus
MSNs	Mesoporous silica nanoparticles
NMR	Nuclear Magnetic Resonance
NPs	Nanoparticles
OD	Optical Density
PBS	Phosphate Buffered Saline

PDMAEMA	poly(2-dimethylaminoethyl methacrylate
PhD	Doctor of Philosophy of Philosophy Doctorate
PMB	Polymyxin B
PXRD	Powder X-ray diffraction
RhB	Rhodamine B
RNA	Ribonucleic acid
RT	Room Temperature
SD	Standard deviation
SDAs	Structure-directing agents
TBA	Thrombin-binding aptamer
TEM	Transmission electron microscopy
TEOS	Tetraethyl orthosilicate
TGA	Thermogravimetric analysis
TRIS	Tris(hydroxymethyl)aminomethane
UPV	Universidad Politécnica de Valencia
UV/VIS and UV-Vis	Ultraviolet–visible
WHO	World Health Organization
λexc	Excitation wavelength

Table of Contents

Chapter 1: General Introduction

General Introduction

This PhD thesis is devoted to the synthesis and characterization of new gated nanosystems based on mesoporous silica nanoparticles. These gated nanodevices are constructed taking into account concepts of supramolecular chemistry and nanotechnology. For this reason, in this introduction, the main concepts of nanotechnology and supramolecular chemistry will be briefly explained in the following pages.

1.1 Nanotechnology

Nowadays nanotechnology is a highly multidisciplinary scientific field involving chemistry, physics, biology, material science, engineering, and electronics. Therefore, requires the collaboration of scientists with different backgrounds to deal with the study, design, synthesis, and application of materials with dimensions in the nanoscale (nanometer = 10^{-9} m). A nanometer is equivalent to a distance 100000 times smaller than the diameter of a human hair (Figure 1).[1]

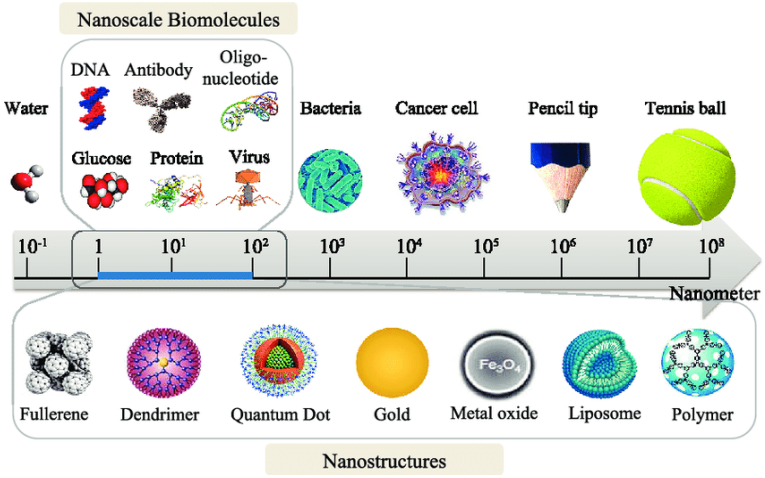

Figure 1. Scheme to compare the range of sizes of nanomaterials, cells and other items.

Since 1959, after the physicist, R. Feynman had proposed the manipulation of matter at the nanoscale,[2] and later in 1974, when N. Taniguchi used for the first time the term nanotechnology,[3] significant advances in the area have been made (for example the reduction of electronic transistors dimensions from 100 μm to less than 100 nm size). Other significative advances were the development of electronic and scanning tunnelling microscopes in 1981 by G. Binnig and H. Rohrer[4] and the atomic force microscope in 1985.[5] Furthermore, other landmarks of the field are the discovery of fullerenes in 1985, carbon nanotubes in 1991, and graphene in 2004[6] with its remarkable features which enable the use of these nanomaterials in a variety of applications. All these factors attracted the attention of the scientific community to nanotechnology and, for these reasons nowadays several nanomaterials have already been developed with different sizes and compositions with applications in different areas such as nanobatteries,[7] nanocarriers[8] and nanomotors.[9]

Nowadays, it is well-known that nanomaterials presented different features when compared to those observed when they are on the bulk scale. For example, gold always exhibits yellow shiny color while gold nanoparticles can show different colors, such as red or blue, depending on the interaction of its surface electrons with light known as surface plasmon resonance. The high surface area presented by these nanomaterials enables them to be used in several applications such as catalysis, biosensors and nanocarriers for controlled release protocols in cells. Besides, some nanomaterials such as graphene or carbon nanotubes, exhibit highly efficient conductivity and excellent mechanical properties and have been extensively used in electronics.[10] Nanotechnology helps to reduce the size of electronic elements as well as increase

their efficiency and power. Furthermore, nanotechnology holds great potential in the development of solar cells. Besides, there are several commercial products used in our daily life with enhanced features thanks to the use of nanomaterials such as bicycles (with improved lightness and resistance thanks to the use of carbon fiber), paints and deodorants (with antibacterial nanoparticles) and television screens (containing quantum dots).

Of all the technological fields in which nanomaterials find applications nanomedicine is, perhaps, one of the most remarkable and several advances can be envisioned in the near future.[11] For instance, the development of delivery nanosystems able to release drugs or biomolecules at specific regions, tissues or cells has been extensively explored in the last years. These delivery nanosystems increased the specificity and localization of the treatments avoiding therapy-derived side effects. Besides, also inside the field of nanomedicine, the development of sensitive and specific nanosensors for the detection of biological markers for disease diagnosis is also a field that deserves great concern. The fact that there are already more than 40 nanomedicines approved by the FDA[12] show the importance and the fast effect of nanotechnology in our life that will be seen clearly in the next few decades.

Nanotechnology, for many experts, is the revolution of the 21st century and remarkable advancements can be envisioned for the next decades. The research to improve and use nanoparticles for several applications is ongoing so fast and still, much progress is needed. A better understanding of nanomaterials features and the improvement in the preparation processes will lead to the development of new nanomaterials with advanced applications in several fields. A crucial role to achieve these advances and accelerating the translation of nanotechnology from the lab to our

daily life is played by the collaboration between researchers from different fields and between academics and industry.

1.2 Supramolecular Chemistry

In the last decades, supramolecular chemistry became a well-established field in chemistry playing an important role in the design and synthesis of nanomaterials and in the development of hybrid nanosystems with advanced functionalities. [13]

The concept of supramolecular chemistry appears in the late nineteenth century when intermolecular forces were discovered in 1873 by J. Van der Waals, Nobel Prize in physics in 1910.[14] Another important early contribution was the synthesis and study of cyclodextrins by Villiers in 1891.[15] These studies were followed by the seminal works of A. Werner about the theory of coordination and the study of metal complexes presented in 1893.[16] Later, in 1987, J. M. Lehn, D. J. Cram and C. J. Pedersen received the Nobel Prize in Chemistry for their contributions that led to the establishment of this new branch of chemistry. According to J. M. Lehn, Supramolecular chemistry can be defined as the chemistry that controls the non-covalent interactions between molecules (as shown in Figure 2), while molecular chemistry is related to the study of the interaction between the atoms that form molecules through covalent bonds.[17]

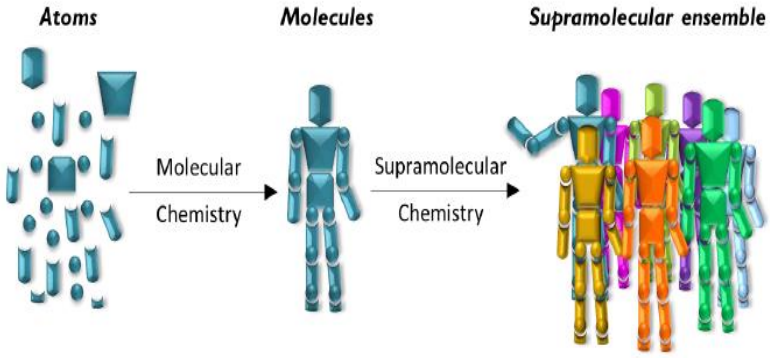

Figure 2. A schematic presentation that illustrates the difference between molecular and supramolecular chemistry.

These non-covalent interactions involved hydrogen bonding, metal coordination, hydrophobic forces, van der Waals forces, π-π interactions and electrostatic forces, which generated unique nanostructured supermolecules which showed different features than that of the individual components.[18]

Several examples of supramolecular interactions can be found in nature. For instance, it is known that water physical properties (such as boiling and freezing points or volume expansion after freezing) are a consequence of hydrogen bonding interactions between water molecules. Supramolecular interactions determine also the structure and function of proteins, enzymes and pathogen-cell interactions. Besides, one of the most important examples of supramolecular interaction and its effect on functionality can be seen clearly in the DNA double helix structure. Single DNA strands are composed of cytosine, thymine, adenine and guanine bases linked to a sugar and a phosphate and connected through covalent bonds. In the double DNA helix, two complementary strands are held together by supramolecular interactions such as (i) hydrogen bonds between complementary bases in different strands and (ii) π-π interactions between the aromatic rings of the bases (Figure 3).

This complex assembly gives DNA the ability to adapt its structure to achieve the optimal manner of function.

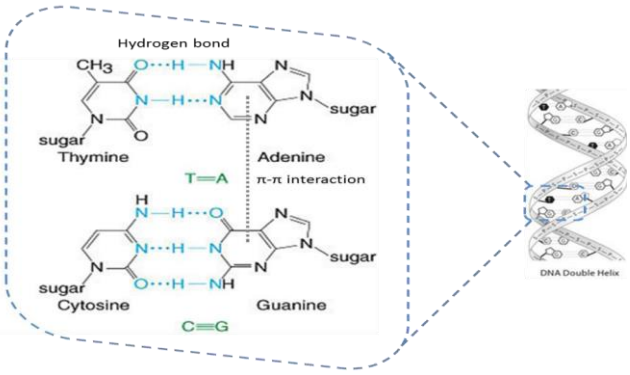

Figure 3. Chemical structure of the DNA double helix showing hydrogen bonds between base pairs (G-C and A-T) and π-π interactions between aromatic rings.

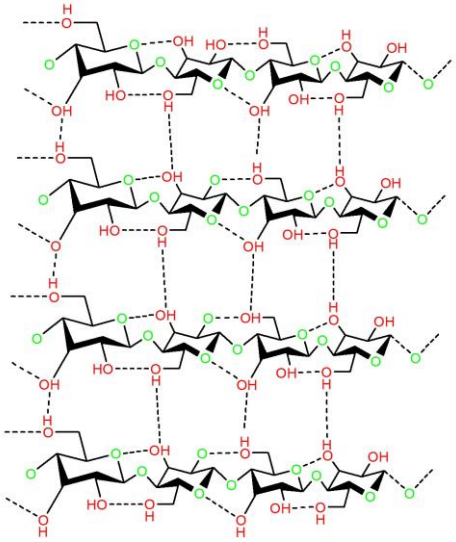

Figure 4. Intermolecular interactions in cellulose: side-to-side hydrogen bonds between hydroxyl groups of the polysaccharide chains in the same horizontal layer.

Another example of supramolecular assembly is the chemical structure of cellulose. Different cellulose layers are linked through the formation of hydrogen bonds between hydroxyl groups of one

saccharide unit with another hydroxyl group in neighbour sugar in the same polysaccharide chain or hydroxyl group in other chains (Figure 4). As a result, these hydrogen bonds reduce the distance between polysaccharides to form mono horizontal layers like a sheet. In addition to hydrogen bonds, van der Waals forces make sheets stacked tightly into layers to form a microfibril.[19]

Inside the vast realm of supramolecular chemistry, two seminal concepts emerged due to their significance as a consequence of the remarkable applications that have been produced: (i) molecular recognition and (ii) self-assembly.

- **Molecular recognition**: Molecular recognition can be defined as the specific binding of a guest molecule to a host compound to form a supramolecular complex. The host, or receptor, is usually a large molecule (such as an enzyme) with a geometric size or shape complementarity to the guest. The guest molecule may be a cation, anion or a more complex (bio)molecule. The basis of molecular recognition is laid on the lock and key principle, *i.e* the discrimination by a host between different guests (see Figure 5).[20] The host-guest interaction is the base of the molecular sensor concept. Typical molecular sensors consist of recognition and signalling subunits linked through a covalent bond. The recognition unit is able to interact with the target guest in a selective and specific way while the signalling subunit (a fluorophore or chromophore) translates the microscopic recognition to a measurable optical signal.[21] Several recognition host molecules have been synthesised (cyclodextrins, cucurbiturils, crown ethers, calixarenes and pillarenes) as shown in Figure 6.[22] This knowledge has been transferred to the nanotechnology field. For instance, using these supramolecular receptors as

functional components of nanoparticles for the detection of different molecules with biological or industrial interest even in the aqueous or gas phase. [23]

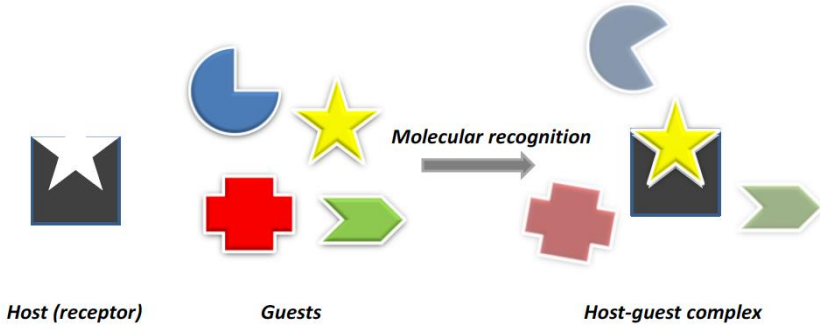

Figure 5. Schematic presentation of molecular recognition between a host and several guests.

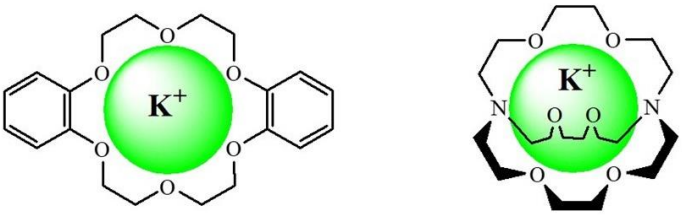

Figure 6. Examples of the host-guest chemistry between as crown ethers left and cryptands right with guest ion K^+.

- **Self-assembly:** Self-assembly can be defined as a process in which molecules spontaneously undergo arrangement to a defined structure guided by its chemical properties. A molecular self-assembly is a recurrent tool in nanotechnology for the construction of nanomaterials because can promote the formation of larger structures such as micelles, membranes and vesicles.[24] The formation of larger molecules is directly and spontaneously built from the assembly between smaller molecular entities, and thus it avoids the use of complicated equipment and overcomes synthetic steps. Furthermore, scientists were able to inspire by examples of self-assembly in nature and use interactions between biological

components to assemble nanodevices. Besides, the capability to incorporate biological components into the final abiotic system, formed by self-assembly using mild conditions, preserved their functionality.

The importance of supramolecular interactions, recognition chemistry and self-assembly concepts in the design and synthesis of nanoparticles, mesoporous silica-based materials and gated nanodevices is remarkable as can be assessed from the following examples:

- Design of capping agents or molecular gates based on supramolecular (host-guest) ensembles like those based on cyclodextrins, cucurbiturils, crown ethers, and so on.
- Self-organization of surfactant molecules into predetermined structures in the synthesis of porous materials.
- Condensation of porous materials through supramolecular electrostatic interactions.
- Uncapping of gated porous materials by the specific molecular recognition between protein and organic compounds.

1.3 Organic-Inorganic Hybrid Materials

Organic-inorganic hybrid materials are obtained by the covalent anchoring of organic compounds into 2D and 3D solid supports. The anchoring of organic molecules (such as receptors) on the surface of nanoscopic inorganic materials (support) can lead to hybrid organic-inorganic solids which present different properties often better than those of the isolated components.[25]

These new materials emerged from the need to develop new applications that are difficult to obtain by using classical chemistry. These hybrid materials presented enhanced functionalities by the combination of supramolecular concepts with nanoscopic inorganic solids.[26]

This could be achieved by using preorganized nanoscopic solid structures and molecular functional units attached to the surface of the inorganic supports in a synergic fashion.[27] Taking this fact into account, it was found that the anchoring of molecular entities onto 3D nanoscopic scaffoldings offers the opportunity to develop and explore new supramolecular concepts that are hard to achieve on 2D surfaces.[28] This is especially clear in the field of gated nanochemistry and in the design of nanoscopic supramolecular architectures incorporating chemical entities that can act as functional gatelike scaffoldings allowing mass transport at the nanometric scale.[29,30,31,32]

The main advantages of anchoring organic molecules on solid supports are the following:

- Pre-organization of the receptor leads to the formation of a dense monolayer (depending on the degree of surface functionalization) of binding/coordination sites arranged in specific positions onto the solid surface. This effect maximizes the interaction with the target analyte.
- Modulation of properties of the hybrid material by multi-functionalization in successive steps.
- Improvement of the recognition process due to the restriction of the receptor movement upon anchoring onto the solid surface.
- Reversibility of the sensing system. If the coordination processes are reversible, the material could be reused several times.
- The possible control of size, shape and surface area can provide interesting changes in the physical and chemical properties of the inorganic surface,[33] improving selectivity and sensitivity.[34]

1.4 Mesoporous Silica Materials

The International Union of Pure and Applied Chemistry (IUPAC) classified pore sizes into three main categories, namely micro-pores (<2 nm), mesopores (2-50 nm) and macro-pores (>50 nm).[35] As a result of their large internal surface area, microporous and mesoporous materials are attracting research attention due to their technological applications in catalysis,[36] filtration and separation,[37] gas adsorption and storage,[38] enzyme immobilization,[39] drug delivery,[40] and chemical/biochemical sensing.[41] Zeolites are examples of microporous aluminosilicates porous materials with pore sizes usually between 3 to 10 Å which are used in applications like catalytic preparation of pharmaceuticals, in petroleum production processes and for water purification.[42] They can act as molecular "sieves" allowing selected molecules to diffuse through their pores and favour the formation of specific products with high yields and minimum waste. However, the small pore size of zeolites makes them not suitable for applications involving chemicals with a larger size. On the other hand, MCM mesoporous silica materials (where MCM stands for **M**obil **C**omposition of **M**atter), discovered in 1992 by Mobil Oil Company, were the first mesoporous solid synthesized.[43] These materials showed a regular ordered pore arrangement and a very narrow pore-size distribution. It was demonstrated that by using different synthesis conditions (solvent, pH, temperature, concentration) different phases were obtained such as MCM-41 (with a hexagonal arrangement of the mesopores), MCM-48 (with a cubic arrangement of mesopores) and MCM-50 (with a lamellar structure) (see Figure 7). Besides, these materials are chemically inert, possess high thermal stability, have large specific surface areas (between 500 and 1000 $m^2 g^{-1}$), homogeneous pore size and

a high pore volume (in the order of 1 cm^3 g^{-1}). Among these phases, the MCM-41 is the most studied and used due to the relative simplicity of its synthesis and its particular honeycomb-like structure.

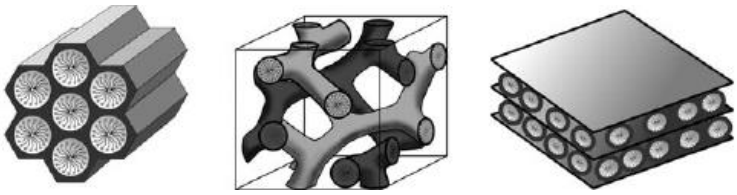

MCM-41 ***MCM-48*** ***MCM-50***

Figure 7. Scheme of structures of mesoporous M41S phase materials. (Reprinted with permission from F. Hoffmann et al., Angew. Chem. Int. Ed., 2006, 45, 3216. Copyright © 2006 Wiley-VCH Verlag GmbH & Co. KGaA, Weinheim).

1.4.1 *Synthesis Of Mesoporous Silica Materials*

The synthesis of these materials used a surfactant, as a structure-directing agent, and as a silica source. Several parameters (such as the nature of structure directing agent, relative concentrations of surfactant and silica source, pH, temperature, synthesis time, solvent) controlled pore formation and the type of phase obtained.

However, two main components are necessary to build up these mesoporous materials with a highly ordered porous structure and homogeneous pore dimensions:

- Structure-directing agents (SDAs) or templates whose function is to direct the construction of a highly ordered porous network.
- A polymeric precursor has to self-organize around the template and upon polymerization, build up the final rigid structure.

SDAs, used as templates in the synthesis of mesoporous materials, are usually surfactants (long-chain alkyl

trimethylammonium halides). Under certain experimental conditions form a lyotropic liquid-crystalline phase, which leads to the assembly of an ordered mesostructured composite during the condensation of the silica precursors under basic conditions. As explained above, MCM-41 is one of the best-known most widely studied mesoporous support and its synthesis is schematically represented in Figure 8. MCM-41 materials are usually synthesized in alkaline media using the cationic surfactant cetyltrimethylammonium bromide (CTABr) as the SDAs.

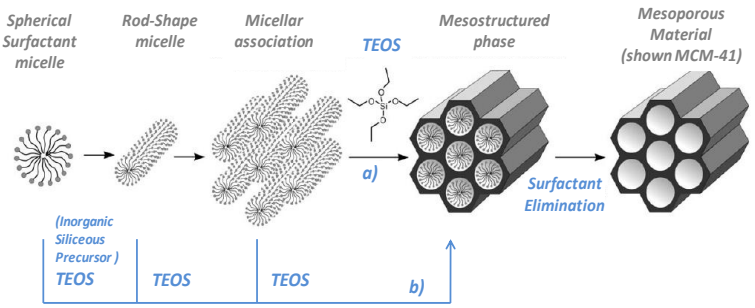

Figure 8. Scheme synthesis of MCM-41 by structure-directing agents: a) hexagonal template formation by the surfactant and b) polymerisation of the silica precursor. (Reprinted and adapted with permission from F. Hoffmann et al., Angew. Chem. Int. Ed., 2006, 45, 3216. Copyright © 2006 Wiley-VCH Verlag GmbH & Co. KGaA, Weinheim).

The first step in the synthesis of MCM-41 material is the preparation of the template using the proper conditions of temperature, pH and concentration. The surfactant firstly self-organizes into micelles and secondly, micelles form hexagonal-shaped supra micellar aggregates by self-assembly. After adding tetraethyl orthosilicate (TEOS) precursor to the solution at basic pH, it polymerizes around the template giving rise to the final mesoporous scaffold with its pores full of surfactant. Depending on

various reaction parameters (temperature, concentration, and reaction time) nano or micro-particles can be specifically obtained.

The second step is the removal of surfactant by high-temperature calcination (500-600 °C) or by extraction with adequate solvents. These procedures allowed us to obtain the final mesoporous inorganic scaffold which presents cylindrical unidirectional empty channels of approximately 3 nm in diameter (when CTABr is used as surfactant) arranged in a hexagonal distribution. The principal advantage of this synthetic method is the fact that the high grade of homogeneity of the initial elements (surfactant and polymer) is transmitted to the final material, which presented a system of pores not only homogeneously in size but also in form and regularity. Making small changes in the synthetic procedure, it is possible to modify the final important features of the solid such as pore size (from 2 up to 50 nm) only by changing the surfactant used as directing agent.[44]

1.4.2 *Functionalisation of Inorganic Silica Scaffolds. Preparation Of Organic-Inorganic Mesoporous Hybrid Materials*

Functionalisation refers to the incorporation of organic groups onto the surface of inorganic supports which leads to the production of hybrid materials. Hybrid organic-inorganic materials are highly interesting for a wide range of applications (e.g. chromatography, sensing, catalysis, etc.) since they combine the high surface area, stability and easy functionalisation of the inorganic support with the organic functionalities.

Silica-based mesoporous scaffolds can be easily functionalised due to the presence of a high concentration of silanol (Si-OH) groups on its surface. These silanols can easily react with trialkoxysilane derivatives $(R'O)_3$-Si-R to generate organic−inorganic

nanocomposites. By changing the chemical nature of R moiety different hybrid materials with selected features and for different purposes can be prepared. Besides, these R groups can contain one or more reactive functional moieties, which can be later chemically modified. Two main procedures for the preparation of the organic-inorganic mesoporous hybrid materials have been described, namely co-condensation or grafting (see Figure 9).[45]

- ***Co-condensation***

In this method, trialkoxy organosilanes of the type $(R'O)_3$-Si-R together with SDAs were incorporated simultaneously in the first step of the synthesis. The resulting silica matrix contains alkoxy functional groups intercalated in the main silica skeleton and distributed homogenously both on the external and internal surfaces. In this case, the surfactant must be removed by extraction and not by calcination as it would destroy the organic functional groups. This protocol leads to materials with organic residues anchored covalently to the pore walls (see Figure 9). Homogeneous distribution of the organic moieties along the inner and outer surface is obtained by using this procedure.

However, this method presented some drawbacks such as: (a) the mesoscopic order degree of the hybrid material decreases with increasing concentration of $(R'O)_3$-Si-R in the reaction mixture; (b) the fraction of terminal organic groups that are incorporated into the pore-wall network is generally lower than that corresponding to the starting concentration of the reaction mixture as there are homo condensation reactions between silanes groups; (c) the incorporated organic groups can lead to a reduction in the pore diameter, pore-volume, and specific surface areas; (d) the homogeneous distribution of different organic functionalities in the framework cannot be ensured. In this method, care must be taken

to preserve the organic functionality during the removal of the surfactant.[46, 47]

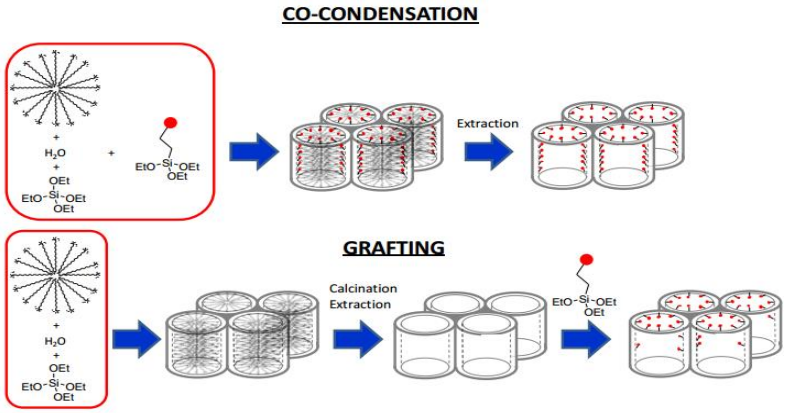

Figure 9. A Schematic representation of the functionalization routes of siliceous mesoporous materials. Adapted from E. Climent PhD Thesis.48

- ***Grafting***

Grafting refers to the subsequent modification of the surface of mesostructured silica phases, after the removal of surfactant by calcination or with solvent, with organic groups as shown in Figure 9. This multi-step process is carried out by reaction of organosilanes of the type $(R'O)_3$-Si-R with the free silanol groups (Si-OH) on the surface of the calcined scaffold. Organosilanes are preferentially located onto the external silica surface because diffusion to the inner of the pores is partially precluded. As there is a wide range of commercially available organosilanes, more than silazanes ($HN(SiR_3)_2$) or chlorosilanes ($ClSiR_3$), these products are by far the most used. Besides, the reaction between the superficial silanol groups with trialkoxysilanes is a simple condensation reaction with high yields.[49]

The two main advantages of using the grafting protocol are that the mesoporous silica support can be synthesized using well-known standard procedures on large scales and later modified with

the selected organosilanes. The second advantage is that the mesostructure of the starting silica phase is usually retained. However, when bulky organic moieties are used for functionalization certain pore blocking can be observed. Also, a superficial modification is usually obtained using this functionalization method.[50]

1.4.3 *Characterization of Mesoporous Silica Materials*

Several characterization techniques are used to confirm the proper formation of the mesoporous structure during the synthesis and the incorporation of different components in the final hybrid material. For example, in the case of MCM-41 mesoporous silica material different features should be considered: (a) the integrity of the mesoporous structure; (b) the high surface and uniform pore volume; (c) the organic matter content in the final material and (d) the particles average diameter and shape. The most common techniques used for the characterization of these hybrid materials are powder X-ray diffraction (PXRD), transmission electron microscopy (TEM), N_2 adsorption-desorption isotherms and solid-state nuclear magnetic resonance spectroscopy (NMR).[51]

Powder X-ray diffraction (PXRD) gives information about the arrangement of the pores in the mesoporous material. In the case of the mesoporous silica materials, there are characteristic peaks on the PXRD pattern which appeared at low angles since the distance between planes of pores is large. This technique is especially useful to verify the integrity of the mesoporous scaffold before and after the removal of the SDAs and after the modification steps that can potentially damage the structure. The typical MCM-41 PXRD pattern, for instance, shows four reflections between $2\Theta = 2^o$ and 5^o, corresponding to the ordered hexagonal

array of parallel silica tubes and can be indexed assuming a hexagonal unit cell as (100), (110), (200), (210) and (300).[52]

N_2 adsorption-desorption isotherms are fundamental in the characterization of mesoporous materials because total surface area, pore size and specific pore volume can be calculated using these data. In this technique, the quantity of nitrogen adsorbed per gram of material, when the pores are empty and when the inner and outer surfaces are functionalised, are calculated. Often the quantity of nitrogen adsorbed is high in the first case due to its adsorption inside the pore channels. On the contrary, when the pores are filled with cargo or have not been properly formed, the quantity of adsorbed nitrogen is significantly lower.[53] Typically, the specific surface area of mesoporous materials is determined by applying the Brunauer-Emmet-Teller (BET) method[54] while the pore size and specific pore volume are calculated by applying the Barret-Joyner-Halenda (BJH) model.[55]

Besides the PXRD pattern, **transmission electron microscopy (TEM)** is used to visualize the size and morphology of the materials with high resolution. For MCM-41 the hexagonal arrangement of the pores can be observed as parallel lines (Figure 10). This is related to the hexagonal repeat between tubes and the uniform pore size (around 2-4 nm) can be observed. Using TEM, the presence of pores on the material and their periodicity can be usually discerned.[56]

Other techniques can be used to evaluate (qualitatively and/or quantitatively) the proper functionalisation of organic molecules during the preparation steps or in the final hybrid material. **Elemental analysis (EA)** gives information about the percentage in weight of carbon, hydrogen, nitrogen and sulphur which is related to the amount of organic functional molecules. **Solid-state nuclear**

magnetic resonance (NMR) allows for confirming the presence of different functional organic molecules onto the solid surface by showing its characteristic NMR peaks. **Thermogravimetric analysis (TGA)** registers the loss in weight of the material as a function of the temperature so the overall percentage of organic matter can be calculated. Furthermore, **Dynamic Light Scattering (DLS)** is used to estimate the hydrodynamic diameter of the particles based on measuring the fluctuation in scattered light due to the motion of the particles in solution while it is irradiated with a laser beam. The particles move faster the smaller they are and thus the fluctuations can be related to the size of the particles. Zeta potential of the particles can be determined from DLS using a special cuvette with two electrodes. Zeta potential measurements can be used to follow the proper functionalization steps followed of the preparation of hybrid materials. Another two techniques that are very useful when working with mesoporous materials are **UV-visible spectrophotometry** and **fluorescence**. Both techniques can be used for quantifying the amount of encapsulated cargo, for monitoring the release of fluorescent or coloured cargo from the pores, for conducting enzymatic assays and so on.

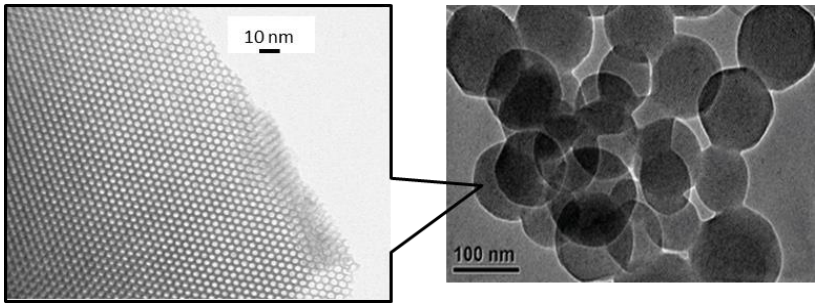

Figure 10. TEM micrographs of MCM-41 at 10 and 100 nm.

1.5 Stimuli-Responsive Gated Materials

As cited above, hybrid materials based on mesoporous silica have been extensively used in different technological fields (heterogeneous catalysis, chemical sensors[57] and environmental studies[58]) and one of the most interesting applications is as reservoirs for the storage and controlled release of (bio)molecules. The remarkable features of mesoporous silica supports (such as chemical inertness, thermal stability, three-dimensional structure, high external surface, uniform pore systems that grant high load capacity, high specific surface area, well-known functionalization procedures and biocompatibility)[59] makes this support the ideal choice for the development on new materials with controlled release features. In particular, functionalized mesoporous solids, have been extensively used in the development of stimuli-responsive gatekeeping materials that can entrap and transport molecules to specific locations,[60] or with the ability to release in a controlled fashion of an encapsulated cargo.[61]

In the beginning, mesoporous materials have been extensively used as vehicles to store and subsequently release certain organic molecules. This application is a direct consequence of the presence of a uniform pore network that grants a high load capacity for large amounts of chemicals. In these materials, the delivery process is regulated by a simple diffusion process and, in general, it is very difficult to control the amount of delivered cargo. In the last years, the use of mesoporous materials functionalised with "**molecular gates**" has suffered a remarkable increase. A molecular gate can be defined as a supramolecular-based device attached onto the external surface of certain inorganic supports in which mass transport can be triggered by a target external stimulus that can control the state of the gate (open or closed) at will.[62] In gated

materials, the chemical features of the anchored molecule (polarity, conformation, size, charge, shape) can be modified on command upon the application of an external stimulus resulting in cargo release (see Figure 11). These gated materials are generally composed of two subunits: (i) a porous inorganic support in which cargo is entrapped and (ii) selected molecular and/or supramolecular entities (molecular gates), grafted onto the external surface, which controls mass transport from the pores to the solution in response to a certain stimulus.

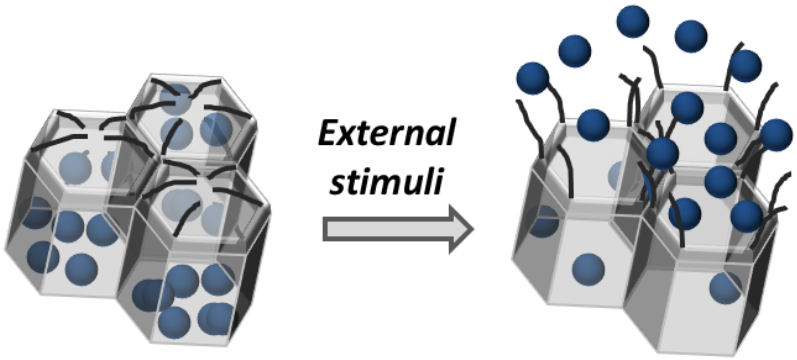

Figure 11. A schematic representation of a gated material. The scheme represents a mesoporous support loaded with certain guest molecules and with a suitable molecular ensemble anchored in the pore outlets (molecular gate). The application of an external stimulus allows the release of the entrapped cargo due to changes in the capping ensemble.

Since the first example of a molecular gate reported by Fujiwara and co-workers,[62a] gated materials have attracted great attention due to their potential applications for the controlled release of chemicals, with promising applications in the biomedical field,[63] and also in the development of new sensing/recognition paradigms.[64] Several molecular and supramolecular systems have been developed which can trigger the release of the entrapped cargo using several external stimuli such as pH,[65] changes in redox potential,[66] temperature[67] and the presence of certain ions, molecules or biomolecules.[68] The most widely used inorganic

support is mesoporous silica nanoparticles (MSNs). Dealing with the gating mechanism, electrostatic or supramolecular interactions, the rupture/formation of covalent bonds, or changes in the physical properties of molecules or macromolecules has been extensively used. Besides, different types of gatekeepers have been used such as polymers, supramolecular ensembles, inorganic nanoparticles, and biomacromolecules. Extensive reviews about gated materials have been published in recent years and give a comprehensive landscape of the work done so far.[69,70,71] Some examples of gated mesoporous silica nanomaterials classified according to the triggering stimuli are described below.

1.5.1 *Light-Sensitive Molecular Gates*

Mesoporous silica hybrid materials capped with light-responsive molecular gates were extensively studied because these nanodevices can be important in biomedical applications due to the fact that cargo release can be achieved only after irradiation with light of a certain wavelength. Since the first example of a molecular gate that used light as the triggering stimulus,[62a] several light-driven molecular gates have been reported.

In these systems, the photocleavage of chemical bonds, directly or assisted by photosensitizers, and photoinduced heating of gold nanostructures are the main mechanisms which induced gate opening. A simple and illustrative example of a light-driven molecular gate is depicted in Figure 12. The authors prepared MSNs loaded with $[Ru(bpy)_3]Cl_2$ and capped with a photo-cleavable bulky *o*-methoxybenzylamine derivative grafted onto the external surface of the support. Upon irradiation with UV light, the bulky group was cleaved allowing the diffusion of the dye to the solution.[72]

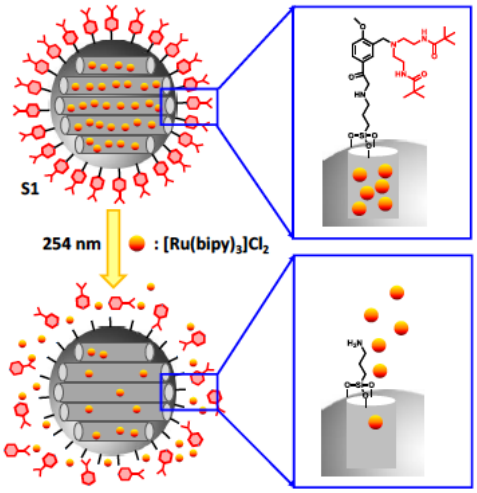

Figure 12. Schematic representation of light-driven gated material. Reprinted with permission from Chem. Eur. J. 2012, 18, 12218.

1.5.2 *Temperature-Sensitive Molecular Gates*

Temperature is also a physical stimulus that has been extensively used as an external trigger in the development of gated materials. The first temperature-driven nanodevice reported consisted of MSNs functionalized with the temperature-sensitive polymer, poly(*N*-isopropyl acrylamide) (PNIPAAm).[73] This polymer exhibits a hydrophilic–hydrophobic transition at a "lower critical solution temperature" (LCST) of about 32 °C in water. Below the LCST, the polymer is in the hydrated state and acquired a coil conformation while above the LCST get collapsed due to dehydration.

Temperature-triggered control of molecular transport through the porous network of the hybrid particles was demonstrated by measuring the release of fluorescein. The fluorescein was slowly released from the pores at room temperature and faster at 40 °C. Several gated nanosystems have been designed using different thermally responsive polymers.[74]

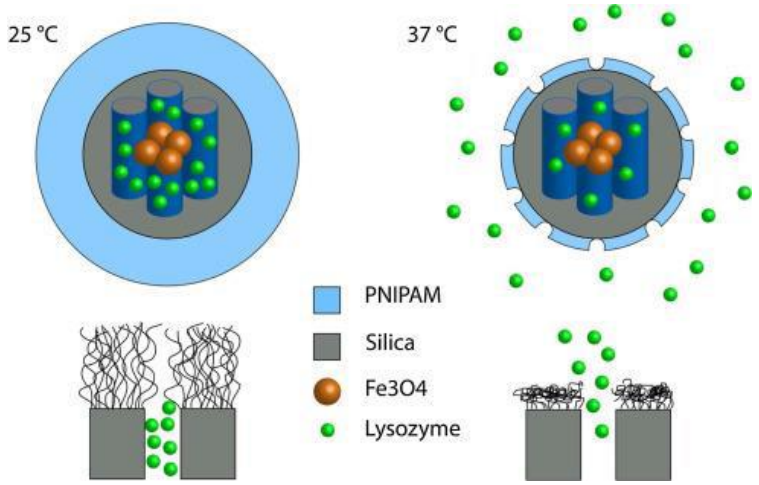

Figure 13. Schematic drawing of the temperature-responsive system based on core-shell nanoparticles loaded with lysozyme and capped with PNIPAM. Reprinted with permission from Colloids Surf. B, 2015, 135, 652. Copyright © 2015 Elsevier B.V.

Yu and co-workers used the same polymer to prepare a cargo delivery system by temperature changes able to release lysozyme.[75] In this respect, core-shell Fe_3O_4-MCM-41 nanoparticles were prepared and used as an inorganic scaffold. The particles were loaded with $[Ru(bpy)_3]Cl_2$ or lysozyme and later capped with PNIPAM for blocking the pore outlets. At room temperature (25 °C), the PNIPAM brushes were hydrated and expanded blocking the pores as depicted in Figure 13. At a physiological temperature (37 °C), an abrupt cargo release was observed due to the collapse of the brushes and the exposure of the pores to the medium. The material was applied as an antibacterial agent and a significant reduction in bacterial growth was observed due to the successful release of lysozyme.

Changes in the conformation of a peptide were also used for the development of a temperature-triggered gated nanosystem. In this respect, MSNs were loaded with safranin O and the external surface functionalized with a peptide which adopted an α-helix

conformation at room temperature. The presence of the bulky α-helix peptide onto the external surface inhibited safranin O release. Upon heating the α-helix conformation of the peptide changed to a disordered structure allowing safranin O release due to a reduction of the steric crowding around pore outlets (Figure 14).[76]

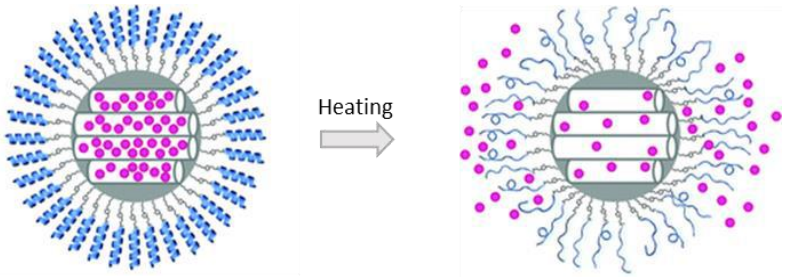

Figure 14. Schematic representation of the temperature-driven peptide-gated material. (Reprinted with permission from Chem. Commun., 2014, 50, 3184. Copyright ©The Royal Society of Chemistry 2014).

1.5.3 *pH-Driven Molecular Gates*

In these systems, the molecular gate structure changes with the pH of the solution due to the addition or abstraction of protons. These modifications in the gating ensemble, which controls the gating mechanism, can be a change of conformation, its rupture or attraction/repulsion interactions between its components. A large number of pH-responsive gated materials have been developed. As capping agents, researchers have reported the use of polyamines, different polymers, supramolecular ensembles, layer-by-layer coatings, biomolecules (like DNA or proteins), lipid bilayers and inorganic nanoparticles, among others.

For instance, Lee and co-workers prepared pH-responsive MSNs capped with a calcium phosphate layer.[77] First, MSNs were loaded with DOX and the system was closed by the enzyme-mediated formation of a calcium phosphate coating using hydroxyapatite and urea. At pH 7.4, the system remained capped, but DOX delivery

was remarkable at pH 4.5 due to the dissolution of the calcium phosphate layer under acidic conditions. The DOX-loaded nanoparticles were tested in cancer cells and marked cell death was observed due to the gradual release of DOX at the lysosomal pH.

Recently, Yang and co-workers reported pH-responsive MSNs using poly (2-dimethylaminoethy l methacrylate) (PDMAEMA) polymer as a capping agent. MSNs were first functionalized with 2-bromoisobutyryl bromide (BIBB) to later link PDMAEMA brushes. The system was then loaded with rhodamine 6G dye. At pH 7.4 no dye release was observed. However, marked dye delivery was observed upon lowering the solution pH to 2.0. The release was ascribed to electrostatic repulsions between the positively charged polymer chains that adopted an extended conformation with subsequent pore opening (Figure 15).[78]

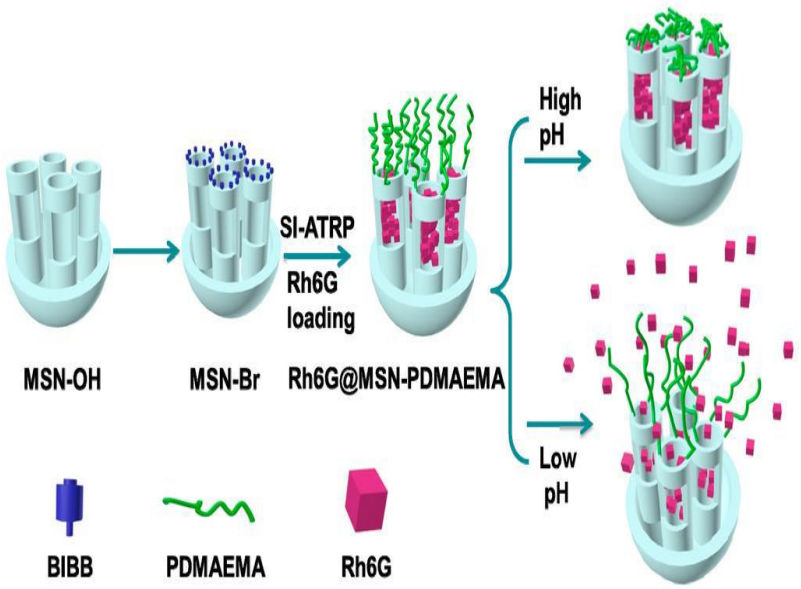

Figure 15. Schematic representation of a pH-driven gated solid based on the protonation of PDMAEMA polymer brushes. Reprinted with permission from Polymers 2016, 8, 277. Copyright © 2016 MDPI AG.

1.5.4 *Redox-Driven Molecular Gates*

The development of redox-driven molecular gates has been widely explored, mainly due to the biological relevance of redox agents and redox reactions. Most of the reported systems can be classified into two main categories:

- Those based on rotaxanes and pseudorotaxes where supramolecular ensembles between macrocycles (like cyclophanes, curcubiturils or cyclodextrins) and an organic chain anchored to the external surface of the porous scaffold control the open/close state of the gate
- Those based on disulphide-linked capping agents (eg. polymers or inorganic nanoparticles) that are detached by reducing agents like glutathione or DTT.[79] Interestingly, some of these systems are reversible which means that the gate can be opened and closed repeatedly by changing the redox conditions of the environment.

Figure 16 shows a prepared nanosystem for O_2 detection, the external surface of MSNs was functionalized with aminopropyl groups that were reacted with ferrocene carboxaldehyde. After loading the inner pores with Rh B, the final capped solid was obtained using bulk β-CDs.

The aqueous suspension solution of the nanoparticles did not release any dye when using gases such as N_2. While upon bubbling with O_2, the entrapped dye starts to release where ferrocene moieties were oxidized to ferrocenium. This resulted in a decrease in the attraction between ferrocene moieties and β-CDs. [80]

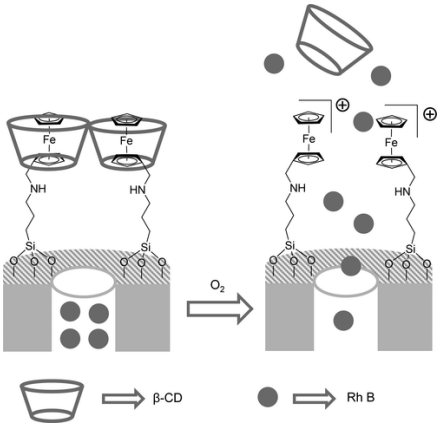

Figure 16. Nanometric silica mesoporous support is loaded with Rh B and capped with the interaction between β-CDs and ferrocene. The oxidation of ferrocene groups by oxygen results in the release of the dye. with permission from ACS Copyright © 2016.

1.5.5 *Magnetically Driven Molecular Gates*

The use of magnetic fields as an external stimulus for the development of gated MSNs has been also reported. Normally, these nanodevices used Fe_2O_3 as a magnetic core surrounded by a mesoporous silica shell. The application of an alternating magnetic field leads to local heating of the nanoparticles followed by cargo release. The importance of these systems in biomedical applications comes from the possibility of guiding these materials to certain tissues with an external magnet and inducing the delivery of the entrapped cargo only at the selected site.

An example of these nanodevices was reported by Stroeve's group where they developed a magnetic-responsive delivery system using iron oxide nanoparticles coated with a mesoporous silica shell, loaded with methylene blue and capped with a thermal responsive lipid bilayer as the molecular gate (Figure 17). The applications of an alternating magnetic field (50 Hz, 1570 G) lead to cargo release in aqueous suspensions of the nanoparticles. The response was ascribed to an increase in the permeability of the

lipid bilayer due to the vibration of the particles upon application of the alternating magnetic field as well as to an increase in the temperature of the nanoparticle that partially disrupted the bilayer. This was confirmed by studying the release of nanoparticle suspensions at 50 °C, which resulted in a massive delivery in short times. [81]

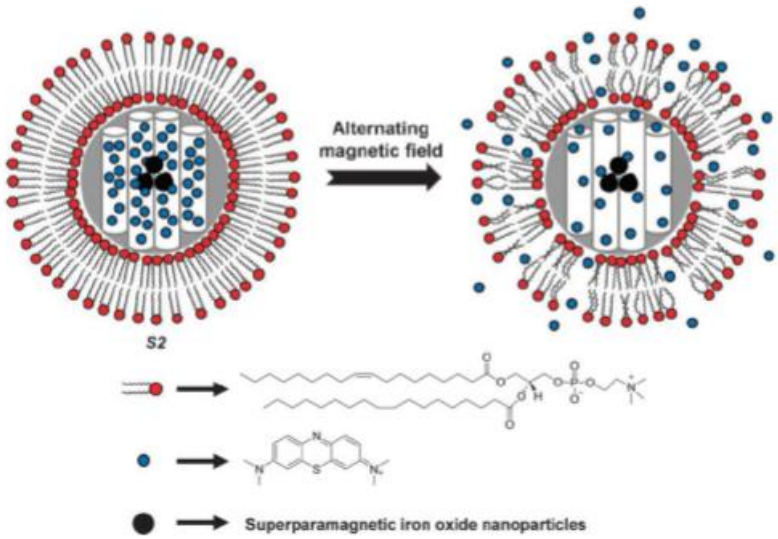

Figure 17. Schematic drawing of the core-shell nanoparticles capped with a lipid bilayer for controlled delivery by an external magnetic field. Copyright © 2012 The Royal Society of Chemistry. with permission from ACS Copyright © 2016.

1.5.6 *Small Biomolecules Driven Molecular Gates*

Several mesoporous capped silica nanosystems have been prepared to deliver the inside cargo in the presence of certain biomolecules such as a specific antigen,[82] and RNA messenger. An example was reported by Xu and co-workers using mesoporous silica nanoparticles coated with a double-stranded DNA fragment with high specificity to Survivin mRNA.[83] The loaded material with anticancer drug DOX was functionalized on the external surface using aminopropyl moieties that later reacted with a double-

stranded DNA sequence as illustrated in figure 18. The electrostatic interactions with the protonated amino groups and double-stranded DNA prevent the inner cargo from being released as illustrated in Figure 18. This double-stranded DNA was formed between a long sequence with high recognition element to Survivin mRNA containing FITC in the other end. While the second strain was a short oligonucleotide functionalized with 7-amino-4-methylcoumarin (AMCA) dye. The fact that using FITC and AMCA were used to monitor the release of the cargo by controlling the changes in fluorescence through of FRET process between these two dyes. The prepared nanomaterials when suspended in buffer solution buffer (20 mM Tris-HCl, 37.5 mM $MgCl_2$ at pH 7.5), no DOX was released to the outer solution. As well excitation of AMCA at 353 nm, results in a dual emission with bands at 450 (from the AMCA) and 520 nm (from the FITC acceptor), this indicates that both the two dyes as close enough which mean that the two strain are held together. While the addition of Survivin mRNA cause the release of DOX and a decrease of the em the emission band at 520 nm, this change in the emission was ascribed to removal of FRET between AMCA and FITC. The added Survivin mRNA selectively hybridized with the long DNA sequence which distributed the blocker gate and led to the separation of the two dyes and changes in emission. The prepared nanodelivery system was found to enter myeloblastic leukemia (HL-60) cell's cytoplasm after and deliver DOX in accordance with the concentration of Survivin mRNA inside the cells.

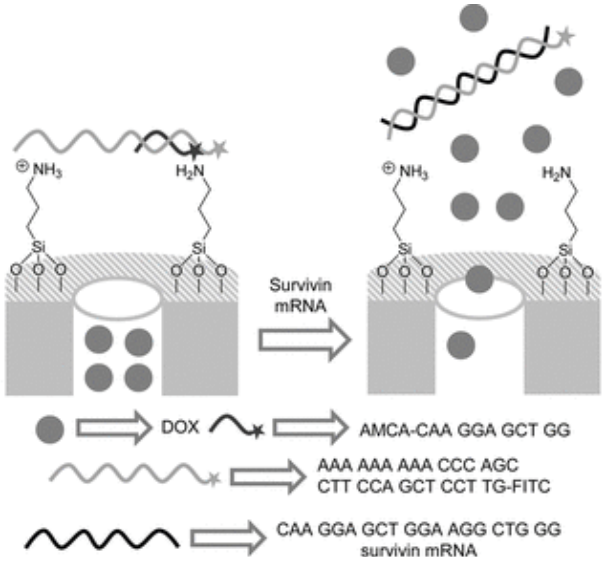

Figure 18. MSNs loaded with DOX and capped with double-stranded DNA. Addition of surviving mRNA induced cargo release. with permission from ACS Copyright © 2016.

1.5.7 *Enzyme Driven Molecular Gates*

Using enzymes as the trigger to uncape gated nano delivery systems is promising to prepare on-demand controlled release systems due to the high selectivity functions known for enzymes even in complex biological environments. For instance, enzyme overexpression in a certain disease has been used to prepare selective capped systems able to be open in a specific cell type. That means a significant reduction of undesirable side effects and a large increase in the effectivity of the drug delivered. Several enzymes have been used as the trigger such as esterases, glycosidases, peptidases, reductases, and DNases. The most used mechanisms were the hydrolysis of ester and phosphodiester groups, [84] hydrolysis of glycosidic linkages,[85] hydrolysis of amide groups, [86] hydrolysis of phosphodiesters[87], elongating DNA sequences[88] and rupture of azo bonds. [89]

For instance, Zhu and co-workers prepared nanodelivery system using mesoporous silica nanoparticles coated with modified oligodeoxynucleotide while the delivery was triggered by α-chymotrypsin.[90] The hollow MSNs, which were loaded with fluorescein and the surface were functionalized with 3-aminopropyl to form a partially positively charged surface. Then particles were coated with a layer-by-layer mechanism (LbL) composed of negatively charged cytosine-phosphodiester-guanine oligodeoxynucleotide and positively charged poly(L-lysine) polymers as shown in Figure 19. The authors found that upon α-chymotrypsin addition, the poly(L-lysine) polymer was degraded, which led to the disassembly of the capping unit and induced the release of the entrapped dye and oligodeoxynucleotide.

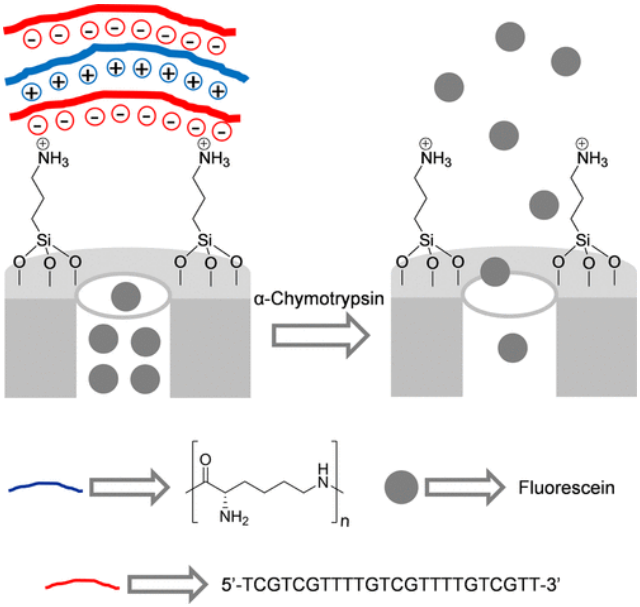

Figure 19. α-Chymotrypsin-induced controlled release of fluorescein from MSNs coated with cytosine-phosphodiester-guanine oligodeoxynucleotide and poly(l-lysine) polymers.

1.6 Silica Mesoporous Gated Materials in Sensing Applications

Most of the mesoporous silica hybrid materials reported were used for on-command delivery applications in the presence of different physical or (bio)chemical stimuli. However, in the last years, the possibility of using these materials, capable of responding specifically to a certain target molecule, as a suitable method for developing new protocols for sensing applications has been described.[91] In these protocols, the main idea relay on the coordination or reaction of a target analyte with the binding sites in the capping ensemble could lead to a release of a dye/fluorophore from pores to the solution and will result in a chromo-fluorogenic signal. Two possible mechanisms can be envisioned (see Figure 18). In the first mechanism, the pore remained opened and the indicator can diffuse into the solution, whereas in the presence of a target analyte this molecule or ion can bind to receptors (grafted onto the external surface of the loaded nanoparticles) and close the gate. In the second mechanism, the starting material is capped, and the presence of a target analyte induces pore opening and dye/fluorophore delivery. One of the advantages of both approaches is the presence of amplification features. In this respect, the presence of few analyte molecules induced the inhibition or the release of a relatively high amount of dye/fluorophore entrapped in the inner of the pores with the subsequent signal amplification.

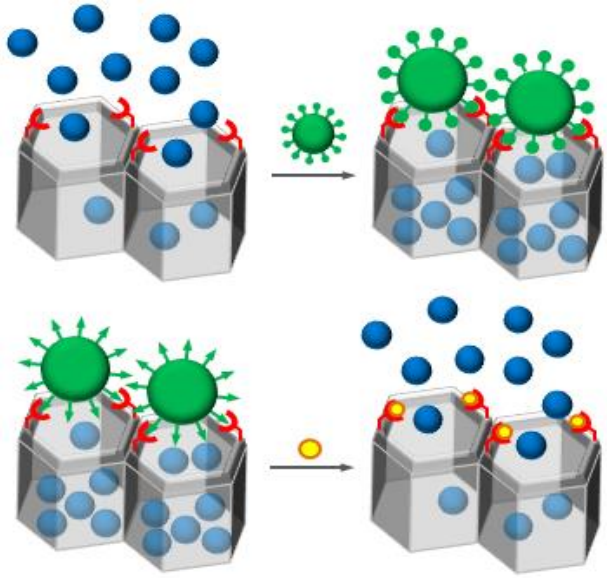

Figure 20. Scheme of the recognition paradigm using nanoscopic gate-like scaffoldings. Up: inhibition of dye release due to the coordination of the selected analyte with the anchored binding sites. Down: uncapping pores by an analyte-induced displacement reaction. Adapted from Acc. Chem. Res., 2013, 46, 339.Copyright © 2013, American Chemical Society.

The first example of a gated mesoporous material used in sensing protocols as described in 2006.[92] The authors reported MCM-41 mesoporous silica microparticles loaded with $[Ru(bpy)_3]^{2+}$ dye as an indicator and with polyamines grafted onto the external surface of the scaffold (see Figure 20). At pH 7.8 the dye was released into the solution because the polyamines are protonated adopting an open conformation. However, the presence of ATP and ADP allowed to selectively inhibit the indicator released by the formation of strong complexes with tethered polyamines through hydrogen bonding and electrostatic interactions. Other anions (such as chloride, sulfate or GMP) are too small or form weak complexes to effectively close pores and they cannot stop the $[Ru(bpy)_3]^{2+}$ dye from leaching.

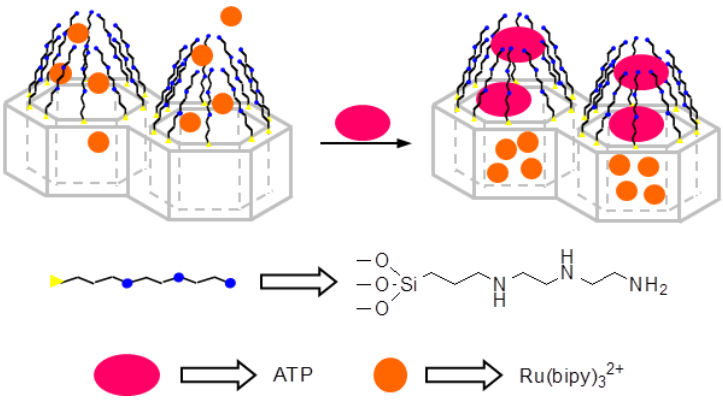

Figure 21. Schematic representation of ATP recognition by inhibiting dye release with nanoscopic supramolecular gate-like systems on mesoporous MCM-41.

Other example based on the open-closed protocol was developed for the detection of borate (Figure 22). The authors used the well-known reaction between polyalcohols and borate anion to form boronate esters as capping mechanims. They prepared MCM-41 silica particles loaded with $Ru(bpy)_3^{2+}$ dye and functionalized with a saccharide derivative on the external surface.[93]

The system was found to detect the presence of borate at pH 7.0 by inducing pore closure and inhibiting dye delivery. Pore closure was produced after the formation of boroesters through the reaction of borate with the hydroxyl moieties of the anchored saccharides. The sensing behaviour was studied and found to be very selective for borate over several anions (e.g. CO_3^{2-}, SO_4^{2-}, Cl^-, Br^-, NO_3^-, PO_4^{3-}) or cations (e.g. Al^{3+}, Cu^{2+}, Fe^{3+}, Na^+, K^+, and Ca^{2+}) tested. By using this simple detection protocol, a limit of detection for borate of 70 ppb in HEPES (pH 7.0) was measured.

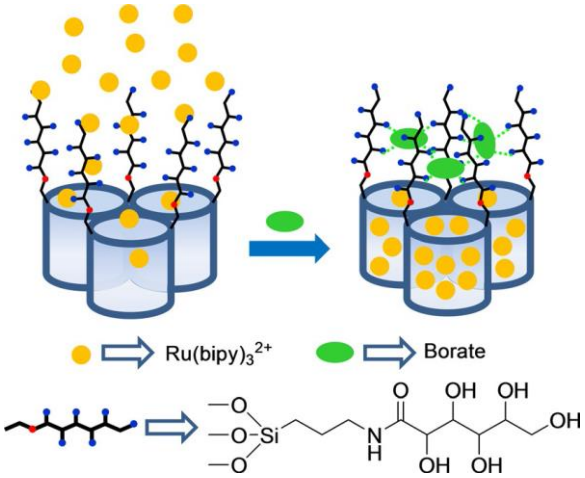

Figure 22. Silica mesoporous support functionalized with polyalcohols for the detection of borate.

The above two examples are based on the "on-off" sensing protocol in which the starting material is uncapped and later the pores are capped in the presence of the target analyte. In contrast to this approach, in "off–on" sensing systems, the starting material is capped and can be opened in the presence of target analytes. An example of the detection of anions using this protocol was reported in 2012 by Tang and co-workers. These authors used aptamer-containing gold nanoparticles as caps (Figure 23).[94] For this purpose, the external surface of MSNs was decorated with amino groups and, in a further step, adenosine-5'-carboxylic acid moieties were grafted, and the pores loaded with fluorescein isothiocyanate. On the other hand, the external surface of gold nanoparticles was decorated with the ATP aptamer 5'-CCT GGG GGA GTA TTG CGG AGG AAG GTT-SH-3' by forming Au-S bonds. The final material was obtained by capping the pores of the loaded support with aptamer-functionalized gold nanoparticles. PBS (pH 7.4) suspensions of the capped solid showed negligible dye leaching, whereas the presence of ATP triggered the release of the

reporter. The uncapping process was ascribed to the selective coordination of gold nanoparticles from the solid surface with ATP.

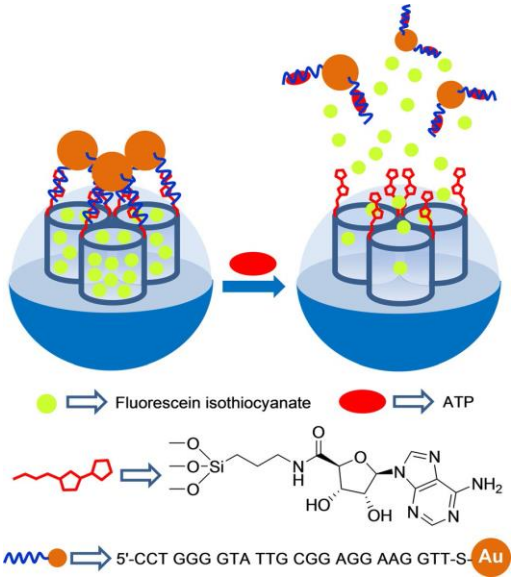

Figure 23. Silica Nanometric silica mesoporous support loaded with fluorescein isothiocyanate and capped with ATP aptamer containing gold nanoparticles for the detection of ATP.

Recently, El Sayed and co-workers reported another "off–on" sensing system for the detection of cyanide. MSNs were loaded with $[Ru(bpy)_3]Cl_2$ dye and its external surface was functionalised with a macrocyclic nickel(II) complex. Finally, pores were capped upon the addition of hexametaphosphate, a sterically hindering anion. As shown in Figure 24, in the absence of cyanide the release was negligible due to pore blockage by the bulky hexametaphosphate anion. In contrast, the addition of cyanide induced demetallation of nickel(II) complexes and the removal of the capping hexametaphosphate anion from the silica surface. As a consequence, a marked enhancement in emission was observed due to the release of $[Ru(bpy)_3]Cl_2$ dye. The system was selective toward cyanide with a limit of detection of 2 μM.[95]

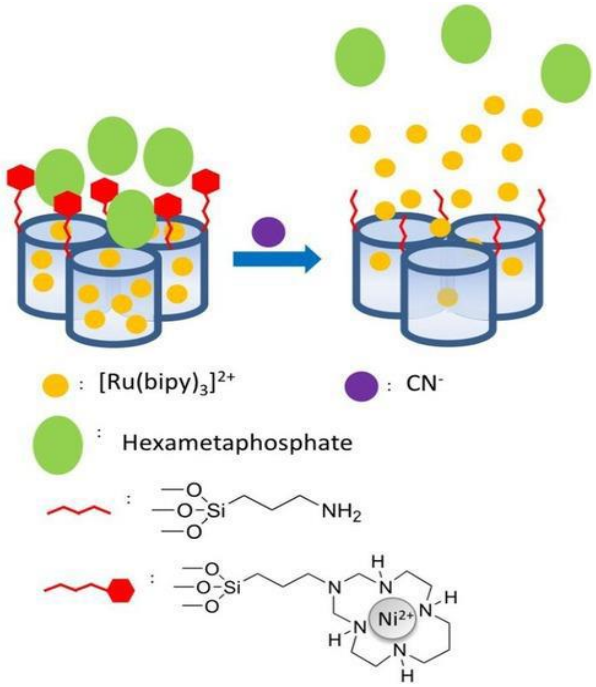

Figure 24. Schematic representation of a gated material for cyanide recognition using a supramolecular complex as the gating ensemble. Reprinted with permission from Chem. Asian J. 2017, 18, 2670. Copyright © 2017 Wiley-VCH.

There are a few examples of capped mesoporous silica nanoparticles designed for the detection of small cations.[96,97,98] The first reported example was designed to sense the presence of CH_3Hg^+.[99] More recently, Zhang and co-workers designed DNA-capped MSNs for the detection of Hg^{2+} cation. In this respect, MCM-41 MSNs were loaded with rhodamine 6G dye and functionalized with isocyanate moieties. Then, pores were capped upon the addition of an amino-modified oligonucleotide strand.[100] The grafted oligonucleotide and its complementary strand (5'- GTT GTT CTT CCT TTG TTT CCC CTT TCT TTG GTT GTT CTTC-3') were able to cap the pores of the material. The authors used an oligonucleotide strand that is very rich in thymine groups which

have a high affinity to Hg^{2+}. In presence of this ion, the thymine-rich strand was displaced from the surface due to the formation of the corresponding Hg^{2+}–aptamer complex, which resulted in dye delivery as shown in Figure 25. The system was able to detect Hg^{2+} in water with a limit of detection of 4 ppb and with high selectivity over other interfering cations (Ni^{2+}, Pd^{2+}, Fe^{2+}, Fe^{3+}, Ba^{2+}, Zn^{2+}, Ca^{2+}, Mg^{2+}, Cu^{2+}, Co^{2+} and Cd^{2+}).

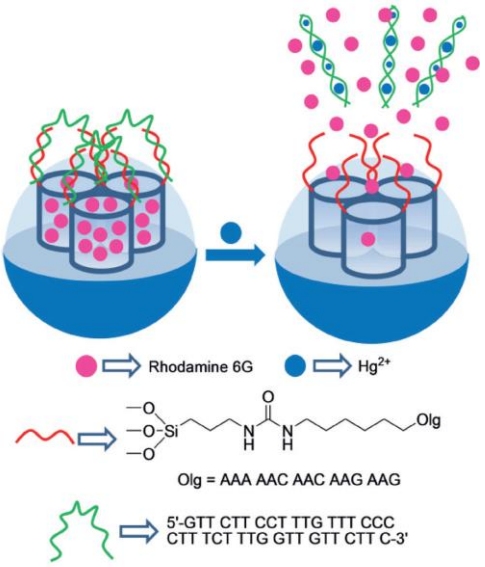

Figure 25. Schematic representation of silica mesoporous support capped with aptamers for the detection of Hg^{2+} cation.

Furthermore, capped MSNs were used for the selective detection of several small neutral compounds such as glucose,[101] nerve agent simulants,[102] sulfathiazole,[103] brevetoxin B,[104] aflatoxin B1[105] and adenosine.[106] Lu and co-workers developed gated MSNs for the detection of glucose. For this purpose, the external surface of MSNs was functionalized with prop-2-in-1-yl(3-(triethoxyxilyl)propyl) carbamate.[107] Then pores were loaded with rhodamine B and the glucose oxidase enzyme (GOx) inhibitor d-(+)-glucosamine was grafted onto the external surface by a click

chemistry reaction. Finally, pores were capped with GOx enzyme, through the formation of a complex with inhibitor d-(+)-glucosamine (Figure 26). A negligible rhodamine B release, in PBS suspensions of the capped material, was observed. However, in the presence of glucose, a marked dye delivery was produced. The observed release, which was proportional to the amount of glucose added, was the result of a displacement reaction of GOx from the pore outlets due to the formation of the corresponding glucose–GOx complex. The uncapping protocol was highly selective and other tested monosaccharides (i.e., fructose, mannose, and galactose) induced negligible dye release.

Figure 26. Schematic silica mesoporous support representation for the detection of glucose.

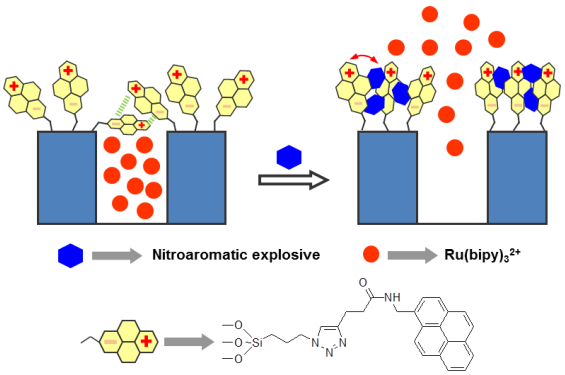

Figure 27. Schematic representation of a gated material for the detection of nitroaromatic explosives. Adapted from J. Mater. Chem. A., 2013, 1, 3561. Copyright ©Royal Society of Chemistry.

Other "off-on" gated MSNs have also been used for the detection of neutral molecules such as nitroaromatic explosives.[108] For this purpose, MCM-41 particles were selected as an inorganic scaffold and then the pores were loaded with $Ru(bpy)_3^{2+}$ dye. Then, the external surface was functionalized with a pyrene derivative using a click chemistry reaction (Figure 27). The presence of a dense pyrene network around the pore outlets inhibited dye delivery. However, upon addition of nitroaromatic explosives (Tetryl and TNT), a massive dye release was observed due to pore opening as a consequence of the formation of strong pyrene (electron donor)-nitroaromatic explosives (electron acceptor) charge-transfer interactions. This material was used for the detection of explosives in soil samples with fine results.

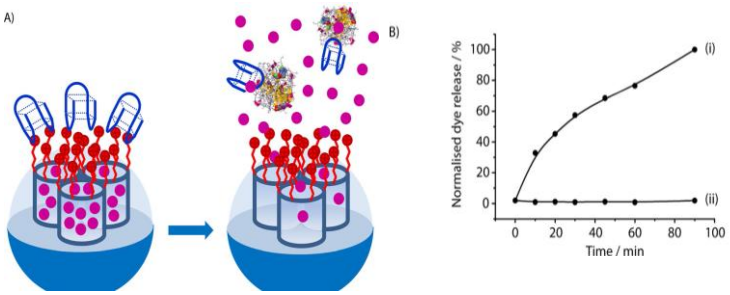

Figure 28. Schematic representation of a gated silica mesoporous material loaded with rhodamine B and capped with thrombin binding aptamer for the detection of thrombin. B) Release profile of rhodamine B from the capped solid in the presence (i) and the absence (ii) of thrombin.

Several biomolecules such as DNA,[109] oligonucleotides[110] and nucleic acid biomarkers were also detected using capped MSNs.[111] For instance, an aptamer-gated nanoparticle to detect thrombin has been developed**.** As shown in Figure 28 the authors used MSNs loaded with dye rhodamine B and with the external surface functionalized with 3-aminopropyl moieties. Finally, pores were capped after the addition of the 15-mer thrombin-binding aptamer 5'-TTT TTTGGTTGGTGTGGT TGG-3' (TBA) through electrostatic interactions. In the presence of thrombin, TBA forms a complex with this biomolecule and the entrapped reporter was delivered. A limit of detection for thrombin of 2 nm in blood serum was reported. Besides, a good selectivity was obtained because other proteins, such as ovalbumin and BSA, were unable to induce pore opening.[112]

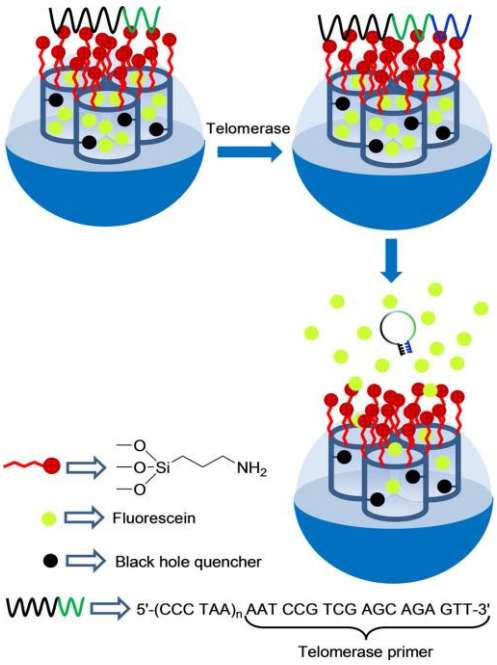

Figure 29. Nanometric silica mesoporous support capped with DNA for the detection of telomerase activity.

Ju and co-workers successfully developed a telomerase-responsive gated system for the sensitive and in situ tracking of the activity of this enzyme in living cells (Figure 29).[113] In their work, MSNs were loaded with fluorescein, functionalized with amino groups on the external surface and capped with DNA sequence 5'-$(CCCTAA)_n$ AATCCG TCGAGC AGAGTT-3', which contains a telomerase primer. In the presence of telomerase and deoxynucleoside triphosphate monomers (dNTPs), the oligonucleotide sequence was extended and formed a rigid hairpin-like DNA structure to allow entrapped fluorescein release. The telomerase-driven response was studied by incubating the enzyme, dNTPs, and capped nanoparticles, and by monitoring fluorescein release by fluorescence and UV/Vis spectroscopy. A gradual increase in fluorescein emission intensity with a prolonged

incubation time and increasing the concentration of telomerase was observed. An extended *in vitro* study on HeLa cells using gated nanoparticles was carried out. They concluded that nanodevice was activated by the action of intracellular telomerase and suggested that it could be used for tracking intracellular telomerase activity and distinguishing between cancer cells and normal cells.

1.7 Mesoporous Silica for Antimicrobial Delivery

Due to remarkable features of MCM-41 mesoporous silica materials (such as high surface area, high pore volume, easy preparation and knowing functionalization methodologies) these supports are ideal candidates to be loaded with antimicrobials for the treatment of bacterial infections.[114]

On the other hand, in recent years, the unjustified and continued use of antibiotics has forced bacteria to develop resistance to common antibacterial drugs.[115,116] In this respect, in 2016, the European Food Safety Authority (EFSA) conducted a study that demonstrates an increased resistance to certain antibiotics in *Salmonella*, *Campylobacter, Escherichia coli*, and *Staphylococcus aureus* bacteria.[117] In addition to this acquired resistance, bacteria have an innate self-defence mechanism that consisted of biofilm formation.[118] As a consequence, it is necessary to increase the dose and frequency of the treatments with antibiotics to be effective. This increase in the antibiotic dose can lead to enhanced resistance and hard side effects due to the high doses administered.[119] As a result, there is a current need for more effective paths to the early detection and treatment of bacterial infections. Numerous efforts are being made to find alternatives such as the use of predatory bacteria,[120] bacteriophages,[121] probiotics and prebiotics.[122]

Very recently, several research groups developed nanomaterials to improve and increase the antimicrobial effect and overcome resistance formation. These studies showed that when nanomaterials are in contact with the bacteria, they can disrupt the bacterial cell wall, inducing toxicity due to a simple matter of size. Recently, there are increasing interest in the development of hybrid nanomaterials for the on-command release of antibiotics.[123] Liposomes,[124] polymeric nanoparticles,[125] and mesoporous silica materials are some of the most common nanocarriers that are used for this purpose.

Mesoporous silica materials, due to their high surface area and pore volume, have been used as reservoirs of antimicrobials.[126] It has been demonstrated that loading antibiotics onto MSNs can improve the effectiveness of the drug. Several examples have been reported as an antibiotic delivery system combining controlled release features with the strong antibacterial properties presented by certain metals such as copper, silver, nickel, and zinc.[127]

For example, in 2009 Zink and co-workers reported their findings on the antibacterial effect of silver nanocrystals encapsulated in MSNs.[128] According to their results, the silica coating reduced the hydrophobicity of the silver nanocrystals, decreasing their aggregation without compromising the oxidation of the silver crystals that were slowly released in the medium. To study the antimicrobial efficacy of the nanoparticles, two different experiments were performed against two types of bacteria; Gram-positive *Bacillus anthracis*, and Gram-negative *E. coli*. It was observed that the presence of the Ag-coated nanoparticles in the agar prevented the formation of colonies of both types of bacteria. On the other hand, in 2017, Zhou and co-workers used silver-decorated MSNs loaded with chlorhexidine against *S. aureus* and *E.*

coli (Figure 29).[129] The combined treatment against both bacteria were more effective than $AgNO_3$ or chlorhexidine separately. Also, it was found that the biocompatibility of the system was enhanced when compared to that of free chlorhexidine or silver ions.

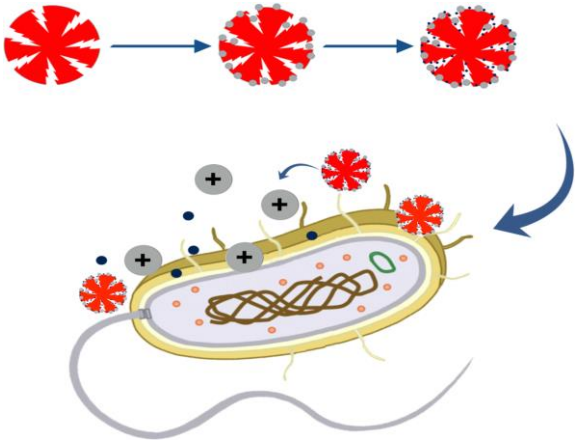

Figure 29. Schematic representation of the mode of action of Ag-MSNs loaded with chlorhexidine.

One of the main challenges in nanomedicine is to achieve selective treatment, acting exclusively on the target area, without affecting healthy tissues, thus reducing the side effects of the drugs. This landmark can be achieved using gated nanodevices. In this respect, several examples of antibiotics delivery systems using gated mesoporous silica materials that open by pH, temperature changes, and the presence of specific toxins or proteins have been reported recently.[130, 131, 132]

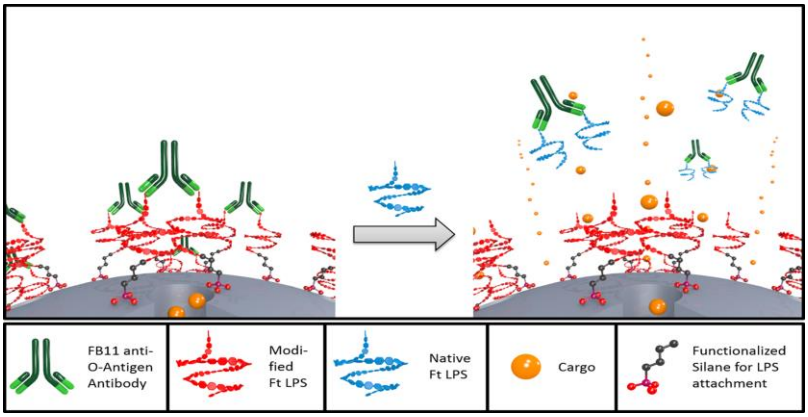

Figure 30. Schematic representation of the triggered release of cargo (orange spheres) loaded into pores due to a competitive displacement of the antibody (green) that caps the pore by naturally occurring *Francisella tularensis* LPS (blue).

For instance, Zink and co-workers prepared a *Francisella tularensis* bacteria detection and delivery system.[133] As illustrated in figure 30, the pores of MCM-41 nanoparticles were loaded with the cargo then the external surface was functionalized using a modified Ft-LPS. The final nanoparticle's external surface was blocked by FB11, an antibody with a high affinity to lipopolysaccharide (LPS) that is present in the *F. tularensis* bacteria wall. The interaction between an FB11 and the modified Ft-LPS blocked the internal cargo from release. In the presence of this pathogen, FB11 interact with native LPS on the bacteria cell wall. This causes pore opening and payload release. The authors used a dye to incubate the *F. tularensis* with the nanoparticles and compared the fluorescence levels after 1 h. They observed that only the presence of *F. tularensis* resulted in an increase in fluorescence. However, the presence of interferent pathogens such as *Francisella novocida* resulted in negligible changes. This indicates the high selectivity of these nanoparticles to detect *F. tularensis* bacteria.

In another example, MCM-41 type MSNs were loaded with the antibiotic vancomycin and the external surface functionalized with the negatively charged *N*-[(3-trimethoxysilyl) propyl] ethylendiaminetriacetate group.[134] Then, the pores were capped by the addition of ε-poly-L-lysine (ε-PL) cationic polymer (Figure 31). The interaction of this nanomaterial with different Gram-negative bacteria (*E. coli* 100, *E.coli 405*, *S. typhi* and *E. carotovora*) was studied. The authors report a remarkable enhancement of the antimicrobial effect of the prepared nanomaterial when compared with free vancomycin. This enhancement of vancomycin toxicity to Gram-negative bacteria was attributed to the interaction of the positively charged nanoparticles with the bacteria. As a consequence of this interaction the capping ε-PL (which binds to the cell wall) was detached inducing bacterial wall damage. Also, the entrapped vancomycin was released and internalized by bacteria. These capped mesoporous nanoparticles may be suitable platforms for the design of smart antimicrobial nanodevices for a wide range of applications.

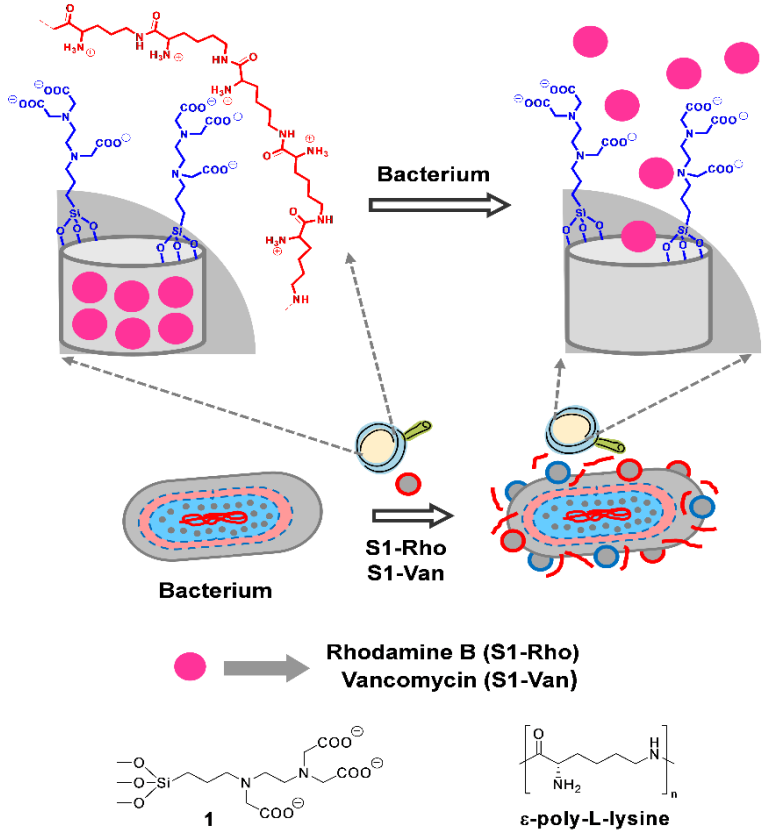

Figure 31. Schematic representation of the action mechanism of the prepared vancomycin loaded MCM-41 in the presence of bacteria.

On the other hand, several studies have demonstrated that loading an antimicrobial agent onto silica pores can reduce biofilm formation since the release of the drug eliminates the surrounding bacteria and their adhesion to the surface of the material.[135,136,137]

Chapter 2: Objectives

Objectives

The main objective of this Ph D thesis is the synthesis, characterization, and evaluation of several nanodevices for biochemical applications as therapeutic agents and sensing systems.

The specific objectives are:

- To develop and evaluate a nanodevice using polymyxin B-gated nanoparticles can fluorogenic detects selectively endotoxin in aqueous solution with a limit of detection in the picomolar range which could be sever for the development of an easy-to-use and rapid kit to detect endotoxin in contaminated environmental samples and doesn't need for special sample preparation like in common kit.
- To design and evaluate a nanodevice based-on curcumin-capped mesoporous silica nanoparticles for the fluorogenic detection of human serum albumin to use it for the sensitive detection of HSA in buffered aqueous solution and in artificial urine as a base to develop a rapid and easy method to use in biomedical applications.
- To explore the beneficial effects of combined linezolid and polymyxin B antibiotic treatment using capped mesoporous nanoparticles in gram negative and positive bacteria. The combined nanosystem can be used to increase the efficient delivery of linezolid gram-positive antibiotic thanks to a synergetic effect with gram negative antimicrobial Polymyxin B in both types of bacteria.

Chapter 3: Simple Endotoxin Detection Using Polymyxin B-Gated Nanoparticle

Simple Endotoxin Detection Using Polymyxin B-Gated Nanoparticles

Ismael Otri,[a,b] Dr. Sameh El Sayed,[a,b] Serena Medaglia,[a,b] Prof. Ramón Martínez-Máñez,[a,b,c]* Dr. Elena Aznar,[a,b]* and Prof. Félix Sancenón[a,b,c]

[a] Instituto Interuniversitario de Investigación de Reconocimiento Molecular y Desarrollo Tecnológico (IDM), Universitat Politècnica de València, Universitat de València. Universitat Politècnica de València, Camino de Vera s/n, 46022, Valencia, Spain.

[b] CIBER de Bioingeniería, Biomateriales y Nanomedicina (CIBER-BBN), Spain.

[c] Departamento de Química, Universitat Politècnica de Valencia, Camino de Vera s/n, 46022, Valencia, Spain.

* Correspondence: elazgi@upvnet.upv.es(E.A.); rmaez@qim.upv.es (R.M.-M.).

Received: December 20, 2018

published: 28 January 2019

Chemistry – A European Journal, **2019**, 25, 3770-3774

Keywords

Endotoxin, Polymyxin B, mesoporous silica nanoparticles, gated materials and fluorogenic detection**.**

My contribution

I performed nanoparticle system design, synthesis, and *in vitro* experiments. I also contributed to the experimental design, data analysis, discussion, and writing.

Graphical Abstract

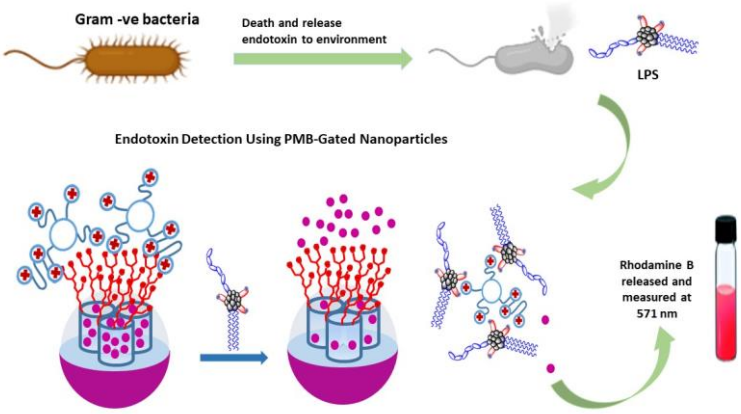

3.1 Abstract

A nanodevice based on mesoporous silica nanoparticles with rhodamine B in the pore framework, functionalised with carboxylates on the outer surface and capped with the cationic polymyxin B peptide was used to selectively detect endotoxin in aqueous solution with a limit of detection in the picomolar range.

3.2 Introduction

Endotoxin, also known as lipopolysaccharide (LPS), is one of the major components of the outer membrane of gram-negative bacteria.[1] Endotoxin is composed of variable polysaccharide chains attached to a phosphorylated glucosamine disaccharide decorated with multiple fatty acids.[2] Gram-negative bacteria, after their death, release this highly stable molecule to the surrounding environment.[3,4] Exposure to endotoxin contaminated environments (water or air) can lead to the development of several health problems such as pulmonary inflammation, respiratory difficulties, asthma, diarrhea, vomiting and fever.[5] Several methods for the detection of endotoxin in environmental samples have been developed.[6] Among them, the Limulus amebocyte lysate (LAL) test is one of the most widely used for endotoxin quantification. However, this test suffers several drawbacks such as false positive readings (by pectic polysaccharides and β-(1,3)-D-glucan),[7-9] is highly affected by temperature and pH changes, requires sample preparation procedures, and the use of controlled experimental conditions.[10] Taking into account the above mentioned facts, the development of reliable, accurate and easy to use sensing methods for endotoxin detection is an issue of interest. In this scenario, optical chemosensors,[11-14] gold nanoparticles,[15] iron oxide-gold

nanoflowers[16] or graphene quantum dots[17] have been explored as alternatives to classical methods for endotoxin sensing.[18]

From another viewpoint, there is an increasing interest in the design of gated porous nanomaterials for sensing and recognition protocols.[19,20] These nanomaterials are composed by a porous inorganic support (usually mesoporous silica) designed in such a way that dye release from the pores is selectively observed only when the target analyte is present. To achieve this functionality, the external surface of the loaded inorganic support is functionalized with molecular or supramolecular entities that inhibit dye delivery. However, in the presence of the analyte, the pores open due to the interaction of the analyte with the capping ensemble leading to cargo release.[21-26] One of the advantages of these solids is the potential existence of amplification features as few analyte molecules may trigger gate opening and induce the release of a high amount of entrapped dye molecules.

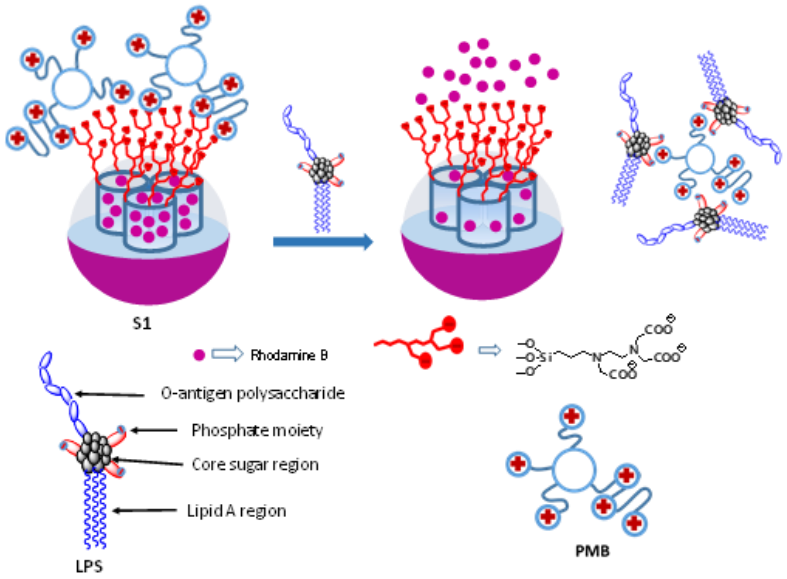

Scheme 1. Representation of the performance of the capped solid **S1** able to detect the presence of endotoxin.

Given our interest in exploring the potential use of gated nanomaterials in sensing protocols, we report herein a new nanodevice based on mesoporous silica nanoparticles (MSNs) functionalized with carboxylate moieties and capped with the cationic peptide polymyxin B for the selective and sensitive detection of endotoxin. The proposed recognition paradigm is depicted in Scheme 1. MSNs are selected as inorganic porous support. The pores of the nanomaterial are loaded with the rhodamine B fluorophore (as reporter) and the outer surface of the rhodamine B-containing nanoparticles is functionalized with carboxylates and finally capped with polymyxin B. Polymyxin B contains two separated lipophilic and hydrophilic domains. The lipophilic domain of polymyxin B is known to shows a very strong affinity for the disaccharide decorated with fatty acids of the endotoxin molecule. In fact, polymyxin B is used in the treatment of gram-negative bacterial infections.[27] In our system, a selective displacement of polymyxin B and rhodamine B release in the presence of endotoxin is expected to occur. To our knowledge, this is the first polymyxin B-capped hybrid nanomaterial used for the fluorogenic detection of endotoxin.

3.3 Experimental section

Mesoporous silica nanoparticles (MSNs) were synthesized according to a described procedure which uses the structure-directing agent *n*-cetyltrimethylammonium bromide (CTAB) and tetraethylorthosilicate (TEOS) as silica source.[28,29] The pore framework of the material was loaded with the fluorescent molecule rhodamine B. In a subsequent step, the external surface was functionalized with *n*-[(3-trimethoxysilyl)propyl] ethylene diamine triacetic acid. Then, pores of the nanoparticles were

capped, through electrostatic interactions, upon addition of the polymyxin B cationic peptide. Finally, nanoparticles were washed with PBS to remove the rhodamine B adsorbed in the outer surface to obtain the final material (solid **S1** in Scheme 1).

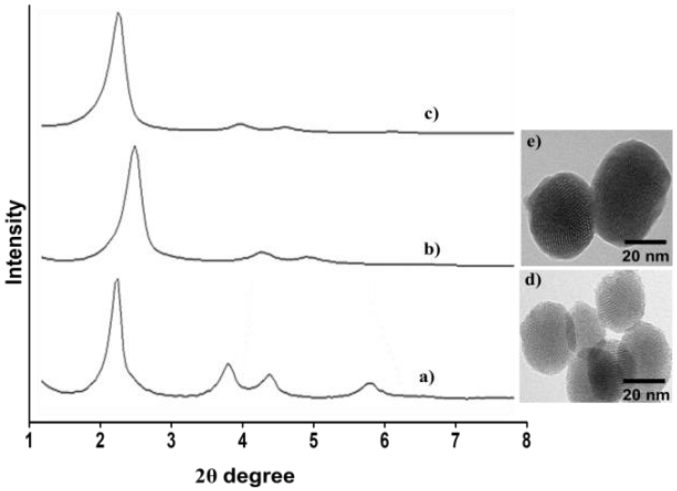

Figure 1. Left: PXRD patterns of (a) mesostructured silica nanoparticles (as-made MSNs), (b) calcined mesoporous nanoparticles and (c) solid **S1**. Right: Representative transmission electron microscopy images of (d) calcined MSNs and (e) solid **S1**.

The starting MSNs (as synthesized and calcined) and **S1** solid were full characterized. Transmission electron microscopy (TEM) and powder X-ray diffraction (PXRD) studies of the nanoparticles confirmed the mesoporous structure of the materials (Figure 1). N_2 adsorption-desorption isotherms of calcined MSNs showed a type IV curve. From BET and BJH models, a specific surface area of 1069 $m^2\ g^{-1}$ and an average pore diameter of 2.66 nm was estimated for the starting MSNs, whereas the specific surface area decreased to 279 $m^2\ g^{-1}$ for **S1** (Table 1). Moreover, elemental and thermogravimetric analysis were used to determine the amount of

rhodamine B, tricarboxylate derivative, and polymyxin B in solid **S1** (Table 2).

Table 1. Main structural features of calcined MSNs and **S1** nanoparticles determined by PXRD, TEM and N_2 isotherm adsorption-desorption measurements.

Sample	Particle diameter[a] (nm)	Surface area, S_{BET} ($m^2\ g^{-1}$)	Pore Volume[b] ($cm^3\ g^{-1}$)	Pore size[c] (nm)
MSNs	110	1011	0.86	2.66
S1	122	279	0.14	-

[a] Measured by TEM.
[b] Pore volume (from BJH for $P/P_0 < 0.6$, associated to mesopores).
[c] Pore size (from BJH model for $P/P_0 < 0.6$).

Table 2. Content (α) of rhodamine B, anchored tricarboxylate and polymyxin B in solid **S1**.

Solid	$\alpha_{rhodamine\ B}$ [mmol g^{-1} SiO_2]	$\alpha_{tricarboxylate}$ [mmol g^{-1} SiO_2]	$\alpha_{polymyxin\ B}$ [mmol g^{-1} SiO_2]
S1	0.073	0.035	0.089

After characterization of the prepared nanoparticles, the sensing behavior of **S1** in the presence of endotoxin (from *E. coli*) was tested. Two portions of solid **S1** (0.5 mg) were suspended in PBS at pH 7.4 (1 mL). Then, endotoxin (1000 μg mL^{-1}) was added to one batch while the volume of the other portion was adjusted with endotoxin-free PBS (blank). At certain scheduled times aliquots of both experiments were separated and filtered. The emission of the rhodamine B released to the solution was measured at 571 nm (λ_{ex} = 555 nm). The obtained results are shown in Figure 2. As it could be seen, when endotoxin is absent, nearly a zero release of rhodamine B was observed according to an efficient pore closure promoted by the strong electrostatic interaction between the grafted tricarboxylate moieties and the cationic polymyxin B. As a

clear contrast, in the presence of endotoxin, a high increase in rhodamine B release was monitored. A 90% of the total released dye was achieved only after 30 min. Thus, the sensing mechanism can be explained in terms of the uncapping event. When the capped nanoparticles are in the presence of endotoxin, this molecule induces pore unblocking and subsequent rhodamine B release due to the formation of a complex between polymyxin and the target endotoxin, which is stronger than the interaction with the solid surface.

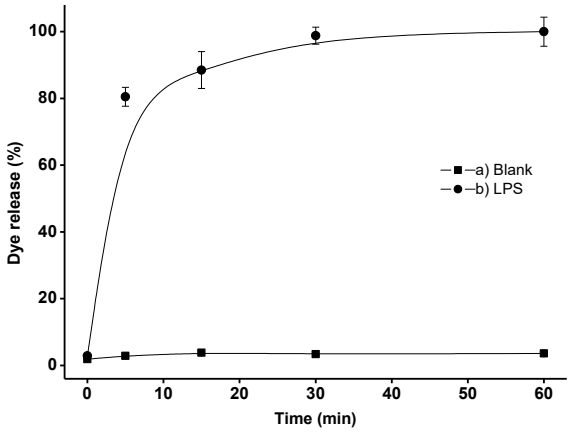

Figure 2. Rhodamine B release profile obtained from suspensions of **S1** when endotoxin is absent and present (1000 μg mL^{-1}) at 25ºC in PBS (pH 7.4).

In a second step, cargo release from **S1** upon addition of increasing concentrations of endotoxin was studied. For this purpose, and following a similar procedure to that described above, rhodamine B release from **S1** at 30 min and using different amounts of endotoxin was registered. Figure 3 shows the obtained calibration curve. As it can be observed, there is a direct correlation between the endotoxin concentration and the amount of rhodamine B delivered from **S1**. From the obtained data a limit of detection (LOD) for endotoxin of 100 pg mL^{-1} was determined. This

LOD is similar to those reported for other hybrid sensors based on the use of gold nanoparticles.[30-32] Besides, **S1** nanoparticles yielded a remarkable fluorescence response in the presence of endotoxin after 10 min, being much faster than the standard LAL method (ca. 60 min) used for the detection of this toxin. In addition, **S1** nanoparticles showed a high stability at 25°C and did not require a special storage or severe temperature requirements. As mentioned above, one interesting feature of gated materials applied in detection protocols is the possibility to observe signal amplification due to a remarkable delivery of the entrapped reporter in the presence of only few analyte molecules. In particular, using **S1**, one LPS molecule (at 1.0×10^{-5} mol dm^{-3} concentration) induced the release of ca. 200 molecules of rhodamine B.

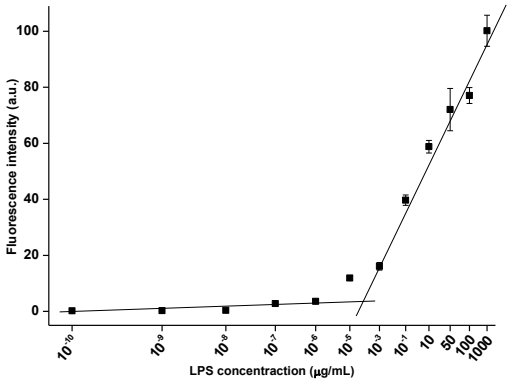

Figure 3. Calibration curve of rhodamine B released from **S1** nanoparticles (PBS, pH 7.4) in response to different quantities of endotoxin after 30 min.

Moreover, the selectivity of solid **S1** toward endotoxin was studied by analyzing cargo release from the nanoparticles in the presence of common interfering agents such as arabinogalactan (AG), β-(1,3)-D-glucan, pectin, EDTA, glucose, GTP, DNA, RNA and dust (endotoxin free). Figure 4 shows the response at 30 min of **S1** nanoparticles suspended in PBS (pH 7.4) or in tap water in the

presence of endotoxin (from *E. coli* and *R. sphaeroides*) and the selected interfering agents (at 50 μg mL^{-1}). As could be seen, only endotoxin was able to induce pore opening and rhodamine B release. This was a remarkable result because the presence of pectin and β-(1,3)-D-glucan usually results in false positives when the LAL method is used.[33] Besides, the same selective response to endotoxin was observed in the presence of a mixture of endotoxin and the selected interfering compounds (see Supporting Information).

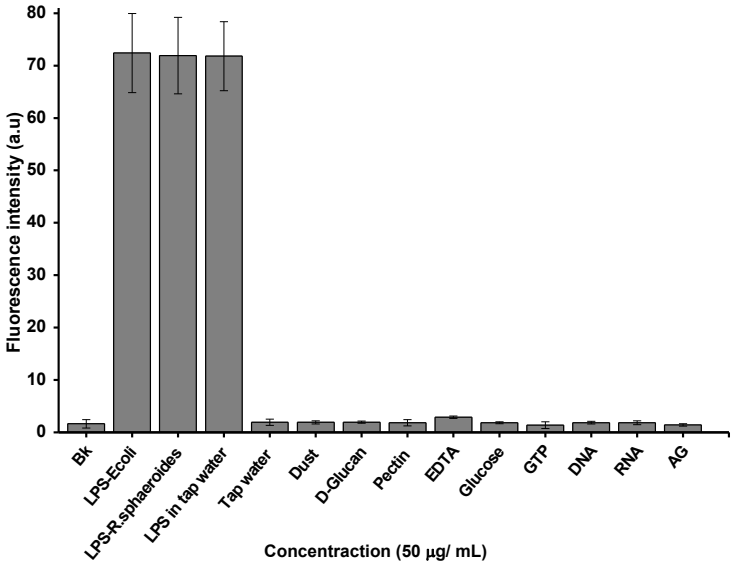

Figure 4. Response of **S1** to endotoxin and selected interfering agents (50 μg mL^{-1}).

In addition, the controlled release behavior of **S1** nanoparticles at different pH was also tested. The pH range in which **S1** nanoparticles could be used to effectively detect endotoxin is 4.0-8.5 (see Supporting Information). As expected, at pH 2, tricarboxylate groups on the external surface of the nanoparticles become fully protonated and negligible interactions with polymyxin B were present. As a consequence, a substantial delivery

of rhodamine B was observed when the material is exposed to acidic pH.

Table 3. Endotoxin determination in different samples of spiked tap water samples using **S1** nanoparticles.

Sample	Spiked endotoxin (μg)	Determined endotoxin (μg)	Recovery (%)
1	500	517	96.7
2	50	52.3	95.6
3	10	9.5	94.8

Finally, we centered our attention in the possible application of **S1** as an endotoxin probe. In the routine practice, the LAL assay is the most widely used endotoxin detection method. However, it requires a controlled workplace to proceed with a complex sample and it is also a time consuming assay. Development of simple alternative methodologies which would give a faster response could be pivotal in many sectors such as health, environment, and food industry. Following these ideas, the applicability of **S1** nanoparticles for endotoxin detection in a more realistic environment such as tap water was studied. Water is one of the most common media that bacteria use to grow and spread to other systems. Aliquots of 450 μL of water were spiked with known amounts of endotoxin (500, 50 and 10 μg). The different samples were mixed with 500 μg of **S1**. Then, rhodamine B release at 30 min was monitored and the corresponding endotoxin concentration was calculated by standard addition. The obtained results are shown in Table 3. As it could be seen, the gated nanomaterial was able to sense the presence of endotoxin in tap water with recoveries in the 95-97% range, which demonstrates the potential applicability of solid **S1** as an effective probe to detect endotoxin in realistic environments.

In summary, we have prepared a new nanomaterial using mesoporous silica nanoparticles as support, rhodamine B as reporter and the cationic peptide polymyxin B as gating mechanism. After characterization, the sensing behavior of the prepared hybrid material against endotoxin was studied. The selective strong coordination, through electrostatic interactions, between endotoxin and the capping polymyxin B induced pore unblocking and the subsequent rhodamine B release. The obtained response was highly selective to endotoxin and other interfering agents such as arabinogalactan, β-(1,3)-D-glucan, pectin, EDTA, glucose, GTP and dust were unable to induce pore opening. Besides, a limit of detection for endotoxin as low as 100 pg mL^{-1} was determined. The probe is stable and allow detection of endotoxin in the 4.0-8.5 pH range. Moreover, the capped nanoparticles were used to detect endotoxin in spiked tap water and obtained high recovery rates. The reported results suggest that polymyxin B-gated nanoparticles could be the basis for the development of an easy-to-use kit to detect endotoxin in contaminated environmental samples.

3.4 Acknowledgments

The authors thank the Spanish Government (MAT2015 64139-C4-1-R) and the Generalitat Valenciana (PROMETEO2018/024) for their support. I.O. thanks to Erasmus Mundus Programme, Action 2, Lot 1, Syria his predoctoral fellowship. S.S is grateful to Spanish Ministerio de Economia y Competitividad for his Juan de la Cierva contract (FJCI-2015-27201).

3.5 References

1 R. J. Ulevitch, P. S. Tobias, Curr. Opin. Immunol. 1994, 6, 125-130.

2 L. S. Young, W. J. Martin, R. D. Meyer, R. J. Weinstein, E. T. Anderson, Ann. Intern. Med. 1977, 86, 456-471.
3 M. Mueller, B. Lindner, S. Kusumoto, K. Fukase, A. B. Schromm, U. Seydel, J. Biol. Chem. 2004, 279, 26307-26313.
4 J. Bhattacharyya, S. Biswas, A. G. Datta, Curr. Med. Chem. 2004, 11, 359-368.
5 C. Braun-Fahrlander, J. Riedler, U. Herz, W. Eder, M. Waser, L. Grize, S. Maishch, D. Carr, F. Gerlach, A. Bufe, R. P. Lauener, R. Schierl, H. Renz, D. Nowak, E. V. Mutius, New Engl. J. Med. 2002, 347, 869-877.
6 M. T. Madigan, J. M. Martinko, J. Parker, T. D. Brock, Brock biology of microorganisms, 2000, 9th ed. Upper Saddle River, NJ: Prentice Hall, pp. 793-794.
7 S. J. Reynolds, D. K. Milton, D. Heederik, P. S. Thorne, K. J. Donham, E. A. Croteau, K. M. Kelly, J. Douwes, D. Lewis, M. Whitmer, I. Connaughton, S. Koch, P. Malmberg, B. M. Larsson, J. Deddens, A. Saraf, L. Larsson, J. Environ. Monit. 2005, 7, 1371-1377.
8 M. Peters, M. Kauth, J. Schwarze, C. Korner-Rettberg, J. Riedler, D. Nowak, C. Braun-Fahrlander, E. V. Mutius, A. Bufe, O. Holst, Thorax 2006, 61, 134-139.
9 M. Peters, P. Fritz, A. Bufe, Innate Immun. 2012, 18, 694-699.
10 F. R. Lourenço, T. D. S. Botelho, T. D. J. A. Pinto, PDA J. Pharm. Sci. Tech. 2012, 66, 542-546.
11 S. Voss, R. Fischer, G. Jung, K. H. Wiesmüller, R. J. Brock, J. Am. Chem. Soc. 2007, 129, 554-561.
12 J. Wu, A. Zawistowski, M. Ehrmann, T. Yi, C. J. Schmuck, J. Am. Chem. Soc. 2011, 133, 9720-9723.
13 L. Zeng, J. Wu, Q. Dai, W. Liu, P. Wang, C.-S. Lee, Org. Lett., 2010, 12, 4014-4017.
14 M. Lan, J. Wu, W. Liu, W. Zhang, J. Ge, H. Zhang, J. Sun, W. Zhao, P. Wang, J. Am. Chem. Soc. 2012, 134, 6685−6694.
15 J. Sun, J. Ge, W. Liu, X. Wang, Z. Fan, W. Zhao, H. Zhang, P. Wang, S. T. Lee, Nano Res. 2012, 5, 486-493.

16 P. Prasad, S. Sachan, S. Suman, G. Swayambhu, S. Gupta, Langmuir 2018, 34, 7396-7403.
17 B. Jurado-Sánchez, M. Pacheco, J. Rojo, A. Escarpa, Angew. Chem. Int. Ed. 2017, 56, 6957-6961.
18 G. Ahn, S. S. Sekhon, Y. -E. Jeon, M. -S. Kim, K. Won, Y. -H. Kim, J. -Y. Ahn, Toxicol. Environ. Health. Sci. 2017, 9, 259-268.
19 F. Sancenón, L. Pascual, M. Oroval, E. Aznar, R. Martínez-Máñez, ChemistryOpen 2015, 4, 418-437.
20 E. Aznar, M. Oroval, L. Pascual, J. R. Murguía, R. Martínez-Máñez, F. Sancenón, Chem. Rev. 2016, 116, 561-718.
21 S. El Sayed, C. Giménez, E. Aznar, R. Martínez-Máñez, F. Sancenón, M. Licchelli, Org. Biomol. Chem. 2015, 13, 1017-1021.
22 Y. L. Choi, J. Jaworski, M. L. Seo, S. J. Lee, J. H. Jung, J. Mater. Chem. 2011, 21, 7882-7885.
23 Ll. Pascual, S. El Sayed, R. Martínez-Máñez, A. M. Costero, S. Gil, P. Gaviña, F. Sancenón, Org. Lett. 2016, 18, 5548-5551.
24 V. C. Özalp, D. Çam, F. J. Hernandez, L. I. Hernandez, T. Schäferd, H. A. Öktem, Analyst 2016, 141, 2595-2599.
25 A. Ribes, S. Santiago-Felipe, A. Aviñó, V. Candela-Noguera, R. Eritja, F. Sancenón, R. Martínez-Máñez, E. Aznar, Sens. Actuators B Chem. 2018, 277, 598-603.
26 A. Ribes, E. Pérez-Xifré, E. Aznar, F. Sancenón, T. Pardo, L. F. Marsal, R. Martínez-Máñez, Sci. Rep. 2016, 6, 38649.
27 D. Ferrari, C. Pizzirani, E. Adinolfi, S. Forchap, B. Sitta, L. Turchet, S. Falzoni, M. Minelli, R. Baricordi, F. Di Virgilio, J. Immunol. 2004, 173, 4652-4660.
28 L. Mondragón, N. Mas, V. Ferragud, C. de la Torre, A. Agostini, R. Martínez-Máñez, F. Sancenón, P. Amorós, E. Pérez-Payá, M. Orzáez, Chem. Eur. J. 2014, 20, 5271-5281.
29 I. Candel, E. Aznar, L. Mondragón, C. de la Torre, R. Martínez-Máñez, F. Sancenón, M. D. Marcos, P. Amorós, C. Guillem, E. Pérez-Payá, A. Costero, S. Gil, M. Parra, Nanoscale 2012, 4, 7237-7245.

30 J. Sun, J. Ge, W. Liu, X. Lung, Z. Fan, W. Zhao, H. Zhang, P. Wang, S. T. Lee, Nano Res. 2012, 5, 486-493.
31 Y. Wang, D. Zhang, W. Liu, X. Zhang, S. Yu, T. Liu, W. Zhang, W. Zhu, J. Wang, Biosens. Bioelectron. 2014, 55, 242-248.
32 W. Su, M. Cho, J. D. Nam, W. S. Choe, Y. K. Lee, Electroanalysis 2013, 25, 380-386.
33 K. Brandenburg, J. Howe, T. Gutsman, P. Garidel, Curr. Med. Chem. 2009, 16, 2653-2660.

3.6 Supporting Information

3.6.1 General Techniques

Powder X-ray diffraction (PXRD), transmission electron microscopy (TEM), N_2 adsorption-desorption, thermogravimetric analysis (TGA) and fluorescence spectroscopy were used to characterize the synthesized materials. PXRD measurements were performed on a D8 Advance diffractometer using CuKα radiation (Philips, Amsterdam, and The Netherlands). Thermogravimetric analyses were carried out on a TGA/SDTA 851e balance (Mettler Toledo, Columbus, OH, USA), using an oxidizing atmosphere (air, 80 mL min^{-1}) with a heating program: gradient of 393-1273 K at 10°C min^{-1}, followed by an isothermal heating step at 1273°C for 30 min. TEM images were obtained with a 100 kV CM10 microscope (Philips). N_2 adsorption-desorption isotherms were recorded with an ASAP2010 automated adsorption analyser (Micromeritics, Norcross, GA, USA). The samples were degassed at 120°C in vacuum overnight. The specific surface areas were calculated from the adsorption data in the low pressure range using the Brunauer, Emmett and Teller (BET) model. Pore size was determined following the Barret, Joyner and Halenda (BJH) method. Dynamic light scattering (DLS) was used to obtain the particle size distribution of the different solids, using a Malvern Mastersizer

2000 (Malvern Instruments, Malvern, UK). For the measurements, samples were dispersed in distilled water. Data analysis was based on the Mie theory using refractive indices of 1.33 and 1.45 for the dispersant and mesoporous silica nanoparticles, respectively. An adsorption value of 0.001 was used for all samples. Variation of this adsorption value did not significantly alter the obtained distributions. Measurements were performed in triplicate.

3.6.2 Chemicals

Tetraethylorthosilicate (TEOS), *n*-cetyltrimethyl ammonium bromide (CTABr), sodium hydroxide, rhodamine B, tris(hydroxymethyl)aminomethane (TRIS), Endotoxin free Dulbecco's PBS (1X), lipopolysaccharide from *Escherichia coli* O55:B5 (LPS), arabinogalactan (AG), β-(1,3)-D-glucan, pectin, EDTA, glucose and GTP were purchased from Sigma-Aldrich Química (Madrid, Spain). LPS from *R. sphaeroides* (LPS-RS) was purchased from InvivoGen, USA. *N*-[(3- trimethoxysilyl)propyl] ethylenediamine triacetic acid trisodium salt was purchased from Fluorochem, UK. Oligonucleotides (DNA: AGGGATTCCTGGGAAAACTGGAC and RNA: GUCCAGUUUUCCCAGGAAUCCCU) were purchased from ThermoFischer Scientific. Finally, polymyxin B sulfate (PMB) was purchased from Tokyo Chemical Industry Co., Ltd. (TCI). Analytical-grade solvents were from Scharlab (Barcelona, Spain). All products were used as received.

3.6.3 Synthesis of Mesoporous Silica Nanoparticles (MSns)

n-cetyltrimethyl ammonium bromide (CTABr, 1.00 g, 2.74 mmol) was first dissolved in 480 mL of deionized water. Then a 3.5 mL of NaOH 2.00 M in deionized water was added to the CTABr solution, followed by adjusting the solution temperature to 80°C. TEOS (5 mL, 25.7 mmol) was then added dropwise to the surfactant

solution. The mixture was allowed to stir for 2 h to give a white suspension. Finally, the solid was centrifuged, washed with deionized water and dried at 60°C (MSNs as-synthesized). To prepare the final mesoporous material, the as-synthesized solid was calcined at 550°C in oxygen atmosphere for 5 h in order to remove the template phase.

3.6.4 Synthesis of S1

In a typical synthesis, 750 mg of template-free MCM-41 MSNs were suspended in a solution of 340 mg of rhodamine B dye in 10 mL of milli-Q water in a round-bottomed flask, (0.8 mmol of dye/g MSNs). After 24 h stirring at room temperature, 15 mmol/g MSNs of *N*-[(3-trimethoxysilyl)propyl] ethylendiamine triacetic acid trisodium salt were added and the mixture was stirred for 5.5 h at room temperature. Then, PMB (2.3 mmol/g MSNs) was added to the suspension. The final suspension was stirred for another 3 h at room temperature. Finally, this solid was filtered and washed with PBS in order to remove the unreacted alkoxysilane and the dye remaining outside the pores. The final solid **S1** was dried under vacuum at ambient temperature for 12 h.

3.6.5 Release Study of S1 at Different pH:

S1 was suspended (500 μg/ml) in water at different pH values (2, 4, and 7) and then kinetic dye release studies were performed at room temperature (25°C) under stirring. At a certain time, aliquots were taken and filtered. The delivery of the rhodamine B dye was then monitored by its fluorescence emission band at 610 nm (λ_{ex} = 453 nm). The release profiles obtained are shown in Figure S1. As could be seen, when solid **S1** is suspended in water at pH 4 and 7 a negligible rhodamine B release is observed. In contrast, at pH 2 a remarkable rhodamine B release was released (ca. 99% after 30 min). As expected, at pH 2, the tricarboxylate

moieties grafted onto the external surface of the **S1** nanoparticles becomes fully protonated and negligible interactions with polymyxin B were present. As a consequence a marked delivery of rhodamine B was observed at acidic pH.

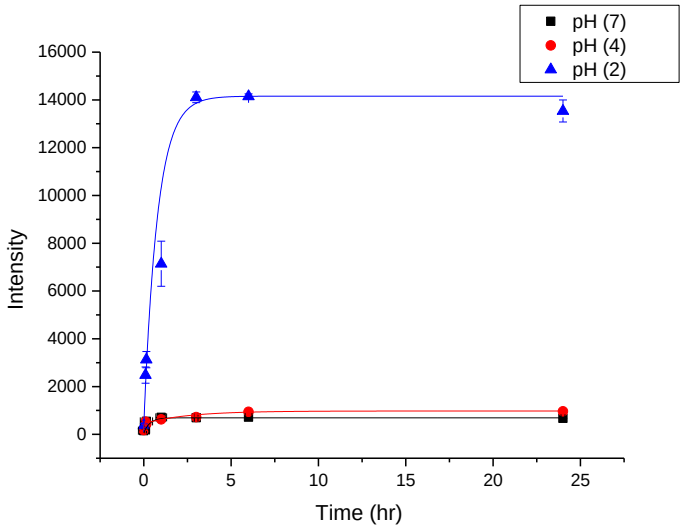

Figure S1. Kinetic release profiles of rhodamine B from solid **S1** at pH 2, 4 and 7.

3.6.6 Interference Studies with S1

In a first step, **S1** (0.5 mg) were suspended in PBS (1 mg/ml). Then, 50 µL of selected interfering species (dust, D-glucan, pectin, EDTA, glucose, GTP, arabinogalactan, and a mixture of all of them at 50 µg/mL concentration) and LPS (also 50 µL at 50 µg/mL concentration) were added to **S1** suspensions. After 30 min aliquots were taken and filtered using 0.2 µm filters. The delivery of rhodamine B dye was then monitored by the fluorescence emission band at 610 nm (λ_{ex} = 453 nm). Results are shown in Figure S2. As could be seen, any of the interfering species induced remarkable changes and the observed response was nearly the same than that obtained for **S1** suspensions in the presence of LPS.

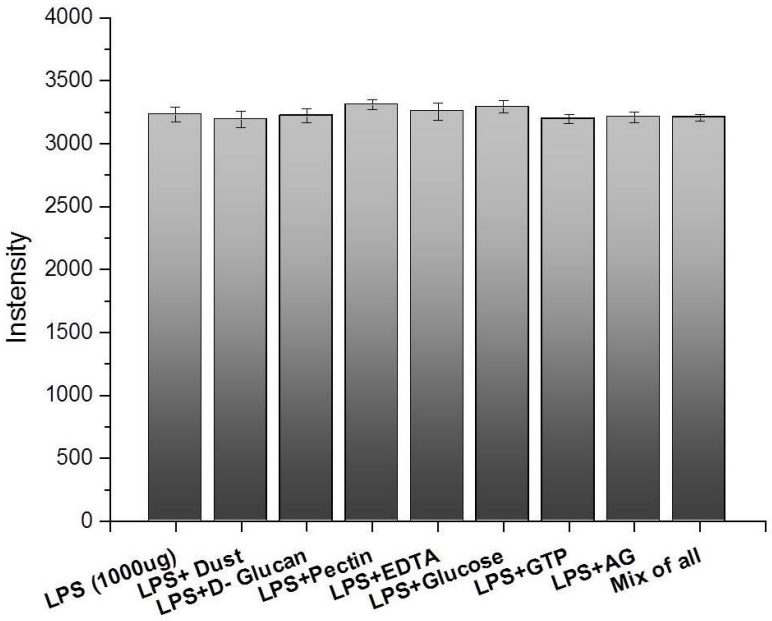

Figure S2. Emission intensity at 610 nm (excitation at 453 nm) of the rhodamine B released from suspensions of **S1** nanoparticles in the presence of LPS and LPS + selected interfering species.

Chapter 4: Fluorogenic Detection of Human Serum Albumin Using Curcumin-Capped Mesoporous Silica Nanoparticles

Fluorogenic Detection of Human Serum Albumin Using Curcumin-Capped Mesoporous Silica Nanoparticles

Ismael Otri,[1,2] Serena Medaglia,[1,2] Elena Aznar,[1,2,3,4,*] Félix Sancenón,[1,2,3,4,5,*] and Ramón Martínez-Máñez [1,2,3,4,5,*]

[1] Instituto Interuniversitario de Investigación de Reconocimiento Molecular y Desarrollo Tecnológico (IDM), Universitat Politècnica de València, Universitat de València, 46022 Valencia, Spain; isot@doctor.upv.es (I.O.); sermed@idm.upv.es (S.M.)

[2] Departamento de Química, Universidad Politécnica de Valencia, Camino de Vera s/n, 46022 Valencia, Spain

[3] CIBER de Bioingeniería, Biomateriales y Nanomedicina (CIBER-BBN), 46022 Valencia, Spain

[4] Unidad Mixta de Investigación en Nanomedicina y Sensores, Instituto de Investigación Sanitaria La Fe (IISLAFE), Universitat Politècnica de València, 46026 Valencia, Spain

[5] Unidad Mixta UPV-CIPF de Investigación en Mecanismos de Enfermedades y Nanomedicina, Centro de Investigación Príncipe Felipe, Universitat Politècnica de València, 46100 Valencia, Spain

*****_Correspondence: elazgi@upvnet.upv.es (E.A.); fanceno@upvnet.upv.es (F.S.); rmaez@qim.upv.es (R.M.-M.)_

***Received**: 20 December 2021*
***Published:** 7 February 2022*
Molecules 2022, 27, 1133-1142.

Keywords

Mesoporous silica; gated hybrid materials; sensors; HSA detection.

My contribution

I performed nanoparticle system design, synthesis, and *in vitro* experiments. I also contributed to the experimental design, data analysis, discussion, and writing.

Graphical abstract

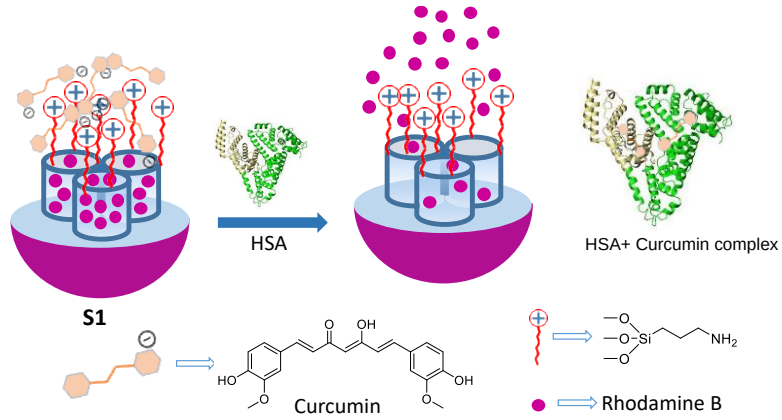

4.1 Abstract

Mesoporous silica nanoparticles loaded with rhodamine B and capped with curcumin are used for the selective and sensitive fluorogenic detection of human serum albumin (HSA). The sensing mesoporous silica nanoparticles are loaded with rhodamine B, decorated with aminopropyl moieties and capped with curcumin. The nanoparticles selectively release the rhodamine B cargo in the presence of HSA. A limit of detection for HSA of 0.1 mg/mL in PBS (pH 7.4)-acetonitrile 95:5 v/v was found, and the sensing nanoparticles were used to detect HSA in spiked synthetic urine samples.

4.2 Introduction

Human serum albumin (HSA) is a vital protein that constitutes around 50% of the total proteins in human plasma [1]. HSA is synthesized in the liver, and it is related with the transport of several endogenous and exogenous biomolecules such as fatty acids, thyroxine, hormones, and drugs [2]. Moreover, HSA also plays a vital role in the regulation of plasma osmotic pressure, maintain water equilibrium between tissues and preserve blood pH [3]. Normal levels of HSA in serum are in the 35–55 g/L range, whereas in urine its concentration is ca. 30 mg/L. However, high levels of HSA in body fluids are related with several human diseases such as kidney failure, diabetes mellitus, cardiovascular disorders, obesity and liver injury [4]. Moreover, low HSA levels are found to cause chronic hepatitis, liver failure and cirrhosis [5].

Currently, HSA is detected and quantified using immune-electrophoresis, enzyme-linked immunosorbent assays (ELISA), radio-immunoassays and liquid chromatography–mass spectroscopy [6,7]. These methods presented several drawbacks, such as the need of complicated instrumentation and the

assistance of trained personnel and are long-time procedures [8]. Recently, as an alternative to these classical methods, fluorescent molecular-based probes, polymers and gold nanoparticles have been described for HSA detection [9,10]. However, some of those methods suffer interferences from molecules in the human serum samples, such as hormones, growth factors, fats, carbohydrates and inorganic substances [11]. Taking into account the above-mentioned facts, the development of fast, easy-to-use, selective and reliable methods to detect HSA in biological matrices for clinical diagnosis and biomedical research is of relevance.

From another point of view, mesoporous silica nanoparticles (MSNs) functionalized with molecular gates able to provide on-command cargo release have been used to design smart nanodevices with application in the biomedical field [12–14], for example as drug-controlled release systems [15,16], for genetic material delivery [17,18], biosensing [19,20], bioimaging [21,22], tissue engineering [23,24], theragnostic applications [25], immunotherapy [26,27] or communication protocols [28–31]. Specifically, the development of new sensing/recognition protocols using mesoporous silica nanoparticles (MSNs) equipped with molecular gates has boosted and several interesting examples has been described in the literature [32]. In these sensing materials, the pores of the nanoparticles are loaded with a dye/fluorophore (acting as reporter) and the external surface is functionalized with bulky (supra)molecular ensembles, which disable the release of the entrapped reporter. In the presence of a target analyte, which selectively interacted with the gating (supra)molecular ensemble, pores opened, the dye/fluorophore is released and a macroscopic signal (changes in color or in the fluorescence) is finally generated [33,34]. Considering that most of the sensing protocols are designed to

detect target analytes in water, the best shape of MCM-41 type mesoporous silica for its use in the preparation of gated sensory materials is nanoparticles of about ca. 100 nm diameter. This allowed the proper suspension of the gated material in aqueous environments and the effective recognition of the target analyte.

Taking into account our interest in the development of new sensing nanodevices to detect biomolecules [35,36], herein we present the synthesis and characterization of curcumin-capped mesoporous silica nanoparticles for the sensitive and selective detection and quantification of HSA. Mesoporous silica nanoparticles (ca. 100 nm diameter) were selected, as inorganic scaffold, and the pores loaded with rhodamine B as reporter. The outer surface of the loaded nanoparticles was decorated with aminopropyl moieties (which are positively charged at neutral pH). Finally, the pores were capped upon addition of curcumin. Nearly half of the curcumin molecules (which have three ionizable hydroxyl groups with pK_a values of 7.8, 8.5 and 9.0) [37] had a negative charge at physiological pH and, for this reason, yielded strong electrostatic interactions with the positively charged protonated amino moieties. The signaling paradigm relies on the fact that HSA shows a marked affinity for complexation with curcumin [38]. In the presence of HSA curcumin molecules are expected to be displaced from the surface of the nanoparticles, due to its preferential coordination with the protein, with subsequent pore opening and rhodamine B release (Scheme 1). The increase in the emission intensity of rhodamine B in then solution would be directly related to the amount of HSA present in the medium. As far as we know, this is the first curcumin-capped hybrid nanomaterial used for the fluorogenic detection of HSA.

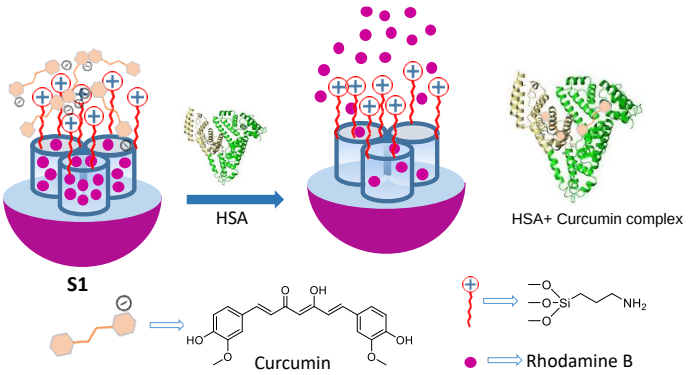

Scheme 1. Schematic representation of the sensing mechanism of **S1** nanoparticles in the presence of HSA.

4.3 Results and Discussion

MCM-41 type MSNs were prepared using *n*-cetyltrimethylammonium bromide (CTABr) as template and tetraethylorthosilicate (TEOS) as a silica source [18,19] and then calcinated to remove the surfactant. MSNs were then loaded with rhodamine B, the loaded solid was reacted with (3-aminopropyl) triethoxysilane and, finally, the pores were capped by addition of curcumin (solid **S1** in Scheme 1).

As-synthesized, calcined and **S1** nanoparticles were characterized using standard techniques such as powder X-ray diffraction (PXRD), transmission electron microscopy (TEM), thermogravimetric analysis, dynamic light scattering (DLS) and elemental analysis. Figure 1A shows the PXRD patterns of the as-made (curve a), calcined (curve b) and **S1** nanoparticles (curve c) which confirmed the mesoporous structure of the materials and the preservation of its structural features after the loading and functionalization process (for **S1**). Moreover, TEM images of calcined MSNs (Figure 1B, image d) and **S1** (Figure 1B, image e) show that nanoparticles were spherical with an average diameter of ca. 110 nm.

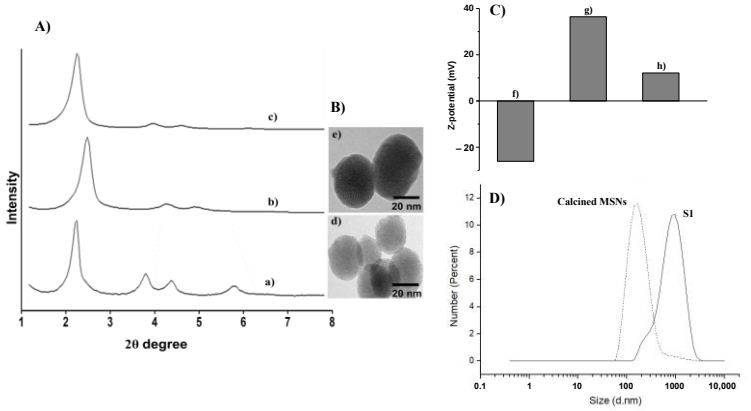

Figure 1. (A) Powder X-ray diffraction patterns of (a) as-synthesized MSNs, (b) calcined MSNs and (c) solid **S1**. (B) TEM images of (d) calcined MSNs and (e) solid **S1**. (C) Z-potential of (f) calcined MSNs, (g) amino-functionalized and loaded MSNs and (h) solid **S1**. (D) Hydrodynamic diameter of calcined MSNs and **S1**.

N_2 adsorption–desorption isotherms of calcined MSNs showed a type IV curve. From BET and BJH models, a specific surface area of 1207.3 $m^2\ g^{-1}$, a narrow pore size distribution and an average pore diameter of 2.56 nm for the starting calcined MCM-41 was obtained. After the loading and functionalization processes the surface area of **S1** markedly decreased to 17.6 $m^2\ g^{-1}$. Structural parameters for calcined MCM-41 and **S1** are listed in Table 1. In addition, Z-potential of the starting calcined MSNs was negative (−26.1 mV) due to the presence of silanolate moieties on the surface of the nanoparticles (see Figure 1C). After loading of the pores with rhodamine B and functionalization of the external surface with aminopropyl moieties, the Z-potential became positive (36.4 mV) due to the presence of ionisable amino groups. The Z-potential of the final **S1** nanoparticles was reduced to (12.1 mV), ascribed to the capping of the pores with the negatively charged curcumin. Moreover, DLS measurements also showed an enhancement of the hydrodynamic diameter of the nanoparticles

from 135 nm for calcined MSNs to 955 nm for **S1** (Figure 1D). The organic matter content in **S1** was 1.56 g/g SiO_2 calculated by thermogravimetric analysis. Moreover, the amount of rhodamine B loaded in **S1** was estimated to be 0.18 g/g SiO_2 using a calibration curve. To infer so, the mesoporous scaffold was hydrolyzed by incubating **S1** with NaOH 20% at 40 °C for 1 h and then the supernatant absorbance was measured.

Table 1. Main structural parameters of calcined MSNs and **S1** nanoparticles determined by TEM, PXRD and N_2 adsorption–desorption measurements.

Sample	Particles Diameter [1] (nm)	Surface Area, S_{BET} ($m^2\ g^{-1}$)	Pore Volume [2] ($cm^3\ g^{-1}$)	Pore Size [3] (nm)
Calcined MSNs	101	1207.3	0.444	2.56
S1	110	17.6	-	-

1 Measured by TEM. 2 Total pore volume according to the BJH model. 3 Pore size estimated by using the BJH model applied to the adsorption branch of the isotherm, for P/P0 < 0.6, which can be associated with the surfactant-generated mesopores.

After characterization, the cargo-controlled release studies in the absence and in the presence of HSA were carried out. In a typical experiment, solid **S1** (0.5 mg) was suspended in PBS (pH 7.4)-acetonitrile 95:5 v/v (1 mL) in the absence and in the presence of HSA (1000 μg mL^{-1}). At selected times (0, 5, 15, 30 min) aliquots (120 μL) were collected and the supernatant was separated using a 0.22 μm filter. Then, rhodamine B emission at 571 nm (λ_{ex} = 555 nm) in the supernatant was measured. The obtained kinetic release profiles of rhodamine B from **S1** in the absence and in the presence of HSA are shown in Figure 2. As could be seen, in the absence of HSA a nearly zero release of rhodamine B was observed due to an efficient pore closure as a result of strong electrostatic interactions between the grafted positively charged aminopropyl moieties and the anionic curcumin. In a clear contrast, a marked rhodamine B release was observed (ca. 75% of the maximum amount of

delivered fluorophore after 5 min) in the presence of HSA, which was ascribed to pore opening due to the formation of a complex between the HSA and curcumin (the logarithm of the stability constant for the HSA-curcumin complex is 4.74) [39].

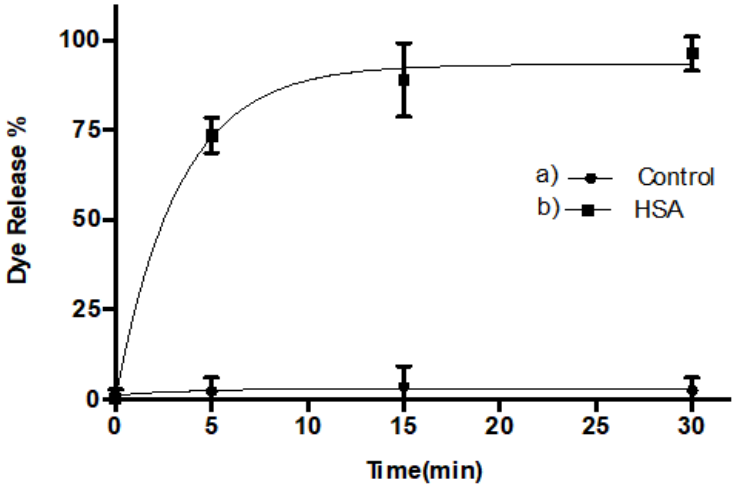

Figure 2. Release of rhodamine B versus time from PBS (pH 7.4)-acetonitrile 95:5 *v/v* suspensions of **S1** nanoparticles (a) in the absence and (b) in the presence of HSA (1000 μg mL^{-1}) at 25 °C (100% is the maximum of rhodamine B released from **S1** solid).

Once the proper working of the gating mechanism in **S1** was assessed, rhodamine B release in the presence of increasing amounts of HSA was evaluated after 5 min upon addition (at this time 75% of the maximum amount of rhodamine B delivered was released from **S1** and this quantity is enough to produce a marked fluorescent signal for analytical purposes). The obtained results are shown in Figure 3. As could be seen, the addition of increasing amounts of HSA induced a clear emission enhancement at 571 nm ascribed to an enhanced rhodamine B released from **S1**. From the emission titration profile, a limit of detection as low as 0.1 mg/mL of HSA was determined (using 3SD/S, where SD is the standard deviation and S is the slope of the linear range). **S1** nanoparticles

are stable at room temperature and did not require a special temperature for storage [40,41]. Another advantage of **S1** is the signal amplification observed [42]. In particular, it was confirmed that the presence of one HSA molecule (at a concentration of ca. 1.0×10^{-5} mol/L) results in the release of ca. 120 molecules of rhodamine B from **S1**.

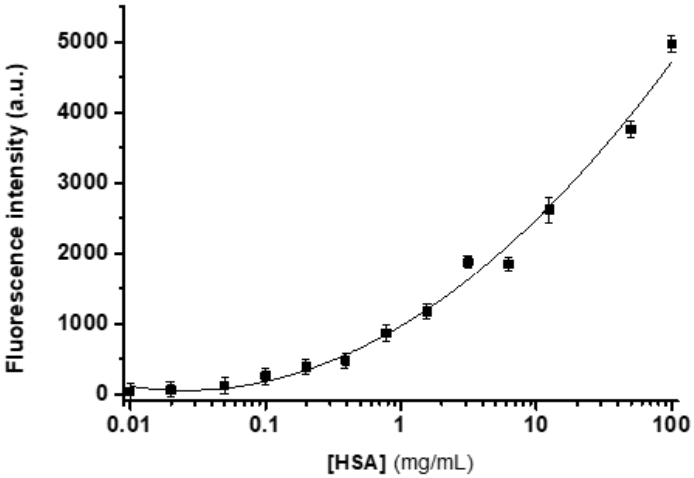

Figure 3. Calibration curve of **S1** nanoparticles suspended in PBS (pH 7.4)-acetonitrile 95:5 v/v upon addition of increasing concentrations of HSA (0.1 to 100 mg/mL). All aliquots were taken after 5 min. Error bars are expressed as 3σ for three independent experiments. The lines are included only as a guide to the eye for better illustration.

Then, the selectivity of **S1** toward HSA was assessed by testing cargo release against common interfering molecules present in biological samples. Figure 4 shows the emission of rhodamine B (at 571 nm) released from **S1** nanoparticles suspended in PBS (pH 7.4)-acetonitrile 95:5 *v*/*v* in the presence of HSA and other selected interfering molecules such as anions, cations, amino acids, urea (at 10 μM) and synthetic urine in PBS [43]. As could be seen, only HSA was able to induce pore opening and rhodamine B release. These results indicated the high selectivity achieved with **S1**

nanoparticles, as only the presence of HSA induced pore opening and rhodamine B release.

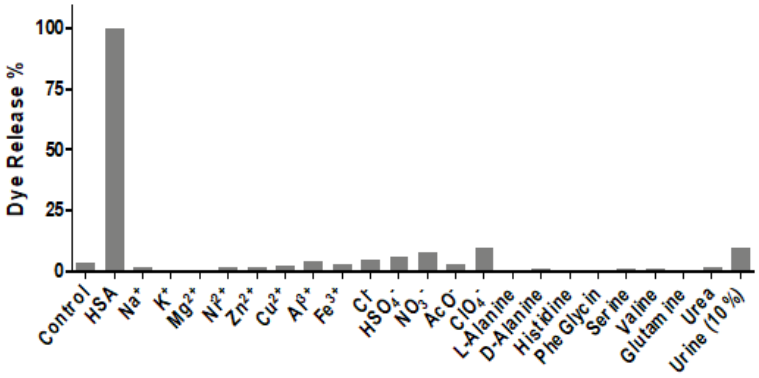

Figure 4. Fluorescence intensity at 571 nm of rhodamine B released from **S1** suspensions in PBS (pH 7.4)-acetonitrile 95:5 *v*/*v* after 5 min of HSA (10 µM) and selected interfering molecules (10 µM) addition. Synthetic urine was dissolved in PBS (pH 7.4)-acetonitrile 95:5 *v*/*v* at 10% concentration.

Finally, in order to test the applicability of **S1** to detect HSA in a complex biological environment, we evaluated the possible use of the sensing nanoparticles to determine HSA in synthetic urine. For this purpose, synthetic urine was spiked with known amounts of HSA and the concentration was determined using **S1** nanoparticles by means of a calibration curve in the same media. Results are shown in Table 2. As it can be seen, **S1** was satisfactorily applied to the detection of HSA with high recovery ratios in the 87–108% range. These results demonstrate the potential application of **S1** for the detection and quantification of HSA in realistic urine samples.

Table 2. Determination of HSA spiked in synthetic urine samples using **S1** nanoparticles.

Sample	Spiked HAS (µg)	Determined HSA (µg)	Recovery (%)
1	100	108	108
2	350	316	90.3
3	500	436	87.2

4.4 Materials and Methods

4.4.1 General Techniques

Powder X-ray diffraction (PXRD), transmission electron microscopy (TEM), N_2 adsorption–desorption, thermogravimetric analysis (TGA) and fluorescence spectroscopy were employed to characterize the synthesized materials. PXRD measurements were performed on a D8 Advance diffractometer using CuKα radiation (Philips, Amsterdam, The Netherlands). Thermogravimetric analyses were carried out on a TGA/SDTA 851e balance (Mettler Toledo, Columbus, OH, USA), using an oxidizing atmosphere (air, 80 mL min^{-1}) with a heating program: a gradient of 393–1273 K at 10 °C min^{-1}, followed by an isothermal heating step at 1273 °C for 30 min. TEM images were obtained with a 100 kV CM10 microscope (Philips). N_2 adsorption–desorption isotherms were recorded with an ASAP2010 automated adsorption analyser (Micromeritics, Norcross, GA, USA). The samples were degassed at 120 °C in vacuum overnight. The specific surface areas were calculated from the adsorption data in the low pressure range using the Brunauer, Emmett and Teller (BET) model. Pore size was determined following the Barret, Joyner and Halenda (BJH) method. Dynamic light scattering was used to obtain the particle size distribution of the different solids, using a ZetaSizer Nano ZS (Malvern Instruments, Malvern, UK) equipped with a laser of 633 nm and collecting the signal at 173°. For the measurements, samples were dispersed in distilled water. Data analysis was based on the Mie theory using refractive indices of 1.33 and 1.45 for the dispersant and mesoporous silica nanoparticles, respectively. An adsorption value of 0.001 was used for all samples. Variation of this adsorption value did not significantly alter the obtained distributions. Measurements were performed in triplicate.

4.4.2 Chemicals

Tetraethylorthosilicate (TEOS), *n*-cetyltrimethyl ammonium bromide (CTABr), curcumin, sodium hydroxide (NaOH), rhodamine B, tris(hydroxymethyl) aminomethane (TRIS), (3-aminopropyl) triethoxysilane, HSA, L-alanine, D-alanine, histidine, phenyl glycine, serine, valine, glutamine, and urea were purchased from Sigma Aldrich. Curcumin was purchased from Tokyo Chemical Industry Co., Ltd. (TCI, Tokyo, Japan). Analytical-grade solvents were from Scharlab (Barcelona, Spain). All products were used as received.

4.4.3 Synthesis of Mesoporous Silica Nanoparticles (MSNs):

n-cetyltrimethylammonium bromide (CTABr, 1.00 g, 2.74 mmol) was first dissolved in 480 mL of deionized water. Then a 3.5 mL of NaOH 2 M in deionized water was added to the CTABr solution, followed by adjusting the solution temperature to 80 °C. TEOS (5 mL, 25.7 mmol) was then added dropwise to the surfactant solution. The mixture was allowed stirred for 2 h to give a white suspension. Finally, the solid was centrifuged, washed with deionized water and dried at 60 °C (MSNs as-synthesized). To prepare the final mesoporous material, the as-synthesized solid was calcined at 550 °C in oxygen atmosphere for 5 h to remove the template phase.

4.4.4 Synthesis of S1

In a typical synthesis, 750 mg of template-free MCM-41 were suspended in a solution of 340 mg of rhodamine B dye in 10 mL of miliQ water in a round-bottomed flask, (0.8 mmol of dye/g MCM-41). After 24 h stirring at room temperature, (3-aminopropyl) triethoxysilane (15 mmol/g) was added and the mixture was stirred for 6 h at room temperature. Then, curcumin (2.3 mmol/g) was added to the suspension. This suspension was stirred for 1 h at room temperature. Finally, this solid was filtered and washed with

PBS to remove the unreacted alkoxysilane and the dye remaining outside the pores. The final solid **S1** was dried under vacuum at ambient temperature for 12 h.

4.4.5 Controlled Release Studies

Solid **S1** (0.5 mg) was suspended in PBS (pH 7.4)-acetonitrile 95:5 v/v (1 mL) in the absence and in the presence of HSA (1000 mg mL^{-1}) and dye release studies versus time were performed at room temperature (25 °C) under stirring. At a certain time (0, 5, 15, 30 min), aliquots (120 µL) were collected, and the supernatant was separated using a 0.22 µm filter. The delivery of the rhodamine B dye was then monitored by its fluorescence emission band at 571 nm (λ_{ex} = 555 nm).

4.4.6 Synthetic Urine Preparation

Artificial urine was prepared by dissolving urea (18.2 g), potassium chloride (4.5 g), sodium chloride (7.5 g), sodium phosphate (4.8 g), and creatinine (2 g) in distilled water (750 mL). Then, the pH of the solution was adjusted to 6.

4.4.6 Calibration curve with HSA:

In a first step, **S1** (0.5 mg) was suspended in 1 mL of synthetic urine diluted with PBS (pH 7.4)-acetonitrile 95:5 v/v (10%). Then, increasing amounts (0.1 to 100 mg/mL) of HSA were solubilized in synthetic urine diluted with PBS (pH 7.4)-acetonitrile 95:5 v/v (10%). Then, the solutions of HSA were added to **S1** suspensions. After 5 min aliquots were taken and filtered using 0.2 µm filters. The delivery of rhodamine B dye was then monitored by the fluorescence emission band at 571 nm (λ_{ex} = 555 nm).

4.4.7 Selectivity Studies

S1 (1.5 mg) was suspended in 3 mL PBS (pH 7.4)-acetonitrile 95:5 *v*/*v*. Then, the selected interfering molecules (anions, cations, amino acids, urea) were solubilized in artificial urine diluted with

PBS (pH 7.4)-acetonitrile 95:5 v/v (10%) at a 10 mM concentration. Then, the selected interfering molecules (10 μM) and HSA (10 μM) were added to **S1** suspensions. After 5 min aliquots were taken and filtered using 0.2 μm filters. The delivery of rhodamine B dye was then monitored by the fluorescence emission band at 571 nm (λ_{ex} = 555 nm).

4.4.8 HSA Determination in Synthetic Urine

In a first step, **S1** (0.5 mg) was suspended in 1 mL of artificial urine diluted with PBS (pH 7.4)-acetonitrile 95:5 v/v (10%). Then, known amounts of HSA were solubilized in synthetic urine diluted with PBS (pH 7.4)-acetonitrile 95:5 v/v (10%). Then, solutions of HSA were added to **S1** suspensions. After 5 min aliquots were taken and filtered using 0.2 μm filters. The delivery of rhodamine B dye was then monitored by the fluorescence emission band at 571 nm (λ_{ex} = 555 nm).

4.5 Conclusions

In summary, we describe herein a sensing material based on gated mesoporous silica nanoparticles for the selective and sensitive HSA detection in buffered aqueous solution and in artificial urine. **S1** nanoparticles are composed of a mesoporous inorganic scaffold loaded with rhodamine B, with the external surface decorated with aminopropyl moieties and with the pores caped with curcumin. The sensing mechanism arises from a displacement reaction by the formation of a strong complex between HSA and curcumin that results in uncapping of the nanoparticles and rhodamine B release. A limit of detection for HSA of 0.1 mg/mL in PBS (pH 7.4)-acetonitrile 95:5 v/v was determined. It was also demonstrated that S1 can be used to determine the concentration of HSA in spiked synthetic urine samples with recoveries in the 87–108% range.

Author Contributions

Conceptualization, E.A., F.S. and R.M.-M.; methodology, I.O. and S.M.; validation, I.O. and S.M.; formal analysis, E.A., F.S. and R.M.-M.; investigation, I.O. and S.M.; writing—original draft preparation, I.O. and S.M.; writing—review and editing, E.A., F.S. and R.M.-M.; supervision, E.A., F.S. and R.M.-M. All authors have read and agreed to the published version of the manuscript.

Funding

This research was funded by the Spanish Government (RTI2018-100910-B-C41 (MCUI/FEDER, EU)) and the Generalitat Valenciana (PROMETEO 2018/024). I.O. was funded by Erasmus Mundus Programme, Action 2, Lot 1, Syria (predoctoral fellowship). S.M. was funded by Generalitat Valenciana (Santiago Grisolía fellowship).

Conflicts of Interest: The authors declare no conflict of interest.

Sample Availability: Samples of the compounds are not available from the authors.

4.6 References

1. Fanali, G.; di Masi, A.; Trezza, V.; Marino, M.; Fasano, M.; Ascenzi, P. Human serum albumin: From bench to bedside. *Mol. Aspects Med.* **2012**, *33*, 209–290.
2. Liu, X.; Song, D.Q.; Zhang, Q.L.; Tian, Y.; Liu, Z.Y.; Zhang, H.Q. Characterization of drug-binding levels to serum albumin using a wavelength modulation surface plasmon resonance sensor. *Sens. Actuators B Chem.* **2006**, *117*, 188–195.
3. Arques, S.; Ambrosi, P. Human serum albumin in the clinical syndrome of heart failure. *J. Card. Fail.* **2011**, *17*, 451–458.
4. Hoogenberg, K.; Sluiter, W.J.; Dullaart, R.P. Effect of grown hormone and insulin-like growth factor I on urinary albumin excretion: Studies in acromegaly and growth hormone deficiency. *Acta Endocrinol.* **1993**, *129*, 151–157.

5. Amin, R.; Widmer, B.; Prevost, A.T.; Schwarze, P.; Coope, J.; Edge, J.; Marcovecchio, L.; Neil, A.; Dalton, R.N.; Dunger, D.B. Risk of microalbuminuria and progression to macroalbuminuria in a cohort with childhood onset type 1 diabetes: Prospective observational study. *Br. Med. J.* **2008**, *336*, 697–701.
6. Wang, R.E.; Tian, L.; Chang, Y. A homogenous fluorescent sensor for human serum albumin. *J. Pharm. Biomed. Anal.* **2012**, *63*, 165–169.
7. Tu, M.C.; Chang, Y.Z.; Kang, Y.T.; Chang, H.Y.; Chang, P.; Yew, T.R. A quantum dot-based optical immunosensor for human serum albumin detection. *Biosens. Bioelectron.* **2012**, *34*, 286–290.
8. Ghai, R.; Falconer, R.J.; Collins, B.M. Applications of isothermal titration calorimetry in pure and applied research—Survey of the literature from 2010. *J. Mol. Recognit.* **2012**, *25*, 32.
9. Reja, S.I.; Khan, I.A.; Bhalla, V.; Kumar, M. A TICT baser NIR-fluorescent probe for human serum albumin: A pre-clinical diagnosis in blood serum. *Chem. Commun.* **2016**, *52*, 1182–1185.
10. An, F.F.; Zhang, X.H. Strategies for preparing albumin-based nanoparticles for multifunctional bioimaging and drug delivery. *Theranostics* **2017**, *7*, 3667–3689.
11. Kang, N.; Kasemsumran, S.; Woo, Y.A.; Kim, H.J.; Ozaki, Y. Optimization of informative spectral regions for the quantification of cholesterol, glucose and urea in control serum solutions using searching combination moving window partial least squares regression method with near infrared spectroscopy. *Chemom. Intell. Lab. Syst.* **2006**, *82*, 90–96.
12. Chen, L.; Liu, M.; Zhou, Q.; Li, X. Recent developments of mesoporous silica nanoparticles in biomedicine. *Emergent Mater.* **2020**, *3*, 381–405.
13. Jafari, S.; Derakhshankhah, H.; Alaei, L.; Fattahi, A.; Varnamkhasti, B.S.; Saboury, A.A. Mesoporous silica nanoparticles for therapeutic/diagnostic applications. *Biomed. Pharmacother.* **2019**, *109*, 1100–1111.
14. García-Fernández, A.; Aznar, E.; Martínez-Máñez, R.; Sancenón, F. New advances in in vivo applications of gated mesoporous silica as drug delivery nanocarriers. *Small* **2020**, *16*, 1902242.
15. Vallet-Regí, M.; Colilla, M.; Izquierdo-Barba, I.; Manzano, M. Mesoporous silica nanoparticles for drug delivery: Current insights. *Molecules* **2018**, *23*, 47.

16. Murugan, B.; Sagadevan, S.; Fatimah, I.; Fatema, K.N.; Oh, W.C.; Mohammad, F.; Johan, M.R. Role of mesoporous silica nanoparticles for the drug delivery applications. *Mater. Res. Express* **2020**, *7*, 102002.
17. Zhou, Y.; Quan, G.; Wu, Q.; Zhang, X.; Niu, B.; Wu, B.; Huang, Y.; Pan, X.; Wu, C. Mesoporous silica nanoparticles for drug and gene delivery. *Acta Pharm. Sin. B* **2018**, *8*, 165–177.
18. Radu, D.R.; Lai, C.Y.; Jeftinija, K.; Rowe, E.W.; Jeftinija, S.; Lin, V.S.Y. A polyamidoamine dendrimer-capped mesoporous silica nanosphere-based gene transfection reagent. *J. Am. Chem. Soc.* **2004**, *126*, 13216–13217.
19. Kordasht, H.K.; Pazhuhi, M.; Pashazadeh-Panahi, P.; Hasanzadeh, M.; Shadjou, N. Multifunctional aptasensors based on mesoporous silica nanoparticles as an efficient platform for bioanalytical applications: Recent advances. *Trends Anal. Chem.* **2020**, *124*, 115778.
20. Pla, L.; Santiago-Felipe, S.; Tormo-Mas, M.A.; Ruiz-Gaitán, A.; Pemán, J.; Valentín, E.; Sancenón, F.; Aznar, E.; Martínez-Máñez, R. Oligonucleotide-capped nanoporous anodic alumina biosensor as diagnostic tool for rapid and accurate detection of *Candida auris* in clinical samples. *Emerg. Microbes Infect.* **2021**, *10*, 407–415.
21. Pascual, L.; Cerqueira-Coutinho, C.; García-Fernández, A.; de Luis, B.; Bernardes, E.S.; Albernaz, M.S.; Missailidis, S.; Martínez-Máñez, R.; Santos-Oliveira, R.; Orzaez, M.; et al. MUC-1 aptamer-capped mesoporous silica nanoparticles for controlled drug delivery and radioimaging applications. *Nanomedicine* **2017**, *13*, 2495–2505.
22. Cha, B.G.; Kim, J. Functional mesoporous silica nanoparticles for bioimaging applications. *Nanomed. Nanobiotechnol.* **2019**, *11*, e1515.
23. Polo, L.; Gómez-Cerezo, N.; Aznar, E.; Vivancos, J.L.; Sancenón, F.; Arcos, D.; Vallet-Regí, M.; Martínez-Máñez, R. Molecular gates in bioactive glasses for the treatment of bone tumors and infection. *Acta Biomater.* **2017**, *50*, 114–126.
24. Chen, L.; Zhou, X.; He, C. Mesoporous silica nanoparticles for tissue engineering applications. *Nanomed. Nanobiotechnol.* **2019**, *11*, e1573.
25. Cheng, Y.; Jiao, X.; Fan, W.; Yang, Z.; Wen, Y.; Chen, X. Controllable synthesis of versatile mesoporous organosilica nanoparticles as precision cancer theranostics. *Biomaterials* **2020**, *256*, 120191.

26. Fontana, F.; Liu, D.; Hirvonen, J.; Santos, H.A. Delivery of therapeutics with nanoparticles: what's new in cancer immunotherapy? *Nanomed. Nanobiotechnol.* **2017**, *9*, e1421.
27. Hao, M.; Chen, B.; Zhao, X.; Zhao, N.; Xu, F.J. Organic/inorganic nanocomposites for cancer immunotherapy. *Mater. Chem. Front.* **2020**, *4*, 2571–2609.
28. Llopis-Lorente, A.; Díez, P.; Sánchez, A.; Marcos, M.D.; Sancenón, F.; Martínez-Ruiz, P.; Villalonga, R.; Martínez-Máñez, R. Interactive models of communication at the nanoscale using nanoparticles that talk to one another. *Nat. Commun.* **2017**, *8*, 15511.
29. de Luis, B.; Llopis-Lorente, A.; Rincón, P.; Gadea, J.; Sancenón, F.; Aznar, E.; Villalonga, R.; Murguía, J.R.; Martínez-Máñez, R. An interactive model of communication between abiotic nanodevices and microorganisms. *Angew. Chem. Int. Ed.* **2019**, *58*, 14986–14990.
30. de Luis, B.; Llopis-Lorente, A.; Sancenón, F.; Martínez-Máñez, R. Engineering chemical communication between micro/nanosystems. *Chem. Soc. Rev.* **2021**, *50*, 8829–8856.
31. de Luis, B.; Morellá-Aucejo, A.; Llopis-Lorente, A.; Godoy-Reyes, T.M.; Villalonga, R.; Aznar, E.; Sancenón, F.; Martínez-Máñez, R. A chemical circular communication network at the nanoscale. *Chem. Sci.* **2021**, *12*, 1551–1559.
32. Sancenón, F.; Pascual, L.; Oroval, M.; Aznar, E.; Martínez-Máñez, R. Gated silica mesoporous materials in sensing applications. *ChemistryOpen* **2015**, *4*, 418–437.
33. Otri, I.; El Sayed, S.; Medaglia, S.; Aznar, E.; Martínez-Máñez, R.; Sancenón, F. Simple endotoxin detection using polymyxin-B-gated nanoparticles. *Chem. Eur. J.* **2019**, *25*, 3770–3774.
34. Pascual, L.; El Sayed, S.; Marcos, M.D.; Martínez-Máñez, R.; Sancenón, F. Acetylcholinesterase-capped mesoporous silica nanoparticles controlled by the presence of inhibitors. *Chem. Asian J.* **2017**, *12*, 775–784.
35. El Sayed, S.; Milani, M.; Licchelli, M.; Martínez-Máñez, R.; Sancenón, F. Hexametaphosphate-capped silica mesoporous nanoparticles containing Cu(II) complexes for the selective and sensitive optical detection of hydrogen sulfide in water. *Chem. Eur. J.* **2015**, *21*, 7002–7006.
36. Ribes, A.; Santiago-Felipe, S.; Xifre-Pérez, E.; Tormo-Mas, M.A.; Peman, J.; Marsal, L.F.; Martínez-Máñez, R. Selective and sensitive

probe based in oligonucleotide-capped nanoporous alumina for the rapid screening of infection produced by *Candida albicans*. *ACS Sens.* **2019**, *4*, 1291–1298.

37. Zebib, B.; Mouloungui, Z.; Noirot, V. Stabilization of curcumin by complexation with divalent cations in glycerol/water system. *Bioinorg. Chem. Appl.* **2010**, *2010*, 292760.
38. Reddy, A.C.P.; Sudharshan, E.; Rao, A.G.A. Interaction of curcumin with human serum albumin-A spectroscopic study. *Lipids* **1999**, *34*, 1025–1029.
39. Bourassa, P.; Kanakis, C.D.; Tarantilis, P.; Pollissiou, M.G.; Tajmir-Riahi, H.A. Resveratrol, genistein, and curcumin bind bovine serum albumin. *J. Phys. Chem. B*. **2010**, *114*, 3348–3354.
40. Argyo, C.; Weiss, V.; Bräuchle, C.; Bein, T. Multifucntional mesoporous silica nanoparticles as a universal platform for drug delivery. *Chem. Mater*. **2014**, *26*, 435–451.
41. Kankala, R.K.; Han, Y.-H.; Na, J.; Lee, C.-H.; Sun, Z.; Wang, S.-B.; Kimura, T.; Ok, Y.S.; Yamauchi, Y.; Chen, A.-Z.; et al. Nanoarchitectured structure and surface biofunctionality of mesoporous silica nanoparticles. *Adv. Mater.* **2020**, *32*, 1907035.
42. Martínez-Máñez, R.; Sancenón, F.; Hecht, M.; Biyical, M.; Rurack, K. Nanoscopic optical sensors based on functional supramolecular hybrid materials. *Anal. Bioanal. Chem.* **2011**, *399*, 55–74.
43. Zeng, X.; Ma, M.; Zhu, B.; Zhu, L. A near infrared fluorescent probe for sensitive determination of human serum albumin. *Anal. Sci.* **2016**, *32*, 1291–129

Chapter 5. Exploring Synergy Between nanoformulated Linezolid and Polymyxin B as a Gram-negative Effective Antibiotic Delivery System Based on Mesoporous Silica Nanoparticles

5.1 Exploring Synergy Between nanoformulated Linezolid and Polymyxin B as a Gram-negative Effective Antibiotic Delivery System Based on Mesoporous Silica Nanoparticles

Ismael Otri,[a,b] Serena Medaglia,[a,b,] Elena Aznar, [a,b,c,d*] and Félix Sancenón,[a,b,c,d*]

[a)] Instituto Interuniversitario de Investigación de Reconocimiento Molecular y Desarrollo Tecnológico (IDM), Unidad Mixta Universitat Politècnica de València - Universitat de València, Spain

[b)] Departamento de Química, Universitat Politècnica de València, Camino de Vera s/n, 46022, Valencia, Spain. E-mail: rmaez@qim.upv.es

[c)] CIBER de Bioingeniería, Biomateriales y Nanomedicina (CIBER-BBN)

[d)] Unidad Mixta de Nanomedicina y Sensores. Universitat Politècnica de València - Instituto de Investigación Sanitaria La Fe (IIS La Fe). Avda. Fernando Abril Martorell, 106, 46026, Valencia, Spain.

**Correspondence:* elazgi@upvnet.upv.es *(E.A.); fanceno@upvnet.upv.es (F.S.)*

Submitted

Graphic abstract

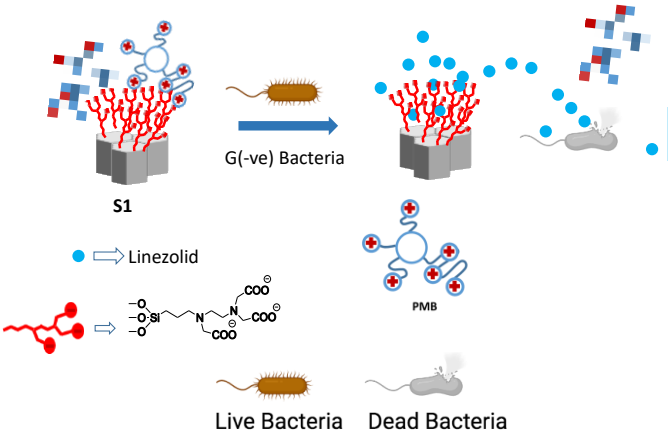

5.1 Abstract

Antimicrobial resistance is a current silent pandemic that needs new types of antimicrobial agents different from the classic antibiotics that are known to lose efficiency over time. Encapsulation of antibiotics inside nanodelivery systems could be a promising effective strategy able to delay the capability of pathogens to develop resistance mechanisms against antimicrobials. These systems can be adapted to deliver already discovered antibiotics to specific infection sites and not to the healthy tissues in a more successful way. Herein mesoporous silica nanomaterials are used for a more efficient delivery of linezolid gram-positive antibiotic thanks to a synergetic effect with gram-negative antimicrobial Polymyxin B in both types of bacteria. For this purpose, linezolid is encapsulated inside the nanomaterial pores and the outer surface is coated with polymyxin B membrane disruptor. The obtained results demonstrate that the prepared nanodelivery system works with a double step mechanism which favors a highly increased antimicrobial efficiency against gram-negative where free linezolid is not effective. Also, enhanced toxicity of the nanoformulation against gram-positive bacteria was confirmed thanks to the combination of both antibiotics in the same nanoparticle.

5.2 Introduction

The world health organization (WHO) considers the raising resistance of microorganisms to antibiotics as the coming pandemic.[1,2] Through the years, microorganisms are becoming more resistant to many existing antimicrobials. It is foreseen that everyday infections will not be able to be treated with current antibiotics in a near future. Antimicrobial resistance (AMR) causes at least 700,000 deaths around the world each

year. These numbers are estimated to reach 10 million by 2050.[3,4] Over the years pathogens were able to increase their resistance to antibiotics by mutation and selection concepts.[5,6,7] This is accelerated by the inappropriate use of these medicines as well as the lack of research and money invested by governments and the pharmaceuticals industry to develop new antibiotics. In the last 10 years, new molecular-based antibiotics are not discovered as it is a slow and expensive process that takes 10–15 years and over 1 billion €.[8] Currently most of the available antibiotics are losing their efficiency. For example, according to WHO report in November 2021, *Staphylococcus aureus* bacterium, which is part of our skin flora and a common cause of infections both in the community and in healthcare facilities, is becoming resistant to most antibiotics treatments. For example, people suffering infections caused by *methicillin-resistant S. aureus (MRSA)* are 64% more likely to die.[9] Huge efforts are needed to tackle AMR to avoid the collapse of the world health systems, the economic impact and the number of deaths caused by infections. A part from governments investment and changing human behavior by introducing awareness to the people about the problem and the current status of the situation, research and development of new antimicrobial medicines, vaccines, and diagnostic tools are urgently required especially for gram-negative bacteria such as *Pseudomonas aeruginosa*, *carbapenem-resistant Enterobacteriaceae, MRSA* or *Acinetobacter baumannii* were most current antibiotics are far away of being sufficiently efficient.

Currently, there are several strategies for the development of new antimicrobials thanks to the discovery of new biological, biochemical o chemical tools such as bacteriocins, phage therapy, antimicrobial heavy metals, lysins, lactam antibiotics[10,11] or antimicrobial peptides.[12] Also in this research area, encapsulation of antibiotics inside porous nanomaterials has emerged as a promising solution to slow down the rapid increase in resistance.[13,14] Antibiotics confinement in porous materials was found to decrease stimulation and activation of the resistance mechanism of resistance organism.[15] At the same time this strategy decreases the side effects and toxicity caused by some antibiotics.[16,17]

For example, gram-negative bacteria develop resistance to antibiotics faster than gram-positive ones due to their membrane structure composed of an inner peptidoglycan thin layer and an outer negatively charged lipopolysaccharide (LPS) membrane, which provides high protection against a wide range of antibiotics.[18] Most of antibiotics used to treat gram-negative infections cause toxicity by distributing the LPS layer through interaction or degradation. As mentioned above, using nanomaterials for the delivery of antibiotics could be a promising strategy to protect antimicrobials from resistance. Nanomaterials can provide protection against enzyme degradation in cells and increase their circulation time in body fluids while the antibiotics are encapsulated inside the nanomaterials. The nanoparticle surface also presents an opportunity to improve antimicrobial efficiency. By functionalization of the outer surface by different molecules such as targeting agents for specific delivery to infective cells, a decrease in the side effects can be achieved. Also coating

the outer surface with hydrophilic and penetrating molecules can improve the ability to cross body membranes and to extend circulation lifetime.[19] Nanomaterials open the possibility to use antibiotics that are hydrophobic, present very short circulation time or need a high dose to be effective. Several nanomaterials were used for the delivery of antibiotics including polymers,[20] liposomes,[21] hydrogels,[22] nanoemulsions,[23] lipid Nanoparticles[24] and others.[25] Mesoporous silica nanoparticles have been investigated over the last decade for delivery applications due to their excellent properties such as a high surface area combined with high cargo capability, their ease of synthesis and functionalization with a wide range of molecules using simple chemistry. Also, the inertness, thermal stability and homogeneity of the inner porous, are features which made these nanomaterials excellent candidates[26] for antimicrobials delivery.[27] In most cases, antibiotics were first loaded in the inner pores of mesoporous silica and then the external surface was coated with different molecules and targeting agents. Coating the outer surface with bulk species was found to be effective in the discontinuation of any release of the loaded antibiotics. At the same time, these blocking molecules can work as stimuli-responsive gates which can be triggered by external conditions to prepare a targeted responsive delivery system. In such systems, antibiotic cargo delivery will be induced in the presence of target stimuli and in the infection site.[28] In this context, many mesoporous silica gated hybrid nanomaterials have been prepared to be stimulated by the change of physical conditions such as temperature, electric or magnetic fields or the change of chemical conditions such as pH, redox environment or

the presence of a specific molecule or enzyme.[29] Bearing in mind our previous experience in the preparation of mesoporous silica nanomaterials as hybrid systems for sensing and delivery applications,[30] herein we develop new mesoporous silica nanoparticles for the efficient delivery of linezolid antibiotic in bacteria.

Linezolid belongs to the oxazolidinones family and it is an aggressive antibiotic effective against serious infections caused by bacteria in the skin and soft tissues.[31] At physiological pH, linezolid has moderate solubility around 3.0 mg/mL.[32] Due to this limited solubility and side effects, it could be noteworthy to prepare a delivery system to release linezolid in specific infection sites. Such system will overcome the limited solubility and provide protection against degradation as well as will slow down the capability of bacteria to develop resistance.

Herein we present a novel hybrid silica nanomaterial for the effective delivery of linezolid based on a polymyxin-gated system. The nanomaterial consist of ordered mesoporous nanoparticles loaded with the antibiotic linezolid and functionalized with carboxylate moieties able to interact with the positively charged antimicrobial agent polymyxin B (PMB). When PMB interacts with carboxylates, it is able to cap the pores and act as stimuli-responsive molecular gate. Thanks to PMB ability to interact with high affinity with LPS of bacteria outer surface,[33,34] when a bacterium is present, PMB will be displaced from nanomaterials surface will i) permeate bacterium outer membrane and ii) trigger the on-site release of linezolid. It was expected that this synergic action facilitates the killing of bacteria as depicted in Scheme 1.

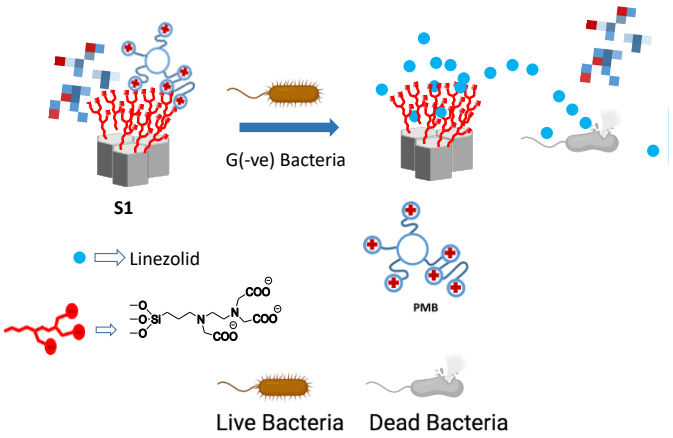

Scheme 1. Schematic representation of the prepared nanomaterial **S1** and its release mechanism.

To obtain the nanomaterial, ordered mesoporous nanoparticles were prepared by known procedures using n-cetyltrimethylammonium bromide (CTABr) as a template and tetraethylorthosilicate (TEOS) as silicon precursor. After removing the surfactant by calcination, the empty pores were loaded with linezolid and the external surface was functionalized using n-[(3-trimethoxysilyl)propyl]ethylene diamine triacetic acid trisodium salt to obtain a negatively charged surface. The final nanomaterial was obtained by adding PMB. The electrostatic interaction between the anionic charge of carboxylate moieties and the cationic PMB block the pores of the nanoparticles as shown in Scheme 1 (See Supporting Information for the detailed procedures).

Different characterization methods were used to examine the correct preparation of the nanomaterial. First, the starting mesoporous silica nanoparticles (MSN) before and after surfactant removal by calcination at 550 °C were characterized using powder X-ray diffraction (PXRD) to determine the correct MCM-41 type hexagonal pore array. Transmission electron microscopy (TEM) was

used to study the size of nanoparticles and isotherm N_2 adsorption-desorption experiments were performed to assess the total surface area and pore size of the MSN. As it can be appreciated in Figure 1a PXRD studies of the parent as-made nanomaterial showed the four typical low-angle reflections of a hexagonal-ordered mesoporous matrix indexed as (100), (110), (200) and (210) Bragg. Additionally, Figure 1b displays the PXRD of calcined MSN were a slight shift of the main (100) peak was observed, which corresponds to a cell contraction of ca. 3 Å due to the condensation of silanol groups in the calcination step. In a further step, Figure 1c shows PXRD pattern of the final material **S1** obtained after loading the pores with linezolid and capping with PMB. A slight intensity reduction in the (100) reflection and loss of the (110) and (200) reflections are observed, most likely due to the reduced contrast after the loading/functionalization process. Nevertheless, the permanence of the (100) reflection in the PXRD pattern strongly evidences that the mesoporous structure is maintained in the final gated nanoparticles as it can be also observed in TEM studies of calcined MSN (Figure 1d) and **S1** (Figure 1e). Representative TEM images of both solids showed spherical nanoparticles with a similar average diameter of ca. 110 nm.

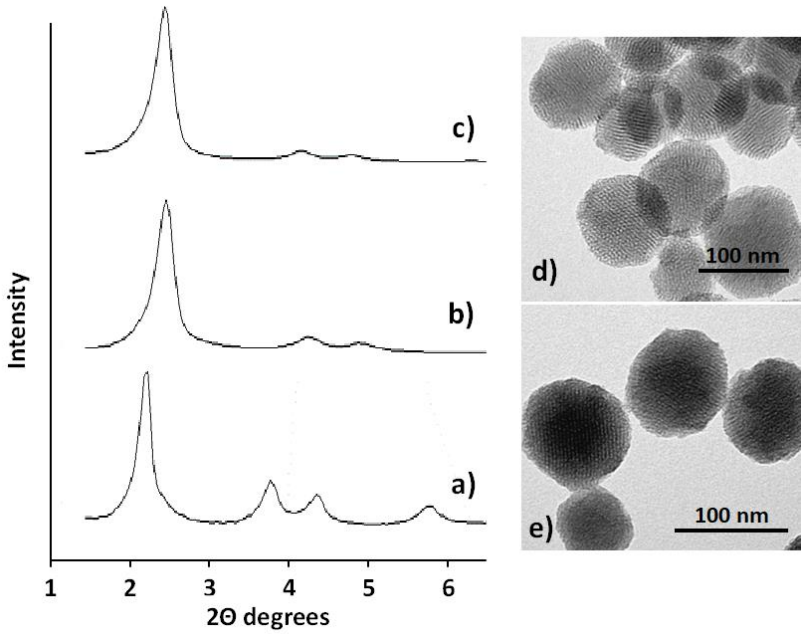

Figure 1. Left: powder X-ray patterns of (a) as-synthesized MSN, (b) calcined MSN and (c) solid **S1**. Right: Representative TEM images of (d) calcined MSN sample and (e) solid **S1**.

N_2 adsorption–desorption isotherm studies were also performed. Specific surface area was calculated by the application of the Brunauer–Emmett–Teller (BET) model.[35] Pore size and pore volume was calculated by using the Barret–Joyner–Halenda (BJH) model[36] on the adsorption branch of the isotherm. Calcined MSN showed the typical curve for mesoporous materials and a high surface area (1069 m^2g^{-1}) and pore volume (2.66 nm) were recorded (Table 1). In contrast, solid **S1** showed a reduced surface area (279 m^2g^{-1}) and no significant pore size due to the filling of mesopores and further external functionalization and capping processes. Table 1 resumes the main structural characterization parameters for both materials.

Table 1. Main structural properties of nano-sized materials determined by TEM and N_2 adsorption analysis.

Sample	Diameter particle (nm)	Surface area, S_{BET} ($m^2\ g^{-1}$)	Pore Volume ($cm^3\ g^{-1}$)	Pore size (nm)
calcined MSN	110	1011	0.86	2.66
S1	122	279	0.14	-

Finally, organic content of **S1** was determined by thermogravimetric analysis (TGA). Table 2 shows the organic content (mmol per gram of SiO_2) of linezolid, carboxylate moieties and PMB in the final material.

Table 1. Content (α) of anchored dye and PMB in S1.

Solid	$\alpha_{Linezolid}$ (mmol g^{-1} SiO_2)	$\alpha_{Carboxylate\ moieties}$ (mmol g^{-1} SiO_2)	α_{PMB} (mmol g^{-1} SiO_2)
S1	0.238	0.060	0.175

In a further step, controlled release experiments to confirm that the electrostatic interaction between the anionic tricarboxylate derivative anchored in the solid surface and the capping cationic PMB was the force that combine the two layers together to prevent cargo release were performed. A release mechanism analysis using pH changes was conducted using a rhodamine B (RhB) loaded solid **S1-Rh** to mimic solid **S1**. 1 mg of **S1-Rh** was suspended in 1 mL of distilled water solution at different pHs (2, 4 and 7). At a certain time, aliquots were taken and filtered. The delivery of the rhodamine B dye was then monitored by measuring the fluorescence emission of RhB at 571 nm (λ_{exc} 555 nm). As shown in Figure 2, only strong acidic pH was able to break these interactions which resulted in rapid release of the dye.

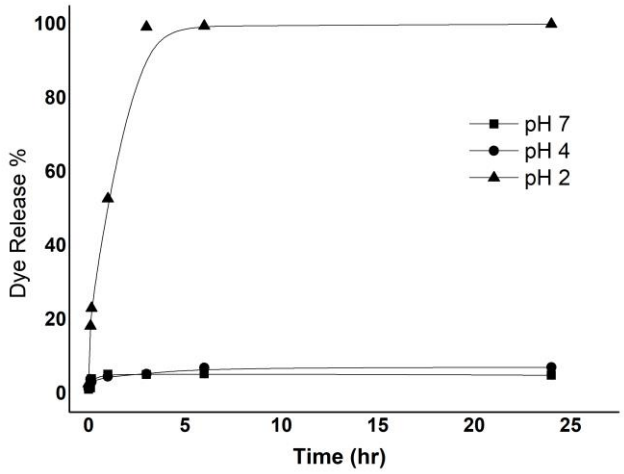

Figure 2. Kinetic release of RhB from **S1-Rh** at different pHs.

In our hypothesis, the recognition of PMB by LPS in the outer cell wall was the stimulus to open the gated nanoparticles. Likewise, the affinity of the PMB capping layer to LPS was tested using solid **S1-Rh**. A kinetic release using LPS was performed in aqueous solutions where 1 mg of **S1-Rh** was suspended in 1 mL of LPS-free phosphate buffer saline (PBS, pH 7.4), in the presence of 2.5 mg of LPS and absence (control). At a certain time, the aliquots were separated and filtered. Delivery of the RhB dye to the bulk solution was then monitored by fluorescence (emission at 571 nm). As it can be appreciated in Figure 3, in the absence of LPS no release of RhB was registered as a result of the strong interaction between the grafted tricarboxylate derivative and PMB. In contrast, the presence of LPS induced a fast release of the dye to the outer solution, which confirmed the gating mechanism associated to the LPS-PMB which triggers the displacement of PMB from the solid surface and allows cargo release.

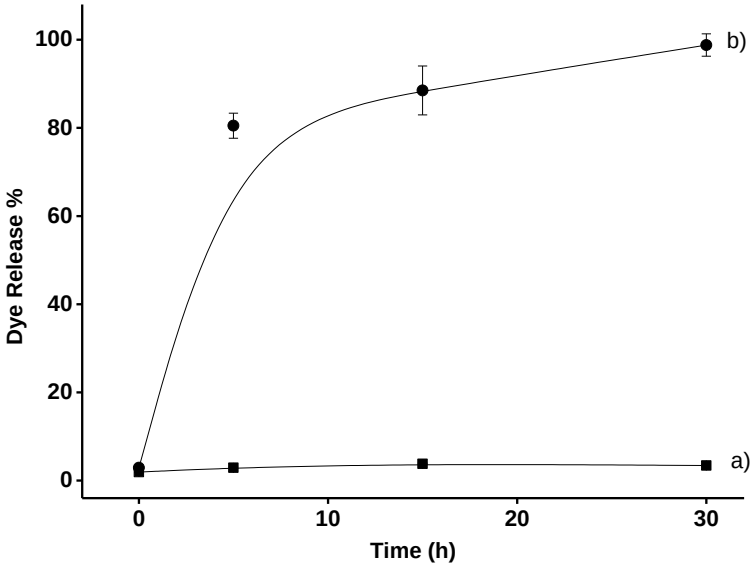

Figure 3. Kinetic release of RhB from **S1-Rh** a) in the absence and b) in the presence of LPS.

Using the same experimental conditions, release profile in the presence of gram-negative bacteria *Escherichia coli* (DH5α strain) was tested. As it can be observed in Figure 4, release of the encapsulated molecule from the gated material is inhibited in the absence of bacteria but a massive cargo release was observed in the presence of bacteria, which confirmed the ability of the prepared nanoparticles to release specifically their content only in a bacterial environment. It is expected that this selectivity of the prepared nanomaterials to target gram-negative bacteria will increase the concentration of antibiotic in the cell surroundings and consequently increase the toxicity caused by linezolid.

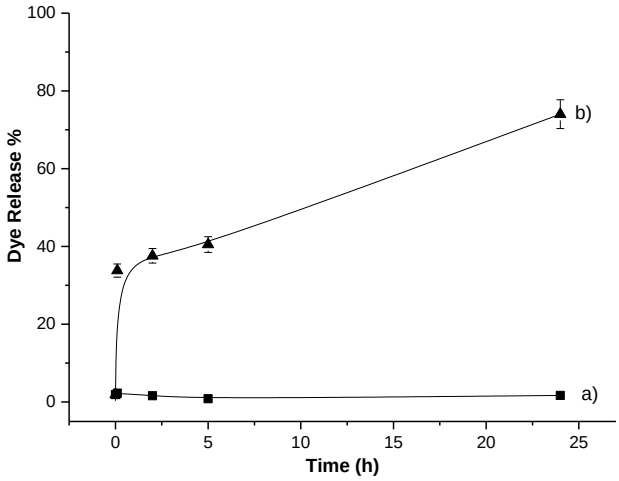

Figure 4. Kinetic release of RhB from **S1-Rh** a) in the absence and b) in the presence of bacteria.

Once the gating mechanism was confirmed. Antimicrobial experiments with **S1** solid loaded with linezolid were performed. *E. coli* (DH5α strain) cell viability was tested upon increasing concentrations of **S1**, (0 to 1 μg/mL in PBS at pH 7.4). Several controls such as free linezolid, and a mixture of free linezolid with PMB were used. For viability studies, *E. coli* (DH5α strain) bacteria cells were enriched in LB agar and LB broth following the recommended conditions. After incubation overnight at 37 °C in LB medium under continuous stirring, bacteria of 1 mL of culture were collected by centrifugation and resuspended in 1 mL of PBS. Then a dilution of 10^5 cells/mL was prepared using turbidimetry measurements (OD_{620}). Clonogenic viability assays of a series of dilutions of **S1**, linezolid and mixture of linezolid and PMB were performed. Each antimicrobial agent (**S1**, free linezolid or the mixture of linezolid and PMB) at the target concentration was mixed with the *E. coli* dilution and stirred for 10 min. Then an

aliquot of 100 µL was diluted 1:10 to get final countable CFU and seeded in a LB agar plate. All plates were incubated at 37°C overnight. CFU were counted in each plate and the percentage of cytotoxicity was determined in comparison with a negative control of *E. coli* bacteria without antimicrobial treatment (100% viability). As in can be appreciated in Figure 5, free linezolid was not toxic to the bacteria even at high concentrations of 1 µg/mL. When the non-sensitive to gram negative linezolid was mixed with equimolar concentrations of membrane disruptor PMB, a decrease of viability was found. A Minimum Inhibitory Concentration (MIC) around $1x10^{-2}$ µg/mL was estimated. Noteworthy, when bacteria were treated with **S1** loaded with linezolid and capped with PMB, the calculated MIC was 10^5 times lower ($1x10^{-7}$ µg/mL) for **S1**.

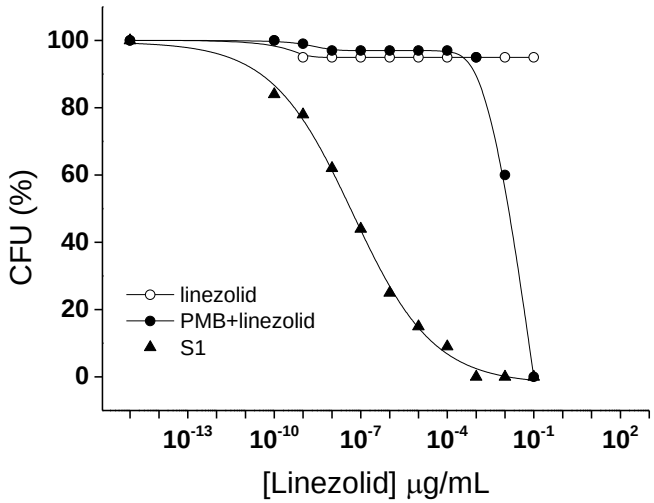

Figure 4: Clonogenic *E. coli* viability assays CFU (%) treated at different concentration of linezolid, mixture of linezolid and PMB and solid **S1**.

These results confirmed that **S1** nanomaterial works as a double toxic agent. First PMB interacts with LPS on the cell membrane causing an efficient membrane disruption which facilitates a

delivery of linezolid closer to the disrupted membrane and resulted more lethal to bacteria. Nanoformulated combination of both antimicrobial agents in **S1** was found to be remarkably more efficient than the combination of both free linezolid and PMB, probably thanks to the simultaneous proximity of both antibiotics to the bacteria. The obtained results demonstrates the benefits of using this nano delivery system to increase the toxicity of current antibiotics against pathogens.

In a step forward, the feasibility of **S1** against gram-positive *S. aureus* compared to gram-negative *E. Coli* was examined. A standard broth microdilution method in a 96-well plate reader was used to determine bacterial growth by OD_{620} and to calculate the antibacterial activity (MIC), see supporting information for more details. For each bacterium, the viability percentage was detected in the presentence of **S1**, free PMB and free linezolid at different concentrations, each sample was repeated 3 times. Linezolid alone was not toxic for *E. coli* (MIC > 1 μg/mL) and slightly toxic for *S. aureus* (MIC $1.22x10^{-1}$ μg/mL). Free PMB showed higher activity (MIC $1.95x10^{-5}$ μg/mL for *E. coli* and (MIC $2.41x10^{-4}$ μg/mL) for *S. aureus*). However, **S1** nanomaterial caused 100-fold and 10-fold stronger growth inhibition than PMB in *E. coli* (MIC $1.23x10^{-7}$ μg/mL) and *S. aureus* (MIC $2.76x10^{-5}$ μg/mL), respectively. For example, as depicted in Figure 6, using only $1x10^{-4}$ μg/mL of **S1**, bacteria viability in both types of bacteria was remarkably reduced. From these experiments, it can be concluded that encapsulation of linezolid in a PMB capped nanomaterial enhanced the antimicrobial efficiency against gram-positive and gram-negative bacteria.

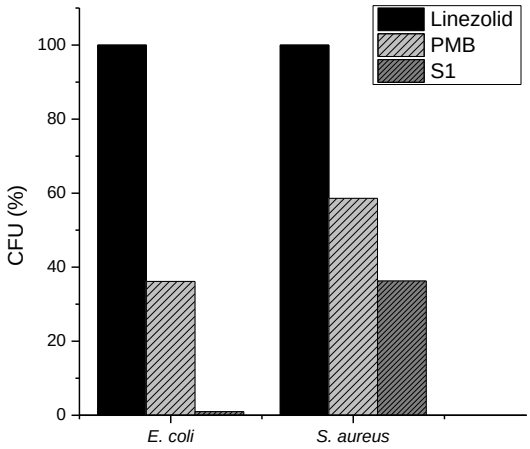

Figure 6. Bacterial viability (% CFU) of *E. coli* and *S. aureus* treated with $1x10^{-4}$ μg/mL of linezolid, PMB and solid **S1**.

In summary, we report herein a new hybrid nanomaterial for the synergic delivery of antibiotics. Linezolid has loaded in silica mesoporous nanoparticles and PMB was used to cap the pores od the nanomaterial and block linezolid release. When the nanomaterial is close to bacteria, PMB interacts with high affinity with LPS of bacteria outer surface and is displaced from nanomaterials surface permeating bacterium outer membrane and triggering the on-site release of linezolid. The antimicrobial activity of the prepared nano delivery system was tested against gram-negative (*E. coli*) and gram-positive *S. aureus*. The results demonstrate that the prepared nanoformulation **S1** enhanced the antimicrobial efficiency against these strains. These results demonstrate the potential of using mesoporous silica nanomaterials as a delivery system for antibiotics with enhanced efficiency, target delivery and the ability to decrease the raising

resistance against antibiotics, which are important factors to overcome antimicrobial resistance.

5.3 Acknowledgements

This research was funded by the Ministerio de Ciencia, Innovación y Universidades (Spanish Government) (projects RTI2018-100910-B-C41 and RTI2018-101599-B-C22-AR (MCUI/FEDER, EU)) and the Generalitat Valenciana (project PROMETEO 2018/024). I.O. thanks Erasmus Mundus Programme, Action 2, Lot 1, Syria, for his predoctoral fellowship. S.M. thanks the Generalitat Valenciana for her Grisolía fellowship.

5.4 References

1 O. J, *Rev. Antimicrob. Resist.*, 2016, 1–81.

2 J. O'Neill, Tackling drug-resistant infections globally: Final report and recommendations" (Wellcome Trust, 2016);https://wellcomecollection.org/works/thvwsuba.

3 WHO, World Health Organization, "No Time to Wait: Securing the Future from Drug Resistant Infections", www.who.int/antimicrobial-resistance/ interagency-coordination-group/final-report/en/.

4 Government of Canada, "Tackling antimicrobial resistance and antimicrobial use: A Pan Canadian Framework for Action" (2017); www.canada.ca/en health-canada/services/publications/drugs-health-products/tackling-antimicrobial-resistance-use-pan-canadianframe.

5 A. Brauner, O. Fridman, O. Gefen and N. Q. Balaban, *Nat. Rev. Microbiol.*, 2016, 320–330.

6 M. A. Kohanski, D. J. Dwyer and J. J. Collins, *Nat. Rev. Microbiol.*, 2010, **8**, 423–435.

7 J. M. A. Blair, M. A. Webber, A. J. Baylay, D. O. Ogbolu and L. J. V. Piddock, *Nat. Rev. Microbiol.*, 2015, **13**, 42–51.

8 M. Miethke, M. Pieroni, T. Weber and E. Al., *Nat Rev Chem*, 2021, **5**, 726–749.

9 WHO, Antimicrobial resistance.
10 D. J. Payne, M. N. Gwynn, D. J. Holmes and D. L. Pompliano, *Nat. Rev. Drug Discov*, 2007, **6**, 29–40.
11 M. E. Evans, D. J. Feola and R. P. Rapp, *Ann. Pharmacother*, 960–967.
12 Y. Wang, A. G. Cheetham, G. Angacian, H. Su, L. Xie and H. Cui, *Adv. Drug Deliv. Rev.*, 2017, **110**–**111**, 112–126.
13 V. Van Giau, S. S. A. An and J. Hulme, *Drug Des Devel Ther*, 2019, **13**, 327–343.
14 Z. Tang, Q. Ma, X. Chen, T. Chen, Y. Ying, X. Xi, L. Wang, C. Ma, C. Shaw and M. Zhou, *Antibiotics*, 2021, **990**, 1–26.
15 J. Ndayishimiye, T. Kumeria, A. Popat, J. R. Falconer and M. A. T. Blaskovich, *ACS Infect. Dis*, 2022, 693–712.
16 P. Severino, E. F. Silveira, K. Loureiro, M. V. Chaud, D. Antonini, M. Lancellotti, V. H. Sarmento, C. F. da Silva, M. H. A. Santana and E. B. Souto, *Eur. J. Pharm. Sci.*, 2017, **106**, 177–184.
17 Z. L. Wu, J. Zhao and R. Xu, *Int J Nanomedicine*, 2020, **15**, 9587–9610.
18 M. J. Hajipour, K. M. Fromm, A. A. Ashkarran, D. J. de Aberasturi, I. R. de Larramendi, T. Rojo, V. Serpooshan, W. J. Parak, M. Mahmoudi and 499 –511 Trends Biotechnol. 2012, 30, *Trends Biotechnol*, 2012, **30**, 499 –511.
19 M. J. Mitchell, M. M. Billingsley, R. M. Haley, M. E. Wechsler, N. A. Peppas and R. Langer, *Nat. Rev. Drug Discov.*, 2021, **20**, 101–124.
20 S. Okonogi, P. Phumat and S. Khongkhunthian, *Bioprocess Biosyst. Eng.*, 2021, **44**, 1289–1300.
21 G. A. Gonzalez and Z. Hosseinidoust, *ACS Infect. Dis.*, 2020, **6**, 896–908.
22 A. . Simonson, A. Lawanprasert, T. D. . Goralski, K. . Keiler and S. . Medina, *Nanomedicine*, 2019, **17**, 391–400.
23 C. . Garcia, M. . Malik, S. Biswas, V. . Tam, K. . Rumbaugh and X. Li, W.; Liu, *Biomater. Sci.*, 2022, **10**, 633–653.
24 S. Khatak, M. Mehta, R. Awasthi, K. . Paudel, S. . Singh, M. Gulati, N. . Hansbro, P. . Ansbro, K. Dua and H. Dureja, *Tuberculosis*, **125**, 02008.
25 Tong-Xin Zong, A. P. Silveira, J. A. V. Morais, M. C. Sampaio, L. A. Muehlmann, J. Zhang, C.-S. Jiang and Shan-Kui Liu 1,

Nanomaterials, 2022, **11**, 1855.
26 Q. Xie, H. Lu, X. Wang, Y. Zhang and N. Zhou, *J. Environ. Chem. Eng.*, 2021, **5**, 105892,.
27 M. Martínez-Carmona, Y. K. Gun'ko and and M. Vallet-Regí, *Pharmaceutics*, 2018, **4**, 279.
28 D. Ş. Karaman, A. Pamukçu, M. B. Karakaplan , O. Kocaoglu and J. M. Rosenholm , *Int J Nanomedicine*, 2021, **16**, 6575–6591.
29 E. Aznar, M. Oroval, L. Pascual, J. R. Murguía, R. Martínez-Máñez and F. Sancenón, *Chem. Rev.*, 2016, 116, 561–718.
30 F. Sancenón, L. Pascual, M. Oroval, E. Znar and R. Martínez-Máñez, *ChemistryOpen*, 2015, 418–437.
31 AP. Wilson, JA. Cepeda, S. Hayman, T. Whitehouse, M. Singer and G. Bellingan, *J. Antimicrob. Chemother.*, 2006, **58**, 470–473.
32 D. J. Herrmann, W. J. Peppard, N. A. Ledeboer, M. L. Theesfeld, J. A. Weigelt and B. J. Buechel , *Expert Rev. Anti-infective Ther.*, 2008, **6**, 825–48.
33 D. Ferrari, C. Pizzirani, E. Adinolfi, S. Forchap, B. Sitta, L. Turchet, S. Falzoni, M. Minelli, R. Baricordi and F. D. Virgilio, *J Immunol.173 4652-4660*, 2004, **173**, 4652–4660.
34 H. Shoji, *Ther. Apher. Dial.*, 2003, **7**, 108–114.
35 S. Brunauer, P. H. Emmett and E. Teller, *J. Am. Chem. Soc.*, 1938, 309–319.
36 E. Barrett, L. Joyner and P. Halenda, *J. Am. Chem. Soc.*, 1951, **73**, 373–380.

5.6 Supporting Information

5.6.1 Chemicals

Tetraethylorthosilicate (TEOS), n-cetyltrimethyl ammonium bromide (CTABr), sodium hydroxide (NaOH), rhodamine B, tris(hydroxymethyl)aminomethane (TRIS), Endotoxin free Dulbecco's PBS (1X) and Lipopolysaccharides from Escherichia coli O55:B5 (LPS) purchased from Sigma-Aldrich Química (Madrid, Spain), LPS from R. sphaeroides (LPS-RS) were purchased from InvivioGen, USA. N-[(3-trimethoxysilyl) propyl] ethylene diamine

triacetic acid trisodium salt from Fluorochem, UK, Polymyxin B sulfte (PMB) was purchased from Tokyo Chemical Industry Co., Ltd. (TCI), Linezolid was purchase from Santa Cruz Biotechnology, Inc, USA. Analytical-grade solvents were from Scharlab (Barcelona, Spain). All products were used as received.

5.6.2 Synthesis of Mesoporous Silica Nanoparticles (MSNs)

N-cetyltrimethylammoniumbromide (CTABr, 1.00 g, 2.74 mmol) was first dissolved in 480 mL of deionized water. Then a 3.5 mL of NaOH 2.00 M in deionized water was added to the CTABr solution, followed by adjusting the solution temperature to 80°C. TEOS (5 mL, 25.7 mmol) was then added dropwise to the surfactant solution. The mixture was allowed stirred for 2 h to give a white suspension. Finally, the solid was centrifuged, washed with deionized water and dried at 60°C (MSNs as synthesized). To prepare the final mesoporous material, the as-synthesized solid was calcined at 550°C in oxygen atmosphere for 5 h in order to remove the template phase.

5.6.3 Synthesis of S1-Rho:

In a typical synthesis, 750 mg of template-free MCM-41 were suspended in a solution of 340 mg of Rhodamine B dye in 10 mL of mili Q water in a round-bottomed flask, (0.8 mmol of dye/g MCM-41). After 24 h stirring at room temperature, 15 mmol/g MCM-41 of N-[(3-Trimethoxysilyl)propyl]ethylendiamine triacetic acid trisodium salt were added and the mixture was stirred for 5.5 h at room temperature. Then, PMB (2.3 mmol/g) was added to the suspension and allowed to stirrer for 2h. This suspension was stirred for 1h at room temperature. Finally, this solid was filtered and washed with PBS in order to remove the unreacted alkoxysilane and the dye remaining outside the pores. The final solid S1 was dried under vacuum at ambient temperature for 12 h.

5.6.4 Synthesis of S1-Linezolid:

750 mg of template-free MCM-41 were suspended in 10 mL of an anhydrous acetonitrile of 375 mg of Linezolid in a round-bottomed flask, (1.1 mmol of Linezolid /g MCM-41). After 24 h stirring at room temperature, 15 mmol/g MCM-41 of N-[(3-Trimethoxysilyl)propyl]ethylendiamine triacetic acid trisodium salt were added and the mixture was stirred for 5.5 h at room temperature. Then, PMB (2.3 mmol/g) was added to the suspension drop by drop and allowed to stirrer for overnight. Finally, this solid was filtered and washed with PBS plus 5% of ACN in order to remove the unreacted alkoxysilane and the linezolid remaining outside the pores. The final solid S1 was dried under vacuum at ambient temperature for 12 h.

5.6.5 Release test with bacterial, free LPS:

In vitro dye-release studies were carried out with S1-Rho solid to test the correct working with bacteria (Escherichia coli, DH5α strain). In a typical experiment, 3000 ug of solid S1-Rho was suspended in PBS at pH 7.2 and divided in three aliquots. 105 cell ml-1 of E. coli, 2500 ug/ml of LPS and blank were added respectively. All suspensions were incubated at room temperature and at given times fractions of suspensions were taken and filtered by 0.22um filter in order to remove the solid. The delivery of the rhodamine B dye was then monitored by the fluorescence emission band at 610 nm (λex=453 nm).

5.6.6 E. coli DH5α culture conditions:

For viability studies, bacteria (Escherichia coli, E. coli) cell culture DH5α was used general enrichment media type LB broth and LB agar from Laboratories Conda. All reagents were used following manufacturer's conditions.

DH5α cells were cultured in LB medium at 37°C overnight with continuous stirring then 1 ml of culture were collected by centrifugation for 30 seconds at 13000 rpm and resuspended in 1 mL PBS. Then a dilution of 10-5 cells/mL was prepared depending on OD620.

5.6.7 Cell viability studies with E. coli DH5α (Clonogenic viability assays to determine S1-Rho, S1- Lin., free PMB And Linezolid cytotoxicity):

Serial dilutions for S1-Rho, S1- Lin., free PMB, free Linezolid and mixed PMB and Linezolid (1000, 100,10, ….10-7 ,0 ug/ml) were prepared in PBS (pH=7.2) then incubated with 10-5 cells ml-1 E.coli DH5α with shaking 150rpm at 37 C for 10 min. then aliquot of 100ul diluted 1:10 to get countable CFU on the plates then 100ul of each was seeded in LB agar plate from each dilution (duplicated each concentration) after that all plates were incubated at 37 C over night. Then Colony Formation Units (CFU) were counted in each plate and the percentage of cytotoxicity was determined in comparison with negative control as 100% viability.

$$\% \text{ viability} = \frac{\#\text{ Of CFU on -ve control}}{\#\text{ Of colony in each concentration}}$$

** The concentration of free Linezolid/PMB was 1mg/ml of each mixed together.

5.6.8 Minimum inhibitory concentrations (MICs) in this case were determined by the standard broth microdilution method in 96-well plate format:

1. 10^{-5} cells ml^{-1} of bacteria was prepared in LB broth for *S. aureus* and *E.coli* then 100ul was filled in 96 well plate for each bacteria separately.
2. Serial dilutions (1000ug to 10^{-7} ml^{-1}) of free linezolid, PMB and S1 were prepared and aliquoted 200ul in each well then added to 10^{-5} cells ml^{-1} of bacteria.

3. Each 96 well plate was prepared for type of bacteria to prevent cross contamination. negative control (media with bacteria only) and blank (media with antibacterial agent only) were performed as well then, all plates were incubated over night at 37 C and repeated three times.
4. Bacterial growth was determined turbidimetrically (OD_{620}) using an Elisa plate reader by calculating the mean of viability for each concentration.

Chapter 6. Discussion

Discussion

The results of this PhD thesis demonstrated the efficacy of MSNs as efficient sensing nanodevices (for the detection of a biological important biomarker such as Human serum albumin, and of lipopolysaccharide) as well as controlled release reservoirs (for linezolid antibiotic with enhanced antimicrobial activity against bacteria).

In the introduction chapter, the beginning of using MSNs as a nanomaterial for both sensing and delivery applications is described. Besides, recent advances and scientific exploitation of these nanomaterials and how are used for forming very sophisticated stimuli responsive nanosystems with several functions and with high sensitivity to external stimulus are also explained. These materials presented several interesting features (such as chemical stability, easy functionalization, high surface area, high loading capacity) and, as a consequence, are excellent candidates for the delivery of several molecules in response to specific external stimuli. Based on this, MSNs were exploited first for the delivery of biomolecules and later as a sensing system for biological molecules of interest. Several examples were illustrated in the introduction chapter to show the state of the art using MSNs for delivery and sensing applications.

In the third chapter, MSNs based nanosystem for the detection of free endotoxin (LPS) was prepared. For this purpose, MSNs are loaded with rhodamine B dye (as the signal molecule) and its external surface was functionalized by n-[(3-trimethoxysilyl)propyl] ethylene diamine triacetic acid. After adding polymyxin B, the electrostatic interaction between polymyxin B and n-[(3-trimethoxysilyl)propyl] ethylene diamine triacetic acid closes the pores and stops the dye from being released. This interaction

mechanism was proved by studying the release of rhodamine B at several pHs (2, 4 and 7). Furthermore, the sensing behavior of the nano-sensor was evaluated based on the release of rhodamine B in the presence of free endotoxin (LPS) in PBS buffer (pH 7.4) over time. In the absence of endotoxin, no significant rhodamine B was released. While in the presence of endotoxin (1000 μg mL-1) a remarkable rhodamine B release was observed (ca. 90% of the total released dye after 30 min). The observed rhodamine B release was ascribed to pore opening due to the formation of a strong complex between the endotoxin and polymyxin B. The high selectivity of the prepared nanosystem was demonstrated by testing cargo release from the nanoparticles in the presence of common possible interfering molecules in environmental samples such as pectin, DNA, RNA, arabinogalactan (AG), β-(1,3)-D-glucan, EDTA, glucose, GTP, endotoxin-free dust and spiked tap water. In addition, the selectivity was tested toward several types of endotoxins from E. coli and R. spheroids. Finally, the limit of detection (LOD) was calculated as low as 100 pg mL-1 using the calibration curve of rhodamine B released from the nanosensor after 30 mins of adding increasing concentrations of LPS. Using standard equations, a very low limit of detection was calculated. As well the prepared nanomaterials present a high recovery rate of around 95-97% when tested with spiked tap water. All the above results make the nanomaterials a powerful candidate for the development of an easy-to-use kit to detect endotoxin in contaminated environmental samples.

In the fourth chapter, considering our interest in the development of new sensing nanodevices to detect biomolecules, the synthesis and characterization of curcumin-capped mesoporous silica nanoparticles for the sensitive and selective

detection and quantification of Human Serum Albumin (HSA) was described. MCM-41 type MSNs were prepared by a standard procedure. Then the inner pores were loaded with rhodamine B and the outer surface was functionalized with (3-aminopropyl) triethoxysilane. Finally, the pores were capped by the addition of curcumin yielding the final nanomaterial. The prepared nanomaterial was characterized using standard techniques such as powder X-ray diffraction (PXRD), transmission electron microscopy (TEM), thermogravimetric analysis, dynamic light scattering (DLS) and elemental analysis. The responsive behavior of the prepared nanosystem in the presence of HSA was measured using fluorescence. Aliquots were taken at scheduled times (0, 5, 15, 30 min), filtered to remove nanoparticles, and cargo release was evaluated by measuring the emission band of rhodamine B at 571 nm. Only the presence of HSA induced a remarkable dye release (nearly 75% of the loaded rhodamine B was delivered after 5 min). As a contrast, in the absence of HSA, rhodamine B release from nanoparticles was negligible. Encouraged by these results, the selectivity of nanomaterials was assessed by testing cargo release against common interfering molecules (such as anions, cations, amino acids, urea and synthetic urine) in biological samples. As a result, only HSA was able to induce pore opening and rhodamine B release. Furthermore, the LOD was evaluated using a calibration curve at the same conditions upon the addition of increasing concentrations of HSA (0.1 to 100 mg/mL). The result showed that the amount of rhodamine B released is proportional to the quantity of HSA added. Finally, we evaluated the performance of the nanosystem to determine HSA in synthetic urine. The results indicated a satisfactory HSA detection with high recovery ratios in the 87–108% range.

In the fifth chapter, MSNs loaded with linezolid and capped with polymyxin B (PMB) are used as antimicrobial agent. As usual, MCM-41 MSNs were prepared and characterized The selectivity of the nanosystem was evaluated at several pHs (2, 4 and 7) with bacteria and free LPS. Only in the presence of Escherichia coli (DH5Aα strain) and LPS cargo was delivered to the outer solution. The prepared nanosystem was used to enhance the antimicrobial efficiency of linezolid. A low water solubility antibiotic normally used at high dosage to reach the needed efficacy normally causes uncomfortable side effects. The efficiency of the nanomaterial was assessed by viability assays with a series of dilutions of free linezolid, a mixture of linezolid with PMB and the prepared nanosystem loaded with linezolid antibiotic. As a result, in the case of using a nanosystem loaded with linezolid and capped with PMB, a remarkable reduction of cell viability was found. After that antimicrobial activity was tested against gram-positive bacteria (S.aureus). Tthe viability percentage was evaluated in the presentence of the prepared nanosystem, free PMB and free linezolid at different concentrations using a standard broth microdilution method Using the prepared nanosystem, a strong growth inhibition to E. Coli and S.aureus was observed. From these results, we demonstrated that encapsulating linezolid in the prepared nanosystem enhanced the antimicrobial efficiency against gram-positive and gram-negative bacteria.

Chapter 7. Future Perspectives and Conclusion

Future Perspectives and Conclusions

This PhD thesis has explored, designed, and synthesized several nanosystems for biochemical applications as sensing systems and for antimicrobial delivery.

The design of stimuli-responsive hybrid silica-based nanomaterials has attracted significant attention for the preparation of sensing devices and for the controlled delivery of biomedical molecules. The present thesis has attempted to explore the possibility to use the recent progress in this research line to design, prepare and test nanomaterials for sensing of biomolecules such as HSA and endotoxin. Besides, stimuli-responsive hybrid silica-based nanomaterials are used also to enhance the antimicrobial efficiency of an antibiotic such as linezolid.

Regarding the first objective of this thesis, in the third chapter, we have prepared a new nanomaterial using mesoporous silica nanoparticles as support, rhodamine B as a reporter and the cationic peptide polymyxin B as a gating mechanism. The obtained nanodevice allowed a highly selective detection of endotoxin. Other interfering agents (such as arabinogalactan, β-(1,3)-D-glucan, pectin, EDTA, glucose, GTP and dust) were unable to induce pore opening. The prepared nanosystem was stable and allow the detection of endotoxin in the 4.0-8.5 pH range. Moreover, the capped nanosystem was used to detect endotoxin in spiked tap water with high recovery rates. The reported results suggest that polymyxin B-gated nanoparticles could be the basis for the development of an easy-to-use kit to detect endotoxin in contaminated environmental samples.

Regarding the second objective of this thesis, in the fourth chapter, we designed a fluorogenic sensing material based on gated mesoporous silica nanoparticles for the selective and

sensitive detection of HSA in buffered aqueous solution and in artificial urine. The prepared nanosystem is based on a mesoporous inorganic scaffold loaded with rhodamine B, with the external surface functionalized with aminopropyl moieties and the pores capped with curcumin. The sensing mechanism arises from a displacement reaction, through the formation of a strong complex between HSA and curcumin, that results in uncapping of the nanoparticles and rhodamine B release. A limit of detection for HSA of 0.1 mg/mL in PBS (pH 7.4)-acetonitrile 95:5 v/v was determined. It was also demonstrated that the prepared nanosystem can be used to determine the concentration of HSA in spiked synthetic urine samples with recoveries in the 87–108% range.

Regarding the last objective of the presented thesis, in the fifth chapter, we designed a new hybrid nanomaterial for the delivery of antibiotics. Linezolid was loaded inside the pores of mesoporous silica nanoparticles and PMB was used to cap the pores of the nanomaterial blocking antibiotic release. Characterization techniques demonstrated the correct preparation of the nanosystem. The antimicrobial activity of the prepared nano-delivery system was tested against gram-negative (E. Coli) and gram-positive (S.aureus) bacteria. The results demonstrate that loading linezolid inside the nanomaterial enhanced the antimicrobial efficiency against these strains. These results demonstrate the potential of using mesoporous silica nanomaterials as a delivery system for antibiotics to enhance its efficiency.

In summary, it can be concluded that several hybrid nanosystems have been developed in this PhD thesis for sensing and controlled release using mesoporous silica nanoparticles. We

hope that the results achieved in this PhD thesis will inspire the development of advanced nanosystems for their application in the field of biomedical areas such as sensing and novel antibiotic nanomedicine to overcome multi-resistance bacteria problems.

References

[1] J. A. Martín-Gago, C. Briones, E. Casero, P. A. Serena, El nanomundo en tus manos: Las claves de la nanociencia y la nanotecnología, Editorial Critica, **2014.**

[2] R.P. Feynman, *Caltech Eng. Sci.* **1960**, *23*, 22-36.

[3] N. Taniguchi, *Proc. Intl. Conf. Prod. Eng. Tokyo, Part II, Japan Society of Precision Engineering*, **1974**.

[4] G. Binnig, H. Rohrer, *Surf. Sci.* **1983**, *126*, 236-244.

[5] G. Binnig, C. Quate, C. Gerber, *Phys. Rev. Lett.* **1986**, *56*, 930-934.

[6] K. S. Novoselov, A. K. Geim, S. V. Morozov, D. Jiang, Y. Zhang, S. V. Dubonos, I. V. Grigorieva, A. A. Firsov, *Science* **2004**, *306*, 666-669.

[7] I. Valov, E. Linn, S. Tappertzhofen, S. Schmelzer, J. van den Hurk, F. Lentz, R. Waser, *Nat. Commun.* **2013**, *4*, 1771.

[8] D. Tarn, C. E. Ashley, M. Xue, E. C. Carnes, J. I. Zink, C. J. Brinker, *Acc. Chem. Res.* **2013**, *46*, 792-801.

[9] S. Sánchez, L. Soler, J. Katuri, *Angew. Chem. Int. Ed.* **2015**, *54*, 1414-1444.

[10] R. Bott, *Springer Handbook of Nanotechnology*, Springer, **2014**.

[11] K. Narendra, S. Kumbhat, *Essentials in Nanoscience and Nanotechnology,* John Wiley & Sons, **2016**.

[12] D. Bobo, K. J. Robinson, J. Islam, K. Thurecht, S. R. Corrie, *Pharm. Res.* **2016**, *33*, 2373-2387.

[13] X. Y. Ling, D. N. Reinhoudt, J. Huskens, Pure Appl. Chem. 2009, 81, 2225-2233.

[14] a) J. D. Van der Waals, Nobel Lecture: Physics 1901-1921, 1967, 255-265. b) J. D. Van der Waals, *"On the continuity of the gaseous and liquid state"*, PhD Dissertation. Leiden University, **1873**.

[15] A. C. R. Villiers, *Hebd. Seances. Acad. Sci*., **1891**, *112*, 536-538.

[16] a) A. Werner, *Nobel Lecture: Chemistry 1901-1921*, **1966**, 256-269. b) K. Bowman-James, *Acc. Chem. Res.*, **2005**, *38*, 671–678.

[17] a) J. M. Lehn, *Nobel Lectures: Chemistry 1981-1990*, World Scientific Publishing Co., **1992**, 444-491; b) G. R. Desiraju, *Nature* **2001**, *412*, 397-40

[18] D. K. Smith, *J. Chem. Edu.,* **2005**, *82*, 393-400.

[19] T. Donglin, L. Tao, Z. Rongchun, W. Qiang, C. Tiehong, S. Pingchuan, R. Ayyalusamy*, J. Phys. Chem. B*, **2017**, 121, 6108-6116.

[20] a) F. P. Schmidtchen, *Chem. Soc. Rev*., **2010**, 39, 3916-3935. b) D. W. Smith, *J. Chem. Edu*., **2005**, 82, 393-400.

[21] a) D. Wua, L. Chen, W. Lee, G. D. Wua, L. Chen, W. Lee, K. Gyeongju, J. Yin, J. Yoon, J. Yin, J, Yoon, *Chem. Rev.*, **2012**, *112*, 1910–1956.; b) H. G. Löhr, F. Vögtle, *Acc. Chem. Res.*, **1985**, *18*, 65-72.; c) M. Takagi, K. Ueno, *Top. Curr. Chem.*, **1984**, *121*, 39-65.

[22] a) B. Kaur, K. Navneet, S. Kumar, *Coord. Chem. Rev.*, **2018**, *358*, 13–69.; b) D. Wua, L. Chen, W. Lee, G. D. Wua, L. Chen, W. Lee, K. Gyeongju, J. Yin, J. Yoon, J. Yin, J, Yoon, *Chem. Rev.*, **2012**, *112*, 1910–1956

[23] a) S. El sayed, M. Licchelli, R. Martínez-Máñez, F. Sancenón, *Chem. Asian J*. **2017**, 18, 2670-2674.; b) M.-V. Salvia, G. Salassa, F. Rastrelli, F. Mancin, *J. Am. Chem. Soc*. **2015**, 137, 11399-11406.; c) S. El sayed, M. Milani, M. Licchelli. Martínez-Máñez, F. Sancenón, *Chem. Eur.J.* **2015**, 21,7002 –7006.; d) M. Oroval, C. Coll, A. Bernardos, M. D. Marcos, R. Martínez-Máñez, D. G. Shchukin, F. Sancenón, *ACS Appl. Mater. Inerfaces*, **2017**, 9, 11332-11336.

[24] K. Ariga, J. P. Hill, M. V. Lee, A. Vinu, R. Charvet, S. Acharya, *Sci. Technol. Adv. Mater.* **2008**, *9*, 014109.

[25] K. Rurack, R. Martínez-Máñez, The supramolecular chemistry of organic-inorganic hybrid materials, **2010**, ed. John Wiley & Sons.

[26] A.B. Descalzo, R. Martínez-Máñez, F. Sancenón, K. Hoffman, K. Rurack, *Angew. Chem.Int. Ed*, **2006**, 45, 5924

[27] R. Casasús, E. Aznar, M. D. Marcos, R. Martínez-Máñez, F. Sancenón, J. Soto, P. Amorós, *Angew. Chem. Int. Ed***. 2006**, 45, 6661.

[28] M. Comes, G. Rodríguez-López, M. D. Marcos, R. Martínez-Máñez, F. Sancenón, J. Soto, L. A. Villaescusa, P. Amorós, D. Beltrán, *Angew. Chem. Int. Ed*. **2005**, 44, 2918.

[29] N. K. Mal, M. Fujiwara, Y. Tanaka, *Nature* **2003**, 421, 350.

[30] N. K. Mal, M. Fujiwara, Y. Tanaka, T. Taguchi, M. Matsukata, *Chem. Mater*. **2003**, 15, 3385.
[31] Q. Yang, S. Wang, P. Fan, L. Wang, Y. Di, K. Lin, F.-S. Xiao, *Chem. Mater*. **2005**, 17, 5999.
[32] P. Nednoor, N. Chopra, V. Gavalas, L. G. Bachas, B. J. Hinds, *Chem. Mater*. **2005**, 17, 3595.
[33] C. Sánchez, *J. Mater. Chem.*, **2005**, *15*, 3557.
[34] a) A. Verma, V. M. Rotello, *Chem. Commun.*, **2005**, *3*, 303; b) U. Drechsler, B. Erdogan, V. M. Rotello, *Chem. Eur. J.*, **2004**, *10*, 5570; c) A. B. Descalzo, R. Martínez-Máñez, F. Sancenón, K. Hoffmann, K. Rurack, *Angew. Chem. Int. Ed.*, **2006**, *45*, 5924; d) F. Mancin, E. Rampazzo, P. Tecilla, U. Tonellato, *Chem. Eur. J.*, **2006**, *12*, 1844; e) I. Willner, B. Basnar, B. Willner, *Adv. Funct. Mater.*, **2007**, *17*, 702.
[35] G. Zhao, *J. Mater. Chem*., **2006**, *16*, 623-625.
[36] D.E. De Vos, M. Dams, B.F. Sels, P. A. Jacobs*, Chem. Rev*., **2002**, 102, 3615.
[37] X. Liu, Y. Du, Z. Guo, S. Gunasekaran, C. -B. Ching, Y. Chen, S. S. J. Leong, Y. Yang, *Microporous Mesoporous Mater*.,**2009**, *122*, 114.
[38] C. Ispas, I. Sokolov, S. Andreescu, Anal. *Bioanal Chem*., **2009**, *393*, 543.
[39] M. Vallet-Regi, M. Colilla, I. J. Izquierdo-Barba, *Biomed.Nanotechnol*., **2008**, *4*, 1.
[40] a) M. Vallet-Regi, F. Balas, D. Arcos, *Angew. Chem., Int. Ed*., **2007**, *46*, 7548; b) K. A. Kilian, T. Bocking, K. Gaus, J. King-Lacroix, M. Gal, J. J. Gooding, *Chem. Commun*., **2007**, 1936.
[41] a) K. A. Kilian, T. Boecking, K. Gaus, M. Gal, J. J. Gooding, *ACS Nano*.,**2007**, *1*, 355; b) A. Jane, R. Dronov, A. Hodges, N. H. Voelcker, *Trends Biotechnol*.,**2009**,*27*, 230.
[42] M. J. Climent, A. Corma, S. Iborra, J. Primo, *J. Catalysis* **1995**, *151*, 60-66
[43] a) K. S. W. Sing, D. H. Everett, R. H. W. Haul, L. Moscou, R. A. Pierotti, J. Rouquerol, T. Siemieniewska, *Pure Appl. Chem.*, **1985**,

57, 603; b) C. T. Kresge, M. E. Leonowicz, W. J. Roth and J. C. Vartuli, Synthetic Mesoporous Crystalline Material, *US Patent* 5,098,684, March 24, **1992**.

[44] S. A. Bagshaw, E. Prouzet, T. J. Pinnavaia, *Science.*, **1995**, *269*, 1242.

[45] A. Vinu, K. Z. Hossain, K. Ariga, *Nanosci. Nanotech*., **2005**, *5*, 347.

[46] S. Huh, J. W. Wiench, J.-C. Yoo, M. Pruski, V. S.-Y. Lin, *Chem. Mater*., **2003**, *15*, 4247.

[47] J. Kecht, A. Schlossbauer, T. Bein, *Chem. Mater*.,**2008**, *20*, 7207.

[48] E. Climent, Desing of new hybrid materials: Study of its application in new detection formats and in controlled release, **2013**, ISBN: 978-84-9048-015.

[49] F. Juan, E. Ruiz-Hitzky, *Adv. Mater*., **2000,** 12, 430.

[50] F. Hoffmann, M. Cornelius, J. Morell, M. Fröba., *Angew. Chem. Int. Ed*., **2006**, 45, 3216.

[51] U. Ciesla, M. Grün, T. Isajeva, A. A. Kurganov, A. V. Neimark, P. I. Ravikovitch, S. Schacht, F. Schüth, K. K. Unger., *Access in Nanoporous Materials;* T. J. Pinnavaia, M. F. Thorpe, Eds, *Plenum Press*, New York, **1995**.

[52] B. Hatton, K. Landskron, W. Whitnall, D. Perovic, G. A. Ozin, *Acc. Chem. Res.* **2005**, *38*, 305-312.

[53] K. S. W. Sing, D. H. Everett, R. A. W. Haul, L. Moscou, R. A. Pierotti, J. Rouquerol, T. Siemieniewska, *Pure Appl. Chem.* **1985**, *57* ,603-619.

[54] S. Brunauer, P. H. Emmett, T. Teller, *J. Am. Chem. Soc.* **1938**, *60*, 309-319.

[55] E. P. Barrett, L. G. Joyner, P. P. Halenda, *J. Am. Chem. Soc.* **1951**, *73*, 373-380.

[56] A. Chenite, Y. LePage, A. Sayari, *Chem. Mater.*, **1995**, *7*, 1015.

[57] K.K. Cotí, M. E. Belowich, M. Liong, M. W. Ambrogio, Y. A. Lau, H. A. Khatib, J. I. Zink, N. M. Khashab, J. F. Stoddart, *Nanoscale*, **2009**, 1, 16.

[58] S.S. Thakur, Chauhan G.S*., Ind. Eng. Chem. Res.*, **2014**, *53*, 4838

[59] a) M. Vallet-Regí, A. Rámila, R. P. del Real, J. Pérez-Pariente, *J. Chem. Mater.* **2001**, *13*, 308. b) B. Muñoz, A. Rámila, J. Pérez-Pariente, I. Díaz, M. Vallet-Regi, *Chem. Mater.* **2003**, *15*, 500

[60] M. Liong, J. Lu, M. Kovochich, T. Xia, S. G. Ruehm, A. E. Nel, F. Tamanoi, J. I. Zink, *ACS Nano*, **2008**, *2*, 889

[61] K.K. Cotí, M. E. Belowich, M. Liong, M. W. Ambrogio, Y. A. Lau, H. A. Khatib, J. I. Zink, N. M. Khashab, J. F. Stoddart, *Nanoscale,* **2009**, *1*, 16

[62] a) N. K. Mal, M. Fujiwara, Y. Tanaka, *Nature*., **2003**, 421, 350; b) I. –I. Slowing, J. L. Vivero-Escoto, B. G. Trewyn, V. S. –Y. Lin, *J. Mater. Chem*., **2010**, *20*, 7924.

[63] a) Z. Li, J. C. Barnes, A. Bosoy, J. F. Stoddart, J. I. Zink, *Chem. Soc. Rev*. **2012**, 41, 2590-2605; b) R. R. Castillo, M. Colilla, M. Vallet-Regí, *Expert. Opin. Drug Deliv*. **2017,** 14, 229-243.

[64] F. Sancenón, L. Pascual, M. Oroval, E. Aznar, R. Martínez-Máñez, *ChemistryOpen* **2015**, *4*, 418-437.

[65] a) Q. Yang, S. Wang, P. Fan, L. Wang, Y. Di, K. Lin, F. –S. Xiao, *Chem. Mater*., **2005**, *17*, 5999; b) S. Angelos, Y. –W. Yang, K. Patel, J. F. Stoddart, J. I. Zink, *Angew. Chem. Int. Ed.*, **2008**, *47*, 2222; c) Y. Klichko, N. M. Khashab, Y. –W. Yang, S. Angelos, J. F. Stoddart, J. I. Zink, *Micropor. Mesopor.Mater.*,**2010**, *132*, 435; d) J. Liu, X. Du, *J. Mat. Chem.*, **2010***, 20*, 3642.

[66] a) R. Liu, X. Zhao, T. Wu, P. Feng, *J. Am. Chem. Soc.*, **2008**, *130*, 14418;b) R. Mortera, J. Vivero-Escoto, I. I. Slowing, E. Garrone, B. Onida, V. S.-Y. Lin, *Chem. Commun.,* **2009***,* 3219; c) Y. N. Cui, H. Q. Dong, X. J. Cai, D. P. Wang, D. P. Li, *ACS Appl. Mater. Interfaces.,***2012**, *4*, 3177.

[67] a) C. Liu, J. Guo, W. Yang, J. Hu, C. Wang, S. Fu, *J. Mat. Chem.*,**2009***, 19*, 4764; b) J. Lai, X. Mu, Y. Xu, X. Wu, C. Wu, C. Li, J. Chen, Y. Zhao, *Chem. Commun.,***2010**, *46*, 7370; c) C. R. Thomas, D. P. Ferris, J. –H. Lee, E. Choi, M. H. Cho, E. S. Kim, J. F. Stoddart, J. –S. Shin, J. Cheon, J. I. Zink, *J. Am. Chem. Soc.*, **2010**, *132*, 10623.

[68] a) C. Coll, R. Casasús, E. Aznar, M. D. Marcos, R. Martínez-Máñez, F. Sancenón, J. Soto, P. Amorós, *Chem. Commun.*,**2007**, 1957; b) T. D. Nguyen, K.C.-F. Leung, M. Liong, Y. Liu, J. F. Stoddart, J. I. Zink, *Adv. Funct. Mater*., **2007**, *17*, 2101; c) E. Aznar, C. Coll, M. D.

Marcos, R. Martínez-Máñez, F. Sancenón, J. Soto, P. Amorós, J. Cano, E. Ruiz, *Chem. Eur. J.*, **2009**, *15*, 6877; d) Y. Zhao, B. G. Trewyn, I. I. Slowing, V. S.-Y. Lin, *J. Am. Chem. Soc.,* **2009***,131*, 8398;e) R.Klajn, J. F. Stoddart, B. A. Grzybowski, *Chem. Soc. Rev*., **2010**, *39*, 2203;f) C. Coll, L. Mondragón, R. Martínez-Máñez, F. Sancenón, M. D. Marcos, J. Soto, P. Amorós, E. Pérez-Payá, *Angew. Chem. Int. Ed*., **2011**, *50*, 2138.

[69] J. G. Croissant, Y. Fatieiev, A. Almalik, N. M. Khashab, *Adv. Healthcare Mater.* **2018**, *7*, 1700831.

[70] E. Aznar, M. Oroval, L. Pascual, J. R. Murguía, R. Martínez-Máñez, F. Sancenón, *Chem. Rev.* **2016**, *116*, 561-718

[71] a) N. Song, Y.-W. Yang, *Chem. Soc. Rev.* **2015**, *44*, 3474-3504; b) J. Wen, K. Yang, F. Liu, Y. Xiu, S. Sun, *Chem. Soc. Rev.* **2017**, *46*, 6024-6045; c) J. Zhu, Y. Niu, Y. Li, Y. Gong, H. Shi, Q. Huo, Y. Liu, Q. Xu, *J. Mater. Chem. B.* **2017**, *5*, 1339-1352.

[72] A. Agostini, F. Sancenón, R. Martínez-Máñez, M. D. Marcos, J. Soto, P. Amorós, *Chem*. Eur. *J*. **2012**, *18*, 12218-12221.

[73] Q. Fu, G. V. R. Rao, L. K. Ista, Y. Wu, B. P. Andrzejewski, L. A. Sklar, T. L. Ward, G. P. López, *Adv. Mat.*, **2003***, 15*, 1262.

[74] a) Q. Fu, G. V. R. Rao, T. L. Ward, Y. Lu, G. P. López, *Langmuir*, **2007**, *23*, 170. b) Y. –Z. You, K. K. Kalebaila, S. L. Brock, D. Oupicky, *Chem. Mater.,* **2008***, 20*, 3354.

[75] E. Yu, I. Galiana, R. Martínez-Máñez, P. Stroeve, M. D. Marcos, E. Aznar, F. Sancenón, J. R. Murguía, P. Amorós, *Colloids Surf. B* **2015**, *135*, 652-660.

[76] C. de la Torre, A. Agostini, L. Mondragón, M. Orzáez, F. Sancenón, R. Martínez-Máñez, M.D. Marcos, P. Amorós, E. Pérez-Payá, *Chem. Commun***., 2014**, 50, 3184.

[77] H. P. Rim, K. H. Min, H. J. Lee, S. Y. Jeong, S. C. Lee, *Angew. Chem. Int. Ed*. **2011**, 50, 8853-8857.

[78] H. Zhou, X. Wang, J. Tang, Y.-W. Yang, *Polymers* **2016**, *8*, 277.

[79] S. Elsayed, C. Giménez, E. Aznar, Ramón Martínez-Máñez, F. Sancenón, M. Licchelli, *Org. Biomol. Chem.*, **2015,** 13, 1017-1021.

[80] G. Q. Silveira, M. D. Vargas and C. M. Ronconi, *J. Mater. Chem*., **2011**, 21, 6034– 6039.

[81] E. Bringas, Ö. Köysüren, D. V. Quach, M. Mahmoudi, E. Aznar, J. D. Roehling, M. D. Marcos, R. Martínez-Máñez and P. Stroeve, *Chem. Commun.,* 2012, **48**, 5647–5649.

[82] K. Ren, J. Wu, Y. Zhang, F. Yan and H. Ju, *Anal. Chem.*, **2014**, 86, 7494– 7499.

[83] X. – L. Li, N. Hao, H.-Y. Chen and J. – J. Xu, *Anal. Chem*., **2014**, 86, 10239– 10245.

[84] F. Porta, G. E. M. Lamers, J. Morrhayim, A. Chatzopoulou, M. Schaaf, H. den Dulk, C. Backendorf, J. I. Zink and A. Kros, *Adv. Healthc. Mater.*, **2013**, 2, 281– 286.

[85] A. Bernardos, L. Mondragón, E. Aznar, M. D. Marcos, R. Martínez-Máñez, F. Sancenón, J. Soto, J. M. Barat, E. Pérez-Payá and C. Guillem, *ACS Nano*, **2010**, 4, 6353– 6368.

[86] J. M. Li, F. Liu, Q. Shao, Y. Z. Min, M. Costa, E. K. L. Yeow and B. G. Xing, *Adv. Healthc. Mater.*, **2014, 3**, 1230– 1239.

[87] G. L. Zhang, M. L. Yang, D. Q. Cai, K. Zheng, X. Zhang, L. F. Wu and Z. Y. Wu, *ACS Appl. Mater. Interfaces*, **2014**, 6, 8042– 8047.

[88] S. Zong, Z. Wang, H. Chen, D. Zhu, P. Chen and Y. Cui, *IEEE Trans. Nanobiosci.*, 2014, **13**, 55– 60.

[89] A. Popat, S. Jambhrunkar, J. Zhang, J. Yang, H. Zhang, A. Meka and C. Yu, *Chem. Commun.*, **2014**, 50, 5547– 5550.

[90] Y. F. Zhu, W. J. Meng, H. Gao and N. Hanagata, *J. Phys. Chem. C*, **2011**, 115, 13630– 13636.

[91] a) C. Coll, A. Bernardos, R. Martínez-Máñez, F. Sancenón, *Acc. Chem. Res*., **2013**, *46*, 339; b) M. W. Ambrogio, C. R. Thomas, Y.-L. Zhao, J. I. Zink and J. F. Stoddart, *Acc. Chem. Res*., **2011**, *44*, 903.

[92] R. Casasús, E. Aznar, M. D. Marcos, R. Martínez-Máñez, F. Sancenón, J. Soto, P. Amorós*, Angew. Chem. Int. Ed*., **2006**, *45*, 6661.

[93] E. Aznar, C. Coll, M. D. Marcos, R. Martínez-Máñez, F. Sancenón, J. Soto, P. Amor, J. Cano, E. Ruiz, *Chem. Eur. J***. 2009**, 15, 6877– 6888.

[94] X. He, Y. Zhao, D. He, K. Wang, F. Xu, J. Tang, *Langmuir* **2012**, 28, 12909–12915

[95] S. Elsayed, M. Licchelli, R. Martínez-Máñez, F. Sancenón, *Chem. Asian J*. **2017**, 18, 2670-2674.

[96] Y. L. Choi, J. Jaworski, M. L. Seo, S. J. Lee, J. H. Jung, J. *Mater. Chem*. **2011**, 21, 7882–7885.

[97] Z. Zhang, F. Wang, D. Balogh, I. Willner, *J. Mater. Chem. B* **2014**, 2, 4449–4455.

[98] Y. Wen, L. Xu, C. Li, H. Du, L. Chen, B. Su, Z. Zhang, X. Zhang, Y. Song, *Chem. Commun*. **2012**, 48, 8410 8412.

[99] E. Climent, M. D. Marcos, R. Martinez-Máñez, F. Sancenón, J. Soto, K. Rurack, P. Amorós, *Angew. Chem. Int. Ed*. **2009,** 48, 8519–8522.

[100] Y. F. Zhang, Q. Yuan, T. Chen, X. B. Zhang, Y. Chen, W. H. Tan, *Anal. Chem*. **2012**, 84, 1956–1962.

[101] a) E. Aznar, R. Villalonga, C. Gimenez, F. Sancenón, M. D. Marcos, R. Martínez-Máñez, P. Diez, J. M. Pingarron, P. Amorós, *Chem. Commun*. **2013**, 49, 6391–6393. b) R. Villalonga, P. Díez, A. Sánchez, E. Aznar, R. Martínez-Máñez, J. M. Pingarrn, *Chem. Eur. J.* **2013**, 19, 7889–7894, c) P. Díez, A. Sánchez, M. Gamella, P. Martínez-Ruíz, E. Aznar, C. de La Torre, J. R. Murgu.a, R. Martínez-Máñez, R. Villalonga, M. J. Pingarrón, *J. Am. Chem. Soc*. **2014**, 136, 9116–9123.

[102] I. Candel, A. Bernardos, E. Climent, M. D. Marcos, R. Martínez-Máñez, F. Sancen.n, J. Soto, A. M. Costero, S. Gil, M. Parra, *Chem. Commun*. **2011**, 47, 8313–8315.

[103] E. Climent, A. Bernardos, R. Martínez-Máñez, A. Maquieira, M. D. Marcos, N. Pastor-Navarro, R. Puchades, F. Sancenón, J. Soto, P. Amorós, *J. Am. Chem. Soc*. **2009**, 131, 14075–14080.

[104] B. Zhang, B. Liu, J. Liao, G. Chen, D. Tang, *Anal. Chem*. **2013**, 85, 9245 – 9252

[105] D. Tang, B. Q. Liu, R. Niessner, P. W. Li, D. Knopp, *Anal. Chem*. **2013**, 85, 10589–10596.

[106] L. Chen, Y. Wen, B. Su, J. Di, Y. Song, L. Jiang, *J. Mater. Chem*. **2011,** 21, 13811–13816.

[107] M. Chen, C. Huang, C. He, W. Zhu, Y. Xu, Y. Lu, *Chem. Commun*. **2012**, 48, 9522–9524.

[108] Y. Salinas, A. Agostini, É. Pérez-Esteve, R Martínez-Máñez, F. Sancenón, M. D. Marcos, J. Soto, A. M. Costero, S, Gil, M. Parra, P. Amorós, *J. Mater. Chem. A*., **2013**,1, 3561.

[109] a) L. Pascual, I. Baroja, E. Aznar, F. Sancen.n, M. D. Marcos, J. R. Murgu.a, P. Amorós, K. Rurack, R. Martínez-Máñez, *Chem. Commun*. **2015**, 51, 1414 – 1416. b) E. Climent, L. Mondragón, R. Martínez-Máñez, F. Sancen.n, M. D. Marcos, J. R. Murguía, P. Amorós, K. Rurack, E. Pérez-Payá, *Angew. Chem. Int. Ed***. 2013**, 52, 8938–8942.

[110] Z. Wang, X. Yang, J. Feng, Y. Tang, Y. Jiang, N. He, *Analyst* **2014**, 139, 6088–6091.

[111] Z. Zhang, D. Balogh, F. Wang, S. Y. Sung, R. Nechushtai, I. Willner, *ACS Nano* **2013**, 7, 8455–8468.

[112] M. Oroval, E. Climent, C. Coll, R. Eritja, A. Aviño, M. D. Marcos, F. Sancenón, R. Martínez-Máñez, P. Amorós, *Chem. Commun*. **2013**, 49, 5480 –5482.

[113] R. Qian, I. Ding, H. Ju, *J. Am. Chem. Soc*. **2013**, 135, 13282–13285.

[114] M. Martínez-Carmona, Y. K. Gun´ko, María Vallet-Regí, *Pharmaceutics* **2018**, 10, 279.

[115] Dodds, D.R. Antibiotic resistance: A current epilogue. *Biochem. Pharmacol.* **2017**, 134, 139–146.

[116] MacGowan, A.; Macnaughton, E. Antibiotic resistance. *Medicine* **2017**, 45, 622–628.

[117] The European Union summary report on antimicrobial resistance in zoonotic and indicator bacteria from humans, animals and food in **2016**. EFSA J. 2018, 16, 5182.

[118] Kumar, A.; Alam, A.; Rani, M.; Ehtesham, N.Z.; Hasnain, S.E. *Int. J. Med. Microbiol*. **2017**, 307, 481–489.

[119] Weledji, E.P.; Weledji, E.K.; Assob, J.C.; Nsagha, D.S. Pros. New Horiz. *Transl. Med*. **2017**, 4, 9–14.
[120] Shatzkes, K.; Connell, N.D.; Kadouri, D.E. Predatory bacteria: *Future Microbiol*. **2017**, 12, 469–472
[121] El-Shibiny, A.; El-Sahhar, S. Bacteriophages: *J. Microbiol*. **2017**, 63, 865–879.
[122] Vitetta, L.; Vitetta, G.; Hall, S. Front. *Immunol*. **2018**, 9, 2240.
[123] Wang, L.; Hu, C.; Shao, L. *Int. J. Nanomed*. **2017**, 12, 1227–1249.
[124] Sammour, O.A.; Hassan, H.M. *Drug Deliv*. **1996**, 3, 273–278, b) Eid, K.A.M.; Azzazy, H.M.E. *Nanomedicine* **2014**, 9, 1301–1310.
[125] Cheow, W.S.; Hadinoto, K.; Donelli, G., Ed.; Springer: New York, NY, USA, 2014; pp. 227–238, ISBN 978-1-4939-0467-9.
[126] Vallet-Regí, M.; Manzano, M.; González-Calbet, J.M.; Okunishi, E. *Chem. Commun.* **2010**, 46, 2956–2958.
[127] Yasuyuki, M.; Kunihiro, K.; Kurissery, S.; Kanavillil, N.; Sato, Y.; Kikuchi, Y. Biofouling 2010, 26, 851–858.
[128] M. Liong, B. France, K. A. Bradley, J. I. Zink, *Adv. Mater*. **2009**, 21, 1684–1689.
[129] M. Lu, Q. Wang, Z. Chang, Z. Wang, X. Zheng, D. Shao, W. Dong, Y. Zhou, *Int. J. Nanomed*. **2017**, 12, 3577–3589.
[130] T. Tamanna, J. B. Bulitta, A. Yu, *J. Mater. Sci. Mater. Med*. **2015**, 26, 117.
[131] W. K. Jung, H.C. Koo, K. W. Kim, S. Shin, S. H. Kim, Y. H. Park, *Appl. Environ. Microbiol.* **2008**, 74, 2171–2178.
[132] Dibrov, P.; Dzioba, J.; Gosink, K.K.; Häse, C.C. Antimicrob. Agents Chemother. 2002, 46, 2668–2670.
[133] B. Ruehle, D. L. Clemens, B. -Y. Lee, M. A. Horwitz, I. J. Zink, *J. Am. Chem. Soc*. **2017**, 139, 6663–6668.
[134] N. Mas, I. Galiana, L. Mondragõn, E. Aznar, E. Climent, N. Cabedo, F. Sancenõn, J. R. Murguía, R. Martínez-Máñez, M. D. Marcos and P. Amorõs, *Chem. - A Eur. J*., **2013**, 19, 11167–11171.
[135] S. Sánchez-Salcedo, S. Hruti, A. J. Salinas, G. Malavasi, L. Menabue, M. Vallet-Regí, *J. Mater. Chem. B*. **2014**, 2, 4836–4847.

[136] A. Aguilar-Colomer, J. C. Doadrio, C. Pérez-Jorge, M. Manzano, M. Vallet-Regí, J. Esteban, *J. Antibiot*. **2017**, 70, 259–263.
[137] R. García-Alvarez, I. Izquierdo-Barba, M. Vallet-Regí, *Acta Biomater*. **2017**, 49, 113–126.